Assessment of soft tissue tension during total hip arthroplasty

Measuring the forces in the neck of a prosthesis

Dieter van der Pol

Graduation thesis
Department of BioMechanical Engineering
TU Delft
2017

Assessment of soft tissue tension during total hip arthroplasty

Measuring the forces in the neck of a prosthesis

by

Dieter van der Pol

to obtain the degree of Master of Science
at the Delft University of Technology,
to be defended publicly on Friday December 22, 2017 at 14:00.

NOTE: Photos of the surgical procedure in the Erasmus hospital are confidential and cannot be made public.

An electronic version of this thesis will be available at `http://repository.tudelft.nl/`.

TUDelft   MISIT

From left to right: MD Bryan Blaauw (Orthopedic surgeon), Reinier van Antwerpen (Technician O&O at TU Delft), Dieter van der Pol (Msc candidate TU Delft), Karin Biermans (Sales Consultant Joint Reconstruction at Johnson&Johnson Medical BV), Dr. ir. Tim Horeman (Supervisor and researcher at MISIT lab TU Delft).

Preface & Acknowledgements

Dear reader,

Before you lies the report of my thesis project. The project started about a year ago. I would say we started out quite ambitious, since the requirements for designing a tool that is used inside the human body are very strict (especially with regards to sterilization) and there is very little physical workspace as well. However, sometimes you have to aim above the mark to hit the mark. Which is exactly what we did and it resulted in this thesis.

Personally, I became a mechanical engineer out of curiosity and with intend to improve the lives of others. Within the specialization of medical equipment, one has the opportunity to affect the lives of many. Mainly, this considers the lives of patients, but you can also make work easier for the surgical teams who are tasked with performing difficult surgeries. I wanted to accomplish the development of a mechanism to reduce the post surgical complications, but also to create a simple, effective and trustworthy tool for the medical teams who perform hip surgery. This mission was challenging, but also a very interesting and fulfilling project.

This brings me to my acknowledgements, because this project would not have been possible without the support of many. Most important were my supervisors. Therefore I would like to thank Tim Horeman, Bryan Blaauw and Jenny Dankelman for making this thesis possible, for their valuable input during the project and for challenging me to come up with new solutions. I would also like to thank Karin Biermans for being our contact person at DePuy/Johnson&Johnson company and providing us with the implant materials we required. Another person I would like to thank is Evert van Langelaan, a very experienced surgeon whom I interviewed about the subject of the thesis. Furthermore, I would like to thank Jan van Frankenhuyzen from the faculty of Mechanical Engineering for helping me to 3D print the first plastic prototypes, and I would like to thank Frank Schilder of the DEMO lab and Reinier van Antwerpen for helping me manufacturing the metal prototype. I would also like to thank Patrick van Holst and Harry Jansen for their technical support during the calibration sessions. Finally, I would like to thank my parents for their support that encouraged me to go to university.

At the end, thanks to you reader. If you read this line after the others, you have read at least one page of my thesis. I hope you will find it enjoyable and interesting to read the rest as well.

Dieter van der Pol
Delft, December 2017

Summary

The goal of this thesis is: *"To create a sterilizable instrument that measures the compressive force in the axial direction of the neck of the hip implant during surgery."*. This measured axial force in combination with a standardized ROM test could be used to objectively assess the soft tissue tension during surgery. It is expected that this instrument will be a helpful tool for inexperienced surgeons, because literature shows that errors made by the surgeon are the biggest cause of early failures and inexperienced surgeons registered twice as much dislocations as experienced surgeons. Therefore, the instrument could improve the success rate and quality of total hip arthroplasty by reducing the number of early failures caused by dislocation resulting from the inadequate soft tissue tension created by inexperienced surgeons. Furthermore, it could improve the patients' quality of living by reducing their limping and pain after the surgery.

The current techniques to obtain the optimal length and angle of the implant are: preoperative radiography, intraoperative leg length assessment and subjective soft tissue tension assessment methods. Factors that influence soft tissue tension, apart from the implant, are either caused by the patient (inter- or intra-personal), the surgeon or the environment.

Although a 3 DOF sensory system integrated in the test stem is preferable, it is likely that measuring only the axial force in a so called 'the neck' of the prosthesis, in combination with a standardized range of motion (ROM) test, provides valuable inside information about the relation between variation in force and success of the procedure. This assessment is not based measuring absolute forces, but on pattern recognition while moving the hip through its range of motion. The validity of this hypothesis should be investigated in future research. Different sensors have been tested to see if they survive the standard sterilization program of an autoclave, which uses hot steam at 134 degree Celsius, at a pressure of 2 bar for 20 minutes. The linear Hall sensor was chosen based on this test and a list of pros and cons. After that, a design was made in SolidWorks. Then it was manufactured and calibrated. The final prototype can be implanted in a few seconds when the stem is in place, by sliding it onto the stem and plugging it into a monitor. The device is intuitive to use, because the monitor produces real time graphs of the axial force that are easy to understand. Immediate adjustments to the soft tissue tension can be made by switching the head of the implant, while keeping the force sensing neck in place, in order to provide the greatest chance for surgical success. Furthermore, the device is highly reusable, because it can be sterilized with the standard autoclave procedure.

Finally, the prototype was tested in a cadaver at the Erasmus hospital in Rotterdam. The axial hip force was measured at rest, when pulling the leg and when moving the leg through its range of motion. Although there were inaccuracies due to the elastic hysteresis of the rubber spring and friction of between axis and cylinder, consistent patterns in the measured axial hip force were observed. Recommendations are proposed in chapter 5 to reduce the errors caused by elastic hysteresis, friction and ROM tracking.

Based on what was learned from the cadaver test and from literature, a standardized test proposal with hypothesis was made. This test should serve as a guideline to get consistent and useful results in future research. This future research should investigate if the axial force measured during these ROM tests provides enough information to objectively assess the soft tissue tension, or if more information is required.

Contents

Introduction

Total hip arthroplasty (THA) has two very important outcomes. The most important is the stability of the hip. The second most important is the symmetry of the legs. One of the factors that influences the stability of the hip is the so called 'soft tissue' tension. These soft tissues consist of tendons, muscles, ligaments, fascia, skin, fibrous tissues, fat, nerves and blood vessels. Of course, the tendons, muscles and ligaments are have the biggest contribution to the stability of the hip joint. Interestingly, very little has been written about the objective assessment of the soft tissue tension in the hip during THA, as all of the current techniques are subjective. Several studies indicate that the soft tissue tension is related to: pain (in for instance the groin and knee), dislocation, range of motion (ROM) of the hip and limping [1], [2], [3]. The instrument could make work easier for inexperienced surgeons in particular, since they lack the "fingerspitzengefühl" to assess what is the correct soft tissue tension. We aim at inexperienced surgeons because errors made by the surgeon are the biggest cause of early failures [4], [5], and inexperienced surgeons registered twice as much dislocations as experienced surgeons [6].

Thus, it would be interesting to measure the soft tissue tension during total hip arthroplasty. Therefore, an instrument that allows the surgeon to **objectively** assess the soft tissue tension will be created. It is important to note that this instrument will only be used intraoperatively. This means it will only be used as a tool to help the surgeon during surgery. It is strongly preferred that the instrument is sterilizable, because in that way it could be re-used for multiple surgeries. The standard procedure for sterilization is by means of hot steam in an autoclave.

During surgery, a modular implant is used that consists of a spherical head, a neck and a stem part. These modular parts can easily be inserted. The surgeon can choose test heads with different diameters and hole depths to vary the length of the implant and thus the soft tissue tension. DePuy company sells three different test necks and more than 20 different spherical test heads. Therefore, it was decided to instrument one of the test necks with one or more sensors. DePuy supplied us with a test neck, a test head and a stem.
It appeared that measuring the forces in three orthogonal directions is technically difficult, because there is little space for multiple sensors and cross talk effects could occur. Therefore, it was decided to measure the force in only one direction, being the axial direction of the neck of the implant. Hence a test neck of a hip implant must be redesigned and instrumented with a sensor, in order to measure the axial hip forces during surgery. This axial force measurement should be combined with a standardized ROM test, in order to provide valuable information about the soft tissue tension of the hip and hence its stability. Thus, the assumption was made that the hip forces are indeed caused by the soft tissue tension of the hip, although disturbances can be created when external forces are applied to the body. Finally, a prototype will be created and tested in a cadaver.

Taking all of this into account, the complete mission statement for the thesis is: *"To create a sterilizable instrument that measures the compressive force in the axial direction of the neck of the hip implant during surgery."* This measured axial force in combination with a standardized ROM test could be used to objectively assess the soft tissue tension during surgery.

Furthermore, I would like to attend the reader that appendix A was created to help the reader understand the anatomical terminology used throughout this report. This appendix contains an overview of all the relevant bone sections, ligaments, muscles, motions and anatomical planes of the hip. If the reader encounters an unknown word in the report considering one of these topics, it can be found in appendix A.

1

Analysis

In this chapter there will be a description of the total hip arthroplasty (THA) procedure in a nutshell. This chapter is written in chronological order, so the reasons for surgery and preoperative techniques are described first. Then a short explanation of the surgical approach and the procedure will be given, along with the intraoperative measurements that can be used to check the symmetry of the legs and the stability of the hip. As said before, the stability of the hip is the most important outcome. The symmetry of the legs is the second most important outcome.

1.1. Reasons for surgery

The most common preoperative diagnosis for THA, which accounts for 63% of cases, is osteoarthritis [7]. Following this diagnosis, rheumatoid arthritis, avascular necrosis and loosening of components from a former hip replacement surgery are also common diagnoses that lead to a hip surgery. Each of these accounts for roughly 8-11% of all cases [7]. Patients have a variety of complaints before they go under the knife. The most mentioned reason for surgery is pain during daily activities such as walking, climbing stairs, driving, using the toilet, and bending over to tie a shoe. Patients may also have developed a slight limp because of this pain.

1.2. Prosthetic Components

Four components can be identified in the final implant (Fig. 1). The shell, also known as the cup, is the component which is placed in the acetabular cup of the pelvis during the surgery. The liner is placed inside of the shell to create an effect that is comparable to the effect of cartilage between a healthy ball and socket joint. The head is the spherical part of the prosthetic. It replaces the femoral head. The head is attached to the stem. The stem is the leg component, which is inserted into the femur by using a special hammer. Both the head and the stem are adjusted to the particular patient during surgery. This will be explained into detail later on.

It is important to note that during the surgery the surgeon makes use of a trial implant, which is slightly different from the final implant. The difference is that the trial implant has the stem part separated into two pieces: a neck part and a stem part that is inside the bone (Fig. 2). In the Corail hip prosthesis that we will be using, there are three different necks available: standard (STD), high offset (KHO), in which the neck is moved laterally, and coxa vara (KLA), in which the angle between the neck and the shaft of the femur is less than normal. Furthermore, more than twenty different trial heads are available.
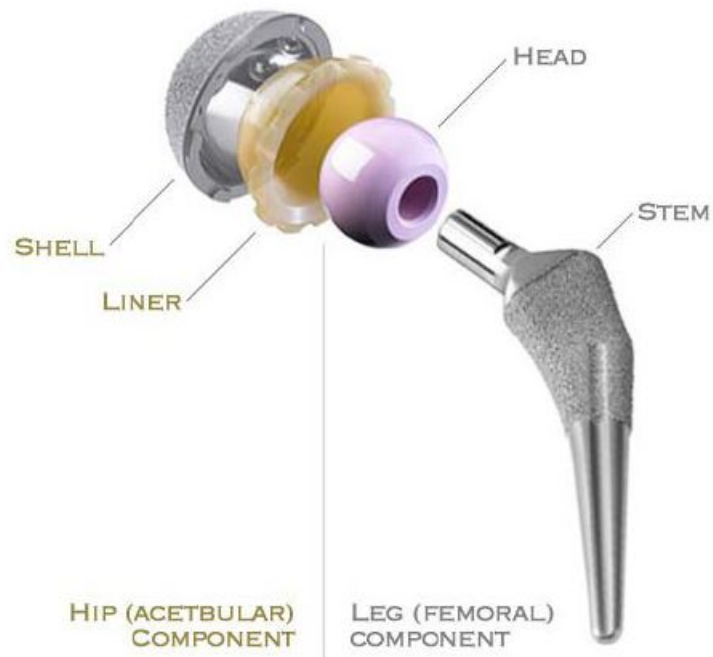
Figure 1: Components of the final implant. Image credit goes to: http://evertsmith.com/innovations. Retrieved 7-6-17. Copyright 2008 by Evert Smith.
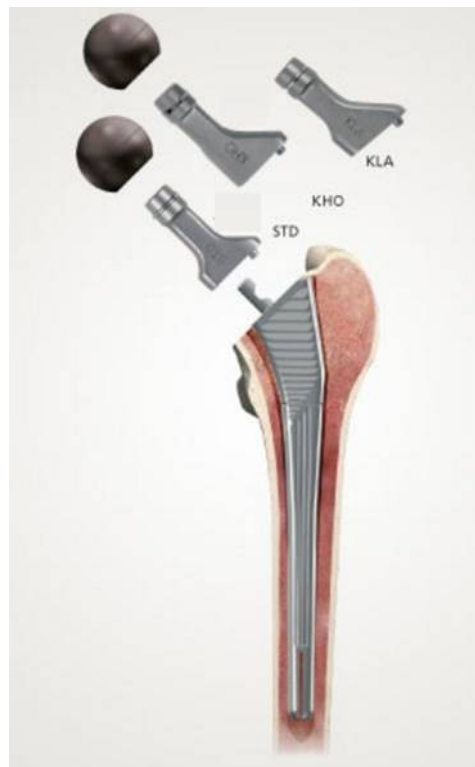

Figure 2: Components of a trial implant. The surgeon can experiment with different heads and necks to influence the soft tissue tension of the hip. Image credit goes to: http://www.corailpinnacle.net. Retrieved 7-6-17.

1.3. Risk factors

Table 1 from Ulrich et al. [5], 2007, shows that instability is the biggest cause of early failures. In this case early means within 5 years after the first surgery. Pain is also listed as a significant reason for early failure. However, we have to investigate what are the causes of instability and pain, before we can talk about solutions.

If the cause of failure is pain, than this is most likely caused by osteonecrosis. Osteonecrosis quickly degenerates the hip. This can be observed in Table 2 from Ulrich et al. [5], 2007, which shows the correlation between the primary diagnosis and the reason for revision. However, this does not mean that the soft tissue tension cannot cause pain. It means that it is not severe enough to be the primary reason for revision.

The risk of instability seems to be present in all diseases, so this is probably not caused by a specific disease, but by the surgical technique and soft tissue tension. This means, objectifying the correct tissue tension could potentially decrease the amount of failures caused by instability. It has to be noted that it is also very important for the patient to exercise their hip muscles after THA, to prevent possible complications like instability caused by weakness of the muscles.

A possible solution to reduce the amount of dislocations is to use larger prosthetic heads. Larger heads tend to be more stable, according to Tansey et al., [8], 2015. The dimensions of these larger prosthetic heads are closer to the anatomical femoral heads. Larger heads also have a larger range of motion, because the impingement between prosthetic neck and liner is delayed. However, three disadvantages of using larger heads are also described in Tanssy et al., [8], 2015. Firstly, the thin polyethylene liners that are necessary to accommodate larger heads may increase the risk of liner fracture. Secondly, larger heads can also cause soft tissue impingement. In particular the iliopsoas is impinged by the distal portion of the larger head. This results in groin pain. Thirdly, larger diameter heads are said to exert larger forces on the femoral trunnion due to the larger moment arm. This contributes to wear, corrosion and metal release. Subsequently, these metal particles can cause adverse local tissue reactions.

Several papers [5], [4], state that errors made by the surgeon are the biggest cause of early failures, especially when unexperienced surgeons perform the procedure. According to Hedlundth et al. [6], 1996, twice as much dislocations were registered for inexperienced surgeons compared to their more experienced colleagues. This frequency of dislocation was lowered to a constant level with increasing numbers of operations. It remained constant after approximately 30 operations. The risk of dislocation decreased by 50% for every 10 primary THAs performed annually. Therefore, it is said these surgeons must remain focused on the technical aspects of the procedure and be vigilant for errors in surgical technique, because these can give rise to early failures. Since the soft tissue tension is one of the factors that influences the risk of dislocation, it could be useful to objectify the soft tissue tension during surgery to prevent these early dislocations.

Time interval to revision	Number of hips requiring revision	Aseptic loosening (%)	Infection (%)	Instability (%)	Component failure (%)	Periprosthetic fracture (%)	Pain (%)
<2 years	79	17.70	24	33	3.80	6.30	15.20
2–5 years	39	46.20	10.30	25.60	0.00	5.10	12.80
5–10 years	49	67.30	14.30	10.30	0.00	2	6.10
>10 years	70	90	5.80	0.00	0.00	2.80	1.40
<5 years	118	27.10	19.60	30.5	2.50	5.90	14.40
>5 years	119	80.70	9.20	4.20	0.00	2.50	3.40
Total	237	51.90	15.60	16.90	2.10	5.50	8

[a] Cause of failure is given in the table as the percentage of the group

Table 1: Relationship between cause of failure and time to failure (time interval to revision) [5].

Diagnosis	Number of hips requiring revision	Causes of failure					
		Aseptic loosening (%)	Infection (%)	Instability (%)	Component failure (%)	Peri-prosthetic fracture (%)	Pain (%)
Osteoarthritis	111	56 (50.5)	24 (21.6)	17 (15.3)	2 (1.8)	9 (8.1)	4 (3.6)
Inflammatory arthritis	20	15 (70)	2 (10)	1 (5)	0 (0.0)	2 (10)	0 (0.0)
Osteonecrosis	62	26 (41.9)	6 (9.7)	13 (21)	2 (3.2)	1 (1.6)	14 (22.6)
Dysplasia	25	15 (60)	1 (4)	6 (24)	1 (4)	1 (4)	1 (4)
Post-traumatic arthritis	14	6 (42.9)	6 (42)	4 (28.6)	0 (0.0)	0 (0.0)	0 (0.0)
Other	5	5 (100)	0 (0.0)	0 (0.0)	0 (0.0)	0 (0.0)	0 (0.0)

[a] Cause of failure is given in the table as the number of hips, with the percentage given in parentheses

Table 2: Relationship between cause of failure and primary diagnosis [5].

1.4. Preoperative procedure

Possible preoperative techniques consist of making a conventional x-ray or CT scan. There are a number of anatomical angles and distances that must be evaluated before the surgery. They will be explained in this chapter. There are also state-of-the-art developments, like the printing of 3D bone models for complicated anatomies, but these special techniques will be disregarded for simplicity.

Conventional x-ray vs CT scan

A simple x-ray of the frontal plane can already provide much useful information. According to Lecerf et al. [9], 2009, preoperative measurement of femoral offset is currently performed with conventional radiographs (x-rays). However, the accuracy of x-ray images is limited. Lecerf et al. [9], 2009, shows that conventional radiography always underestimates the length of the offset, when compared to the CT scan. In 28 % of the cases, the underevalution exceeded 5 mm. One of the reasons for this is that radiographic enlargement is hard to control, because it depends on the patient's build. In postoperative radiographs this is not a problem, since the diameter of the prosthetic head and thereby the magnification factor is known. A second reason for the inaccuracy of the conventional x-ray images could be that the lower limb rotational positioning might also be responsible for offset undervaluation.

Thus, the CT scan is often considered to be the golden standard [9], [10]. Based on the anatomical information provided by this CT scan, the surgeon can make a good initial estimation of the required implant dimensions.

Anatomical landmarks

The surgeon always makes a CT scan of the frontal plane. This radiograph is taken in standing position and can be used to obtain a number of important anatomical and mechanical landmarks. The most important anatomical landmarks are (Fig. 3) [11]:

1. Femoral shaft.

2. Greater trochanter.

3. "Saddle". This point is easily identifiable, even with the minimally invasive frontal approach.

4. Lesser trochanter. The size of the lesser trochanter projected on the radiograph indicates the in plane rotation of the femur. This rotation makes the neck length seem shorter (Fig. 4).

5. Acetabular roof.

6. "Teardrop". This is a purely radiographic landmark created by the superposition of the medial wall and the tip of the horn of the acetabulum.

I Foramen obturatum. Used for radiographic quality assessment.

II Symphysis. Used for radiographic quality assessment.

III Sacrum. Used for radiographic quality assessment.

IV Distance between symphysis and sacrococcygeal joint. This distance is used to determine the pelvic tilt in the frontal and sagittal plane.
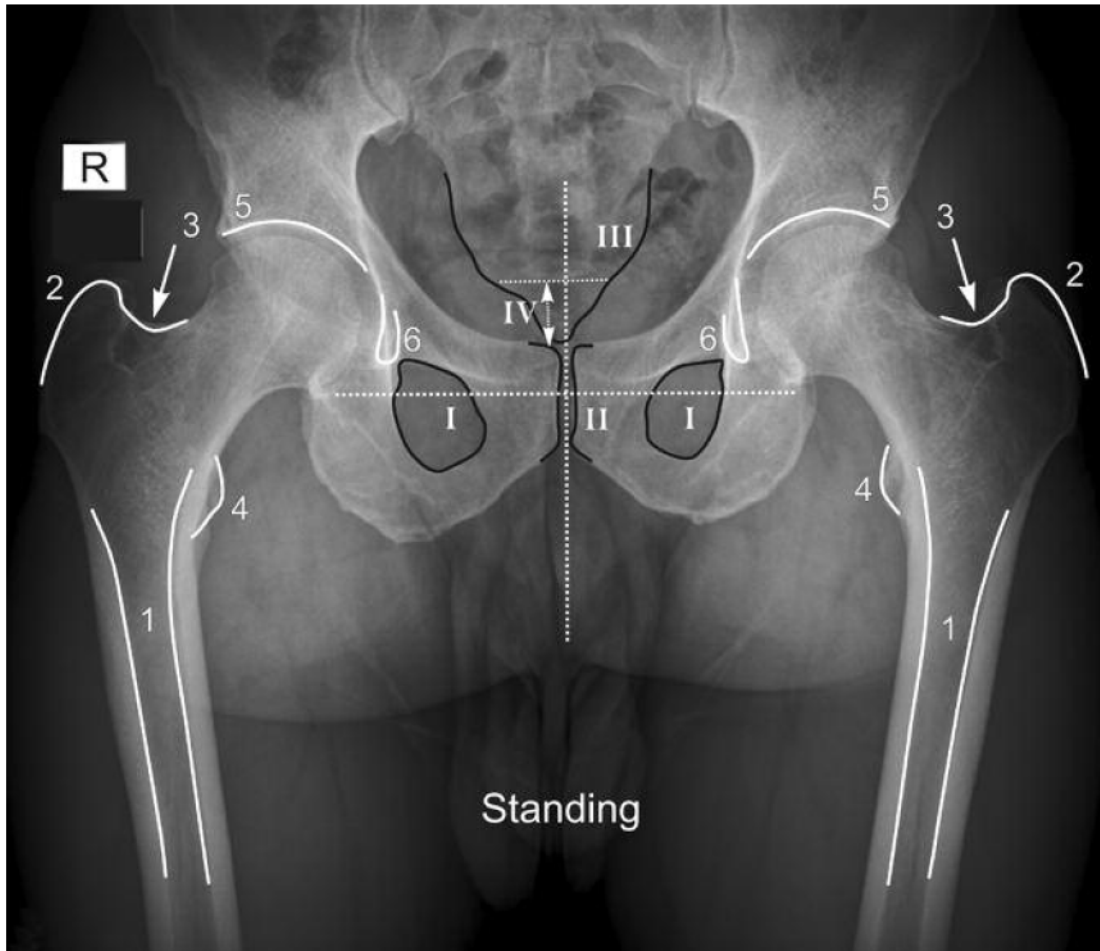
Figure 3: Radiograph of the frontal plane indicating the anatomical landmarks. The patient is standing during this scan [11].
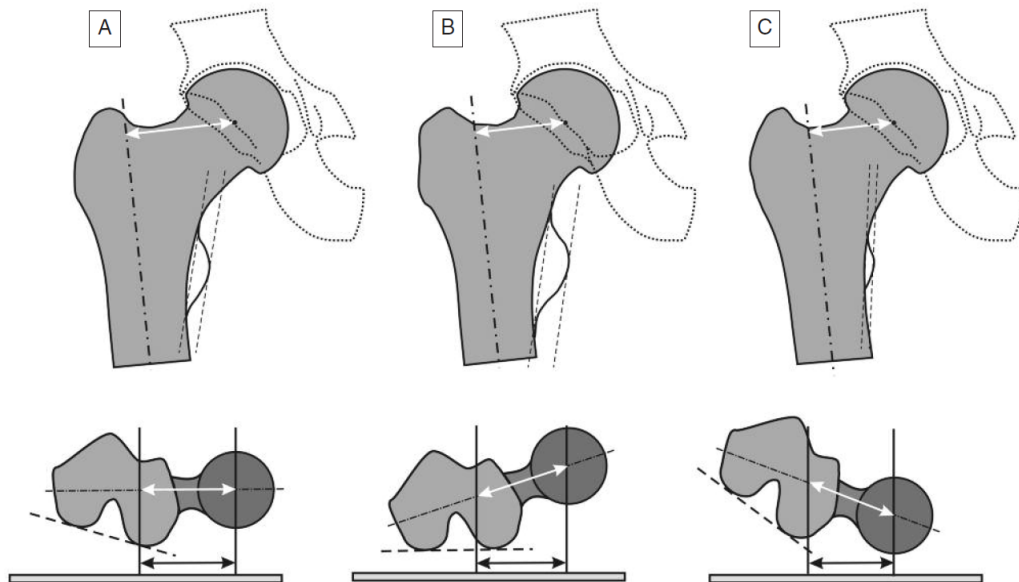

Figure 4: The size of the teardrop indicates the femoral rotation in the radiograph of the frontal plane. A) Correct estimation of neck length. B) Incorrect estimation. C) Incorrect estimation [11].

Mechanical landmarks

From these anatomical landmarks we can determine a number of mechanical landmarks. The most important mechanical landmarks are (Fig. 5):

1. Hip center of rotation.

2. Femoral axis.

3. Femoral offset. Femoral offset is measured as the shortest distance between the center of rotation and the femoral axis.

4. Acetabular offset. The hip center of rotation is determined by the acetabular offset. This offset can be changed by reaming or by inserting a thicker liner into the cup. Both the femoral and acetabular offset strongly correlate to the functioning of the abductor muscles. Therefore, the total hip offset should be defined as the sum of those two. Not all papers do this. These two offsets are also correlated to wear and impingement [12]. This distance is normally 55 mm in males and 48 mm in females (p = 0.001) [13]. The acetabular offset is also important because it serves as the lever arm for the body weight.

5. Hip length. Excessive lengthening is poorly tolerated and can lead to nerve dysfunction, like sciatic nerve palsy or irritation [14]. Furthermore, limb length inequality (LLI) may lead to serious legal issues [15]. Hip length is measured a line which runs perpendicular from the transteardrop line to the apex of the lesser trochanter.

6. Leg length discrepancy. The leg length is measured as the distance between the teardrop and a horizontal line parallel to the floor. The leg length discrepancy is the difference between these lines on left (6L) and right (6R) sides.

Angles

Four different angles can be defined:

I The femoral neck angle (or caput-collum-diaphyseal angle, CCD angle) between the longitudinal axes of the femoral neck and shaft (Fig. 6). This angle usually measures approximately 126 degrees in adults [16], with no significant difference between men and women [13].

II The acetabular inclination (transverse angle of the acetabular inlet plane). This is the angle between a line passing from the superior to the inferior acetabular rim and the horizontal plane (Fig. 6). This angle measures on average 55 degrees in adults, with no significant difference between men and women [16].

III Anteversion angle of the femoral neck, which is the angle between the condylar axis and the axis of the femoral neck (Fig. 7). This angle measures an average of 8 degrees in men and 9 degrees in women [13]. Furthermore, the accuracy of a 2D femoral offset analysis might be compromised by the upper femoral torsion or helitorsion (angle of stem insertion) and femoral anteversion (femoral neck angle). An additional CT scan in the horizontal plane can provide the surgeon with additional information of the anatomy of the patient (Fig. 8). This provides the surgeon with the ability to determine femoral helitorsion and femoral anteversion. Heller et al [17], 2001, has shown that the femoral anteversion has a strong effect on the musculo-skeletal loading around the proximal femur. Increasing the anteversion to an angle of 30 degrees increased the contact forces and moments in the hip joint with 28% during walking and stairs climbing. Once the desired stem anteversion axis is known, it is easy to calculate the alpha angle (the difference between the stem helitorsion and anteversion axis). This can improve the quality of preoperative planning. However, scanning the horizontal plane is not yet common practice [9].

IV Acetabular anteversion. This is the angle between the sagittal plane and the cup (Fig. 7). Adult females have a significantly greater acetabular version of 23 degrees (range 10 to 53) compared to 18 degrees in males (range 7 to 46) (p = 0.02) [13].
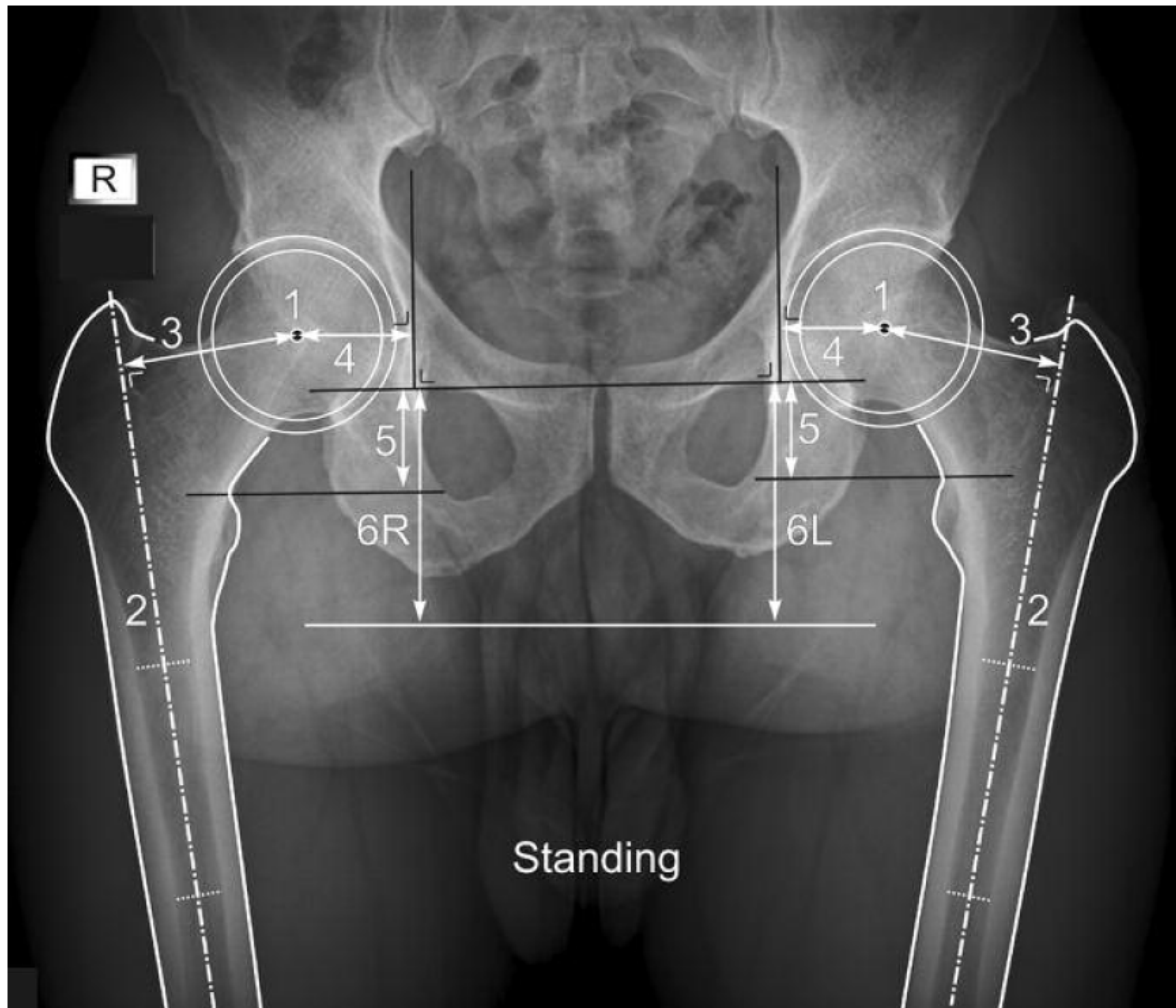
Figure 5: Mechanical landmarks determined by the previous anatomical landmarks. Once the hip rotation center (1) is determined, the femoral hip offset (3) and leg length (5) can be approached by a template of an implant with corresponding dimensions. This will be fine tuned intraoperatively with test neck and head components [11].
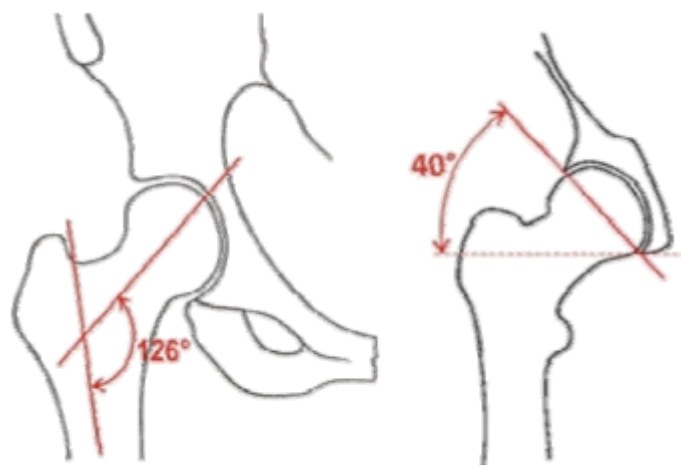

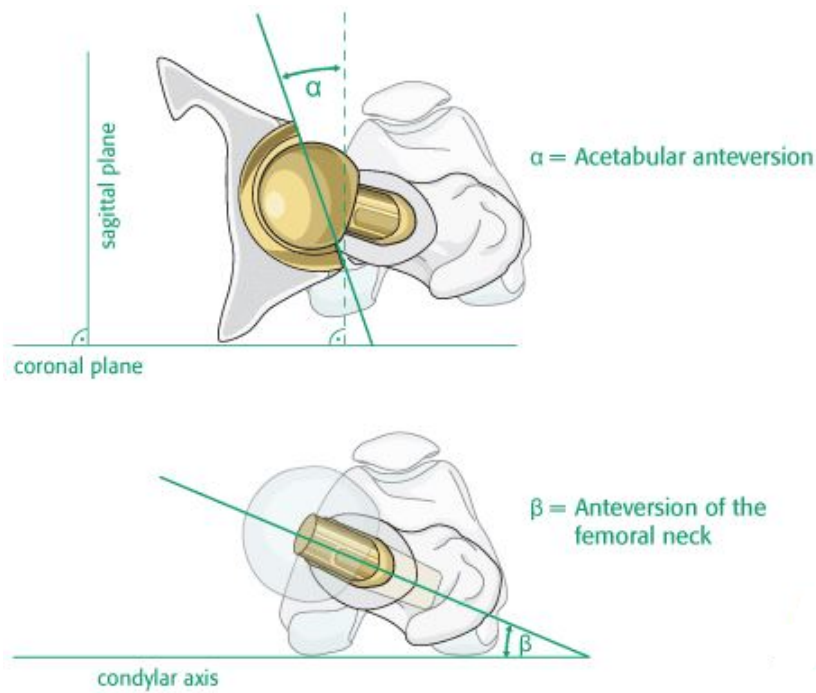Figure 6: Femoral neck angle (CCD angle) and acetabular inclination. [16].

Figure 7: Acetabular anteversion and femoral anteversion. *Image credit: www.aofoundation.org*
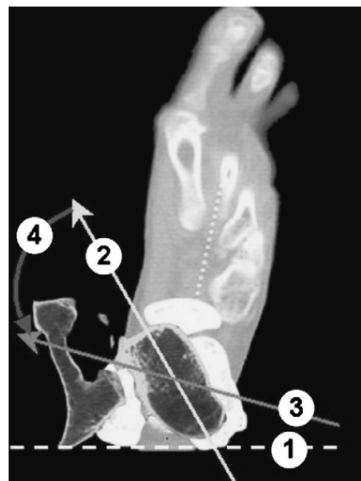

Figure 8: Radiograph of the horizontal plane. This was referred to as a '3D scan'. 1: posterior bicondylar axis; 2: helitorsion axis; 3: prosthetic anteversion axis; 4: alpha angle [9].

Some papers advice to perform extra measurements. According to Lecerf et al. [9], 2009, additional measurements, that have to be determined during the preoperative planning, are the abductor muscle lever arm and the gluteus medius activation angle. However, the author of this report thinks these two measures are already determined by the hip offset. Therefore, adding these two measures would overconstrain the problem.

Preoperative planning has two important limitations that are often overlooked. The first limitation is that a slight intraoperative malpositioning of the femoral implant or acetabular cup can result in an alteration of the dimensions in practice, like the medial femoral offset [15]. The second limitation is that it is not possible to know beforehand what the soft tissue tension will be when the implant is placed. However, this is very important, because the soft tissue tension is related to the stability of the hip, which is the most important outcome. Thus, it is important to use intraoperative methods as well to overcome these limitations.

Mathematical models

There are also mathematical models that describe the optimal geometrical relationships when reconstructing the hip [18], [19], [17], [20]. A clear example is described in Johnston et al. [18], 1979, where they made a model of all the muscles and bones at the hip joint (Appendix A, Fig. A.3). Here they concluded that, for walking and stairs climbing, it is advantageous to:

- Place the center of the acetabulum as far medially, inferiorly and anteriorly as is anatomically possible.

- To use a short prosthetic neck

- To use a femoral shaft-prosthetic neck angle of 130 degrees.

The recommendations for the position of the cup can be a good guideline for surgeons, although the angle of the cup is also very important, because it is the most common cause for dislocation according to emeritus orthopedic surgeon Evert van Langelaan. Moreover, patient anatomy varies over a certain range [21]. Therefore, the optimal angle of the neck is not 130 degrees for every person and the anatomical position and angle of the cup is not the same for everyone. Thus, it is important to perform measurements of anatomical variation and soft tissue tension measurements for each individual separately.

Approach

Most surgeons take a posterior or lateral approach to the hip joint [22]. The operative approach determines which tissues are cut.

During the posterior approach, the surgeon incises the fascia latae overlying the gluteus maximus and splits the muscle down to the short external rotators. After identification of the piriformis, the short external rotators, piriformis and posterior joint capsule are then cut [22]. The muscles are sewed back together at the end of the surgery.

However, there are also surgeons who like to take an anterior approach. No muscles are cut when using this approach. Only the anterior joint capsule is cut [22]. Thus, some surgeons prefer to use the anterior approach, because there is less muscle cutting involved. This results in a faster, less painful recovery. Therefore, it is said to be more minimally invasive.

On the other hand, the anterior approach is more challenging for the surgeon, because he has a limited view of the hip joint. According to Chechik et al. [23], 2013, surgeons were split between the posterior approach (45%) and the direct lateral approach (42%) followed by the anterior approach (10%) or other (3%). North American surgeons favored the posterior approach more often than Europeans (69% compared to 36%, $p < 0.0001$) and surgeons from other countries (69% compared to 45%, $p = 0.01$).

Different hip forces are expected when using the posterior, direct lateral or anterior approach. Therefore, it is important during clinical trials to separate groups not only by disease, age and number of surgeries, but also by the approach taken to the hip joint.

1.5. The procedure step by step

1. A preoperative CT scan of the frontal plane is made.

2. A surgical plan is made. The surgeon considers the bone quality of the patient, the approach to the hip that will be taken (anterior, lateral or posterior), the type of implant used (metal on metal, plastic on metal, ceramic on metal, ceramic on plastic or ceramic on ceramic) and the fixation method (cemented or uncemented).

3. The patient is positioned and anesthesia is applied.

4. The hip joint is exposed by cutting skin, ligaments and muscles.

5. The surgeon dislocates the hip.

6. The head and neck of the femur are cut off.

7. Then the acetabulum is reamed out with a drill like machine to make space for the placement of the metal cup. The anatomical hip center of rotation is restored if possible (Fig 5).

8. The metal cup is placed either as a press fit, or with cement.

9. Then the plastic inner shell, called a liner, is snapped into the metal cup.

10. Next, the femur is hollowed out by hammering in consecutively larger broaches in the femoral canal.

11. A 'test stem' is put in place.

12. On top of this a 'test neck' is placed. A 'test head' is placed on the 'test neck'. The size of the initial test neck and head are determined by putting templates on top of the CT scan. The aim here is to restore the original leg length and hip offset (Fig. 5).

13. The surgeon rejoins the hip joint with test components.

14. Now the surgeon can do a number of measurements and tests to evaluate if he has chosen the right neck and head for the patient. To check the symmetry of the legs, he can apply the techniques described in section 1.7. To check the stability of the hip, he can apply the techniques described in section 1.8.

15. The surgeon can now change the soft tissue tension in three different ways: 1 He can change the neck length of the implant by using a head with different hole depth (Fig. 9). 2 He can lateralise the femur by choosing a neck with higher offset (Fig. 10) or 3 by choosing a neck with smaller neck-shaft angle (Fig. 10). The hip must be dislocated to replace the trial components. No numbers were found in literature on how many times the trial components are switched during surgery. According to orthopaedic surgeon Bryan Blaauw, the neck angle is usually not changed inter-operatively, although there are exceptions. The trial head is switched approximately two times per surgery. The head is changed to compensate for inaccuracies that occur when cutting the femoral neck or when the stem or cup is placed too deep or superficial inside the bone. This influences the soft tissue tension and thus the stability.

16. When the surgeon has fine-tuned the hip with this trial and error technique and is satisfied with the stability of the hip and symmetry of the legs, he dislocates the hip, removes the test components and places the final implant. Remember that the stability of the hip is the most important outcome. In the final implant neck and stem consist out of one piece.

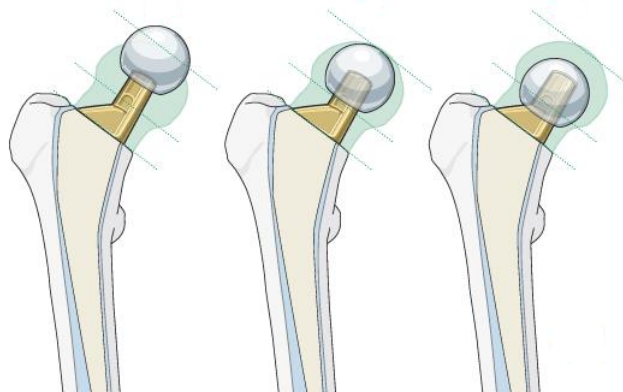17. The surgeon rejoins the hip joint and closes the wound.

Figure 9: The depth of the hole in the head determines the neck length. Heads are also available in different diameters *Image credit: www2.aofoundation.org*

CORAIL Standard   CORAIL High Offset   CORAIL Coxa Vara
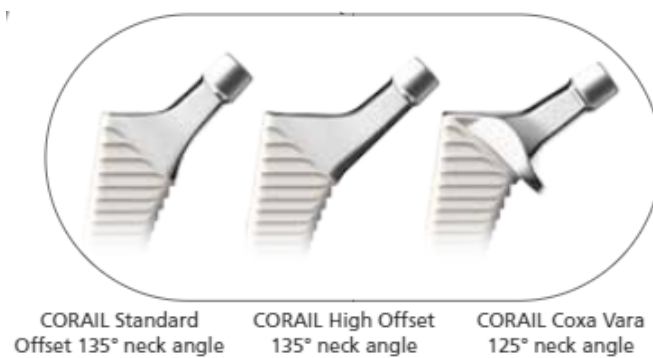Offset 135° neck angle   135° neck angle   125° neck angle

Figure 10: The Corail hip implants we are working with can be chosen in three different neck shapes. The neck can be chosen to have a standard or high offset or a slight varus angle. *Source: Corail hip system Product rationale and surgical technique.*

1.6. Intraoperative leg symmetry measurement

The surgeon also can choose to use radiographs and/or fixed point measurements to check the leg length equality *during* the surgery. A shortcoming of these techniques is that the soft tissue tension can not be assessed this way. They are briefly described below.

Radiography

One way is direct estimation on the operating room table with a radiograph as shown in (Fig. 11). Kuroda et al. [24], 2014, used these kind of radiographs to correct:

1. Component alignment within 2 degrees.

2. Leg length discrepancy (LLD) within within 3 mm.

3. Femoral offset within 3 mm.

4. Adequate canal fill under 2 mm.

There is a downside to this technique, because a slight rotation of one of the legs or pelvis will influence the measurements [25]. Kuroda et al. [24], 2014, states they *"...made an effort to maintain the leg in a neutral position..."*, which does not sound convincing, because it is not clear how this was done. However, Kuroda et al. did estimated the bilateral symmetry of the obturator foramen and the thickness of the lesser trochanter, to check for pelvic and femoral rotation respectively, in order to minimize the rotation errors.

In Kuroda et al. they aimed to recreate the physiological offset, because soft tissue tension around the hip can gradually loosen with a postoperative course. However, many papers argue that the surgeon must check the soft tissue tension during surgery. Otherwise problems like instability and dislocation [1], [3], [2], [26], pain [1], [3], [2], limping [1], [3], [2], [26] or a 'functional long leg' [3] can occur. A 'functional long leg' could last for many months or even become permanent [27]. Some studies even argue that stability due to an adequate soft tissue tension should *always* take precedence over leg length equality, because instability can cause dislocation, which creates more discomfort than leg length inequality [26], [28]. Therefore, aiming for the physiological offset is not always the best approach.

Fixed point references

Many authors describe methods in which the distance between certain points on the pelvis and/or femur are measured, to obtain the limb length discrepancy.

They often use a pin and a mark on the greater trochanter to measure the offset intraoperatively [1]. Two similar examples are: using tranosseous pins with a calibrated caliper [14] or using a Steinman pin and an adjustable caliper [29]. However, it has been shown that using these points can cause significant errors in limb length when there are small errors in the position of the femur in abduction, flexion or rotation [15].

Alternatively, the surgeon can select the points of reference on the femur to negate the variations in measurements caused by errors in the position of the limb [15].

Muscles can also be used to determine the leg length. In the so-called "Abductor shuck method" [14] the abductor muscle is tensioned by a tag suture onto the greater trochanter. The gap or overlap between the tenotomized ends of the abductor is then measured as the amount of limb lengthening.

Finally, the leg length discrepancy can also be determined with "Patella electrocardiogram leads" [14]. Here the operative limb is directly compared to the nonoperative limb by placement of a standard cardiac EKG lead on each patella. Therefore, this method does not require a calculation based on preoperative LLD.
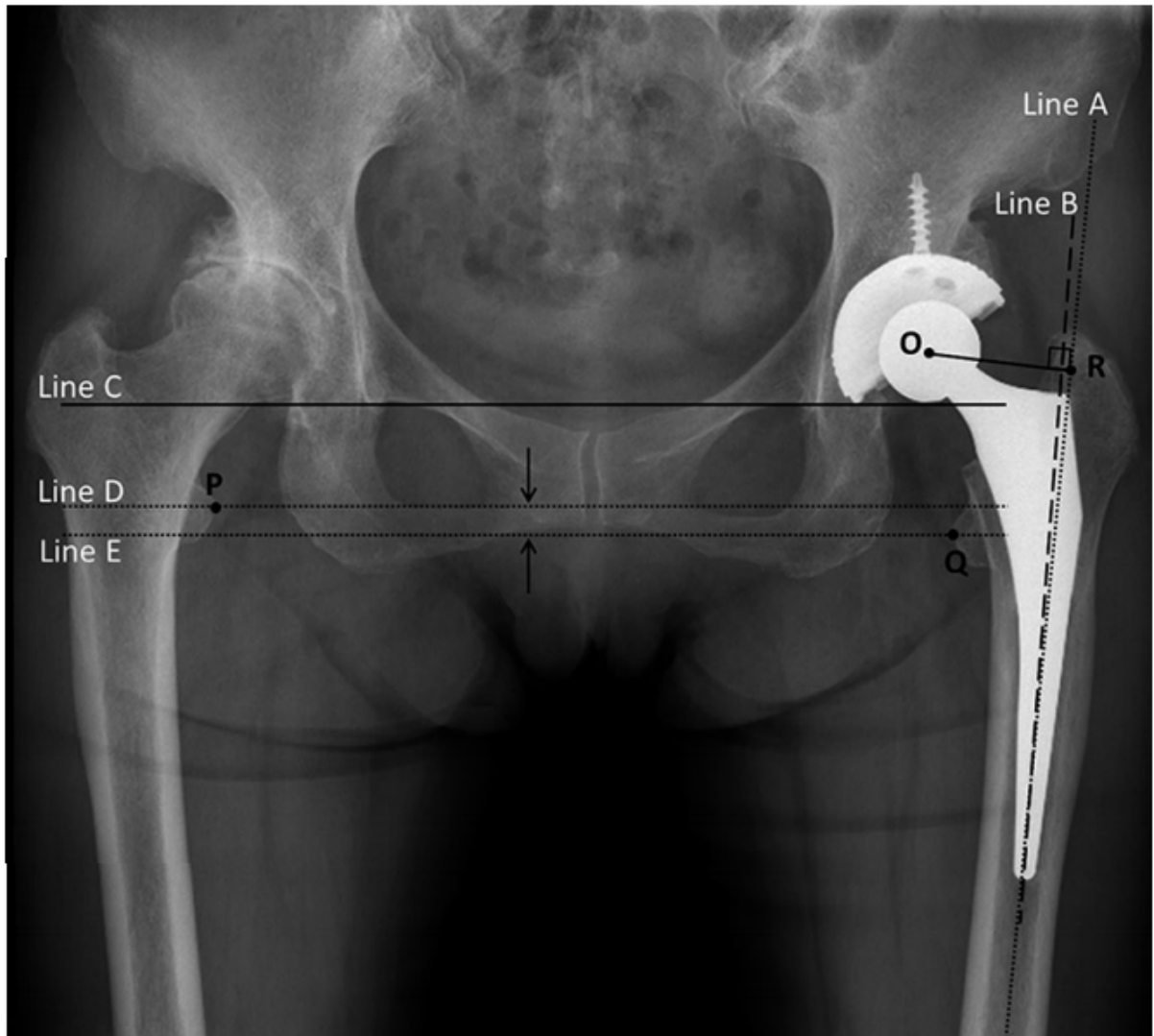
Figure 11: Interoperative radiograph. Line A is the anatomic axis of the femur. Line B is the axis of the femoral component. Line C is the transteardrop line. Line D and line E are parallel to line C through the apex of the lesser trochanter (point P, Q). The angle between line A and line B was measured to evaluate the component alignment. A perpendicular line between line D and line E is the leg length distance (LLD) (which is used to evaluate the leg length). Point O is the center of the inner head of the femoral component. Femoral offset was measured with a perpendicular line from point O to the anatomic axis of the femur line A. [24].

1.7. Intraoperative soft tissue tension assessment

There are a number of different methods that surgeons currently use to assess the soft tissue tension intraoperatively. One method is the so-called 'shuck test'. All other methods involve range of motion tests, which can be combined with palpation of the muscles. The problem is that all of these tests are subjective.

Shuck test

The shuck test allows for a subjective determination of the overall soft-tissue tension around the hip joint. In this test, the leg is put in the 'neutral' (anatomical) position. Traction in the inferior direction is applied distally on the lower limb by an assistant (Fig. 12). The amount of movement of the prosthesis head with respect to the rim of the cup observed by the surgeon, is then used as an indicator of the soft tissue laxity [29], [30]. There is no consensus in literature for the rule of thumb that should be used in this test. According to the book 'Mastering Orthopedic Techniques Total Hip Arthroplasty' [31], 2011, the rule is that no more than half of femoral head should disengage from the liner. According to the book: 'Operative Techniques in Orthopaedic Surgery' [32], 2012, the rule is to have 1 or 2 mm of shuck. Furthermore, this test should not be used in combination with spinal anesthesia, because spinal anesthesia relaxes the muscles beyond their normal tension [30]. By testing various combinations of neck offsets, neck lengths and possibly even lateralized (thicker) cup liners, the surgeon can try which trial components provide optimal tension of the soft-tissue structures [28].

Range of motion tests

If the hip tension is too tight, the range of motion (ROM) will be limited. This especially applies to extension combined with external rotation and flexion combined with internal rotation. Charles et al. [28], 2004, shows two stability tests: one in extension with simultaneous maximal external rotation (Fig. 13) and one in 90 degrees of flexion of the hip and knee with simultaneous maximal internal rotation (Fig. 14).

In a surgical video [33] where they took the lateral approach to the hip joint, the following two ROM tests were observed:

1 The leg is moved in external rotation and extension. The surgeon puts a finger in the hip joint to check if it dislocates.

2 The leg is put in a seated position. Then the hip is rotated internally, which means that the leg is rolled upwards. The hip should not dislocate during this maneuver.

Palpation

Longjohn et al. [3], 1998 describes palpation of the muscles to feel their 'tightness', while moving the leg in certain ways. They suggest that if the surgeon is certain that the tightness is not created by leg lengthening, it is because of the soft tissues. This tightness can be released by cutting these tissues with an electrocautery tool. For example, if the hip does not extend past 10 degrees extension, the iliopsoas tendon will likely be overly tight and can be felt like a 'banjo string'. It must then be recessed or completely released.

Figure 12: The shuck test with the patient in the lateral position. The assistant in the bottom is pulling the leg while the surgeon observes the movement of the head [33].

Figure 13: Full extension and maximal external rotation are tested to assess the stability of the joint [28].

Figure 14: 90 degrees flexion in both the hip and the knee are combined with maximum internal rotation to test the stability of the joint [28].

1.8. Uncontrolled variables influencing soft tissue tension

As mentioned in the intro, the tendons, muscles and ligaments have the biggest contribution to the soft tissue tension. Apart from the implant there are other factors that can influence this tension during the intraoperative measurements. These factors can be split into three categories: patient, surgeon and anesthetics. These will be discussed next.

Patient

The book 'Mastering Orthopedic Techniques Total Hip Arthroplasty' [31], 2012, states that *"soft tissue tension tests are subjective and depend, among other factors, on the muscularity and habitus of the patient"*. So, it seems clear that there is no general soft tissue tension value that is optimal for everyone, because it depends on a variety of interpersonal and intrapersonal factors.

Interpersonal factors

Interpersonal factors are anatomical variations, such as leg length, segment masses and lever arms of muscles like the gluteal muscles [34]. However, it might be possible to define a ROM test, force test or static test that will always result in a joint force in a certain range or pattern. Perhaps one could define a margin or 'safe zone' that recommends a safe amount of muscular tension, that can be checked intraoperatively by such a test. Some papers already take the interpersonal differences a little bit into account by expressing the joint forces in percent body weight of the patient, instead of in Newtons [34].

Intrapersonal factors

Intrapersonal factors are the health and condition of the patient, which can change over time. It is very important that the patient does physio-therapeutic exercises after THA, to prevent instability [34].

Surgeon

The surgeon is a human being and is therefore not 100% accurate. Surgical inaccuracy causes variation in the position of the cup and implant. According to emeritus orthopedic surgeon Evert van Langelaan, the error in position and angle of the cup is the most common cause for dislocation. A cause for this could be that it is very difficult to orientate and fixate the pelvis to the table during surgery.

Furthermore, the surgeon will always cut some amount of soft tissues during the surgery, depending on the approach that he chooses. The surgeon will also apply some force to distract the joint. These actions will influence the soft tissue tension.

Another issue is that the surgeon will influence the measurements of the intraoperative hip forces when he touches the leg.

Anesthesia

Moreover, there is the effect of anesthesia and neuromuscular blocking agents. According to Sathappan et al. [30], 2008, the anesthesia type effects the outcome of the limb length discrepancy. Regional anesthesia, in the spine, was compared to general anesthesia in THA. Regional anesthesia causes significant motor blockade, which relaxes the muscles much more than general anesthesia. This results in a wrong interpretation of intraoperative soft tissue tension tests, like for example, the shuck and ROM tests. This can lead to increased leg length, because the surgeon would underestimate the soft tissue tension and then overcompensate it by choosing larger dimensions for the prosthesis. Therefore, regional anesthesia should never be combined with soft tissue tension tests. Neuromuscular blocking agents also cause relaxation of the skeletal muscles. The applied dose is determined by the anesthetist and is patient specific, according to MD Blaauw.

1.9. Axial force

Appendix B shows the results of a state of the art system called 'Hip III', that was used to measure hip forces in living patients [35]. This system used strain gauges to measure the forces. It has to be noted that the 'Hip III' system was never used to measure forces intra-operatively, but only in patients performing active motions after surgery. Reasons for this might be that the system was not suitable for repeated sterilization and that it is not modular. Therefore, it cannot be taken out once inserted.

It can be seen that the hip force is directed almost completely in the axial direction in the case of isometric contraction while lying in the supine position (Appendix B, Fig.B1-B6). The forces are expressed in percent bodyweight to compensate for naturally higher hip forces in larger patients. Table 3 shows the average hip force, when the hip was *not* being actively contracted, was 34% BW (Appendix B, average of patients 1-6), with a standard deviation of 8% BW [35]. This corresponds with an average hip force of 284 Newton, with a standard deviation of 78 Newton. This already gives an indication of the force that is required for a stable hip joint. Forces measured during surgery are expected to be slightly lower due to the effect of neuromuscular blocking agents that are used during the anesthesia.

Other data [35] (not included in this report) shows that the resultant force often changes direction during active motions of the hip. The active motions performed were: flexion-extension and abduction-adduction. Internal-external rotation was not performed. Furthermore, static and dynamic external loads were applied. These tests with active motions and external loads resulted in similar patterns in all six patients. It might be possible to find similar, repeatable, perhaps symmetrical, patterns when measuring only the axial force in combination with a standardized shuck or ROM test. Research should show if these patterns provide enough information to make a valid prediction about the stability of the hip.

Hip III Patient	BW (kg)	Fmin (%BW)	Fmin (kg)	Fmin (N)
# 1	75.0	18	13.5	135
# 2	88.4	33	29.2	292
# 3	81.2	34	27.6	276
# 4	86.8	40	34.7	347
# 5	78.5	39	30.6	306
# 6	90.8	38	34.5	345
Average	83.5	34	28.4	284
Stdev	6.2	8	7.8	78

Table 3: Hip force measured with the Hip III implant in living patients 1-6, during relaxed lying in the supine position [35]. Fmin is the lowest hip force measured during relaxed lying in these living patients, which already gives an indication of the force that is required for a stable hip joint. Forces measured during surgery are expected to be slightly lower due to the effect of neuromuscular blocking agents.

1.10. Literature on force sensors

The first step was to find suitable force sensors for medical applications from literature. Tiwana et al. [36], 2012, published Table 4, which gives a clear overview of different pressure sensing techniques that have been used in medical applications. However, it is not a complete overview, since force sensors based on the Hall effect are not included.

Strain gauges

The oldest publication found was from as early as 1966 from the University of Göteborg, Sweden. This publication by Rydell et al. [37], 1966, uses strain gauges on the neck of the prosthesis in two locations: one in the center of rotation and one in the distal part of the neck. The neck had to be rather long to obtain accurate results, because they had the sensor technology from 50 years ago. More recent studies have been done in Germany and Japan.

The majority of papers published on force measurements in hip joints were made by the same institutes. The biggest contributor seems to be the Julius Wolff Institute of the Charité in Berlin. They made three instrumented hip implants named the Hip I, Hip II and Hip III implant. All of these use strain gauges [38] and a telemetry system [39]. These were used in many publications. Among these are the publications of: Bergmann et al. [40], [41], [42], [43], [44], [45], [46], [47], [48], [49], [50], Damm et al. [51], [52], [53], Schwachmeyer et al. [34], a Phd thesis and paper by Stansfield et al. [20], Heller et al. [17] and Graichen et al. [54]. They investigated the hip forces during activities of daily living. These are: walking, climbing stairs up and down, two- and one-legged stance, standing up and sitting down, knee bending (squats), slow jogging (7km/h on treadmill) and cycling (90 W, 40 rpm). Two additional activities they studied were 'stumbeling' and walking with crotches. They even studied hip joint forces in sheep [55] and dogs [56]. This institute shares a lot of its data online, like the data in appendix B. It has to be noted that the forces measured during activities are probably much larger than the forces in the hip during surgery. Still, using strain gauges seems to be a reliable method to measure joint forces. However, these instrumented hip implants were permanently implanted and did not require multiple sterilization cycles like a reusable tool does.

The two studies by Otake et al. [57] & [58], published in 2006 and 2007 respectively, used 'pressure sensors', which were likewise made of foil strain gauges. These sensors were integrated in the femoral head. Unfortunately, these papers show no numerical results of the intraoperative measurements.

Capacitive

A rare exception to using strain gauges was found in Müller et al. [59], 2004. Here they use a capacitive sensor array to measure the pressure distribution in artificial joints. A capacitive sensor consists of two conductive plates with a dielectric material in between. In the found study the sensor array was placed between the ball and the cup. Tests were only performed in vitro.

Piezoresistive

Piezoresistive sensors use a pressure sensitive element which changes its resistance when force is applied. They are easy to manufacture and integrate, because they usually require less electronics [36]. The only studies that performed *intraoperative* hip force measurements are from Japan. The poster by Higa et al. [60], 2009, reports the use of 'pressure sensors' (FlexiForce A201-100, Tekscan, Inc., Boston, MA), which is a flexible piezoresistive force sensor. Here the sensors were put inside the head of the prosthesis, but not properly fixated, which could explain the large spread in their measurement outcomes. Another example of a three-axial piezoresistive force sensor designed for prostheses can be found in Beccai et al. [61], 2005.

Piezoelectric

Piezoelectric materials generate a voltage when their crystal lattice is deformed. Their sensitivity depends on their lattice structure. This allows them to distinguish between transverse, longitudinal and shear forces [36]. However, they are limited to measuring dynamic forces, because their large internal resistance is not suitable for measuring static forces [36].

Inductive

Inductive sensors consist of a primary coil that creates a magnetic field. This field is sensed by a secondary coil. One can modulate the mutual inductance between the coils by changing the length of an iron core (as in the case of a linear variable differential transformer). This modulates the amplitude and phase of the voltage measured in the secondary coil [36].

Optoelectric

Optoelectric sensors use a light source, transduction medium and photodetector. The photodetector is usually a camera or a photodiode. The force applied to the transduction medium will modulate either the transmission, or the reflectance intensity, or the spectrum of the light from the source [36].

Transduction technique	Modulated parameter	Advantages	Disadvantages
Capacitive	Change in capacitance	Excellent sensitivity Good spatial resolution Large dynamic range	Stray capacitance Noise susceptible Complexity of measurement electronics
Piezoresistive	Changed in resistance	High spatial resolution High scanning rate in mesh Structured sensors	Lower repeatability Hysteresis Higher power consumption
Piezoelectric	Strain (stress) polarization	High frequency response High sensitivity High dynamic range	Poor spatial resolution Dynamic sensing only
Inductive LVDT	Change in magnetic coupling	Linear output Uni-directional measurement High dynamic range	Moving parts Low spatial resolution Bulky Poor reliability More suitable for force/torque measurement applications
Optoelectric	Light intensity/spectrum change	Good sensing range Good reliability High repeatability High spatial resolution Immunity from EMI	Bulky in size Non-conformable
Strain gauges	Change in resistance	Sensing range Sensitivity Low cost Established product	Calibration Susceptible to temperature changes Susceptible to humidity Design complexity EMI induced errors Non-linearity Hysteresis
Multi-component sensors	Coupling of multiple intrinsic parameters	Ability to overcome certain limitations via combination of intrinsic parameters	Discrete assembly Higher assembly costs

Table 4: Advantages and disadvantage of different pressure sensing techniques. Tiwana et al. [36], 2012.

1.11. Requirements

What technical requirements are needed in order to achieve our goal? In this case important criteria were identified as:

- Biocompatibility *(The device must not have toxic or injurious effects.)*

- Waterproof *(The device must be waterproof, because there will be contact with body fluids.)*

- Sterilizable/disposable *(The force-sensing implant must either be sterilized with sensors or the sensor must be disposed after surgery. If a slide-in sensor is used, it can be disposed after surgery. To reduce costs and time, it is strongly preferred to use the standard sterilization method, which is by autoclave.)*

- Appropriate sizing *(The dimensions of the standard Corail necks that are available to us are: length 38.5 mm, width 10 mm and depth 12 mm. The redesigned neck must fit into the ball and stem parts. Note that different ball sizes can be used to vary the length of the implant.)*

- Sensing range *(On 24-11-16 we performed a test on a cadaver in the Erasmus MC in Rotterdam. The force required to dislocate the hip of the cadaver was roughly 100N (10 kg). According to table 3 the average hip force of six living patients, measured during relaxed lying in the supine position after surgery, is 284N with a standard deviation of 78N. We aim to create a system that can be used on living patients, so we would like to aim at a sensing range of: 0-400N.)*

- Maximum deformation *(The maximum deformation of the neck should not be more than 1 mm under a load of 40 kg, because the dimensions of the test implant should be representative for the final implant. This was decided in consultation with MD Bryan Blaauw.)*

- Safety and reliability *(The expected hip force in a living person is expected to be in the range of 0-400 Newtons. Using a safety factor of 2 the instrumented implant should be able to survive forces in the range of 0-800N without mechanical failure.)*

- Resolution *(The smallest step size should be less than 5N.)*

- Accuracy *(Bergmann et al. [42] classified instrumented implants with a maximum error below 2% as "very accurate," between 2-4% as "accurate," between 4-10% as "inaccurate," and above 10% as "very inaccurate.")*

- Precision *(Results should be repeatable within a range of 10N.)*

- Frequency response *(At least 32 Hz is advised for measuring normal and shear forces [36].)*

- Affordable *(This will be determined in consultation with the supervisors.)*

- Quick insertion *(It should be possible to insert the device in under a minute.)*

- Easy to use *(The device should have an intuitive interface.)*

<div style="text-align: right; font-size: 4em;">2</div>

Design

The choice of the sensor is one of the most crucial step in making the design. There are many sensors to choose from, but in this case the requirements are quite extreme. Among others it was strongly desired to make a design that can be sterilized by the standard autoclave procedure. This procedure uses hot steam at an elevated temperature and pressure. We will see that this greatly limits the sensor options. The process from exploring the varying sensors until the final design will be discussed in this chapter.

2.1. Sensor selection

Sterilization test

At first, it seemed obvious to use strain gauges, as they have already been successfully used in past publications of hip force measurement. Furthermore, they have a resolution so small, that they can measure the strain of the Titanium implant itself, without any need for a spring element to increase the strain. However, the combination of heat and moisture is very damaging to the glue with which the strain gauges are attached. According to the datasheets of Loctite, the glue for strain gauges in medical applications can only be sterilized by autoclave once. There is one exception: a study by Trejos et al. [62], 2014, showed that Loctite M-3981 adhesive in combination with Loctite M-11FL coating provides sufficient protection to allow the strain gauges to survive at least 5 sterilization cycles with excellent performance, even though the coating is only recommended to be used for 3 cycles. They said additional cycles were not conducted due to time constraints. Unfortunately, Loctite M-3981 adhesive is not sold in Europe. Therefore, it was decided to look into more unconventional force sensors as well. Thus, a number of suitable and affordable force sensors that could potentially survive the standard autoclave sterilization procedure were selected, based on their respective data sheets. The selected sensors were: the A1302 Hall sensor (Allegro), the OPR5005 opto-reflective sensor (TT Electronics), the A201 FlexiForce piezoresistive force sensor (Tekscan) and the S8-100N capacitive force sensor (SingleTact). Their functionality was tested with Arduino as shown in (Fig. 15).

Subsequently, these sensors were put to the test in the autoclave at the Misit lab, in which they were sterilized with the standard program, which uses hot steam at 134 degree Celsius, at a pressure of 2 bar for 20 minutes. The result was that the Hall sensor and the opto-reflective sensor kept functioning after sterilization. The piezoresistive and capacitive sensor did not (Fig. 16). A reason for this could be that the Hall and opto-reflective sensor have an epoxy packaging and the other two sensors packaging consisted of glued layers. Therefore, the Hall sensor and opto-reflective sensor have an advantage over the other options.
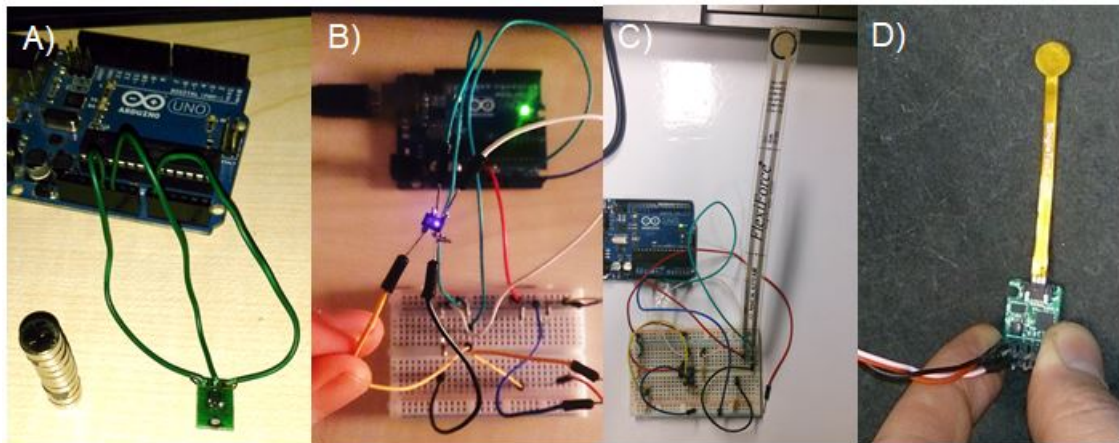
Figure 15: A) A1301 Hall sensor (Allegro) B) OPR5005 Opto-reflective sensor (TT Electronics) C) A201 FlexiForce piezoresistive force sensor (Tekscan) and D) S8-100N Capacitive force sensor (SingleTact).
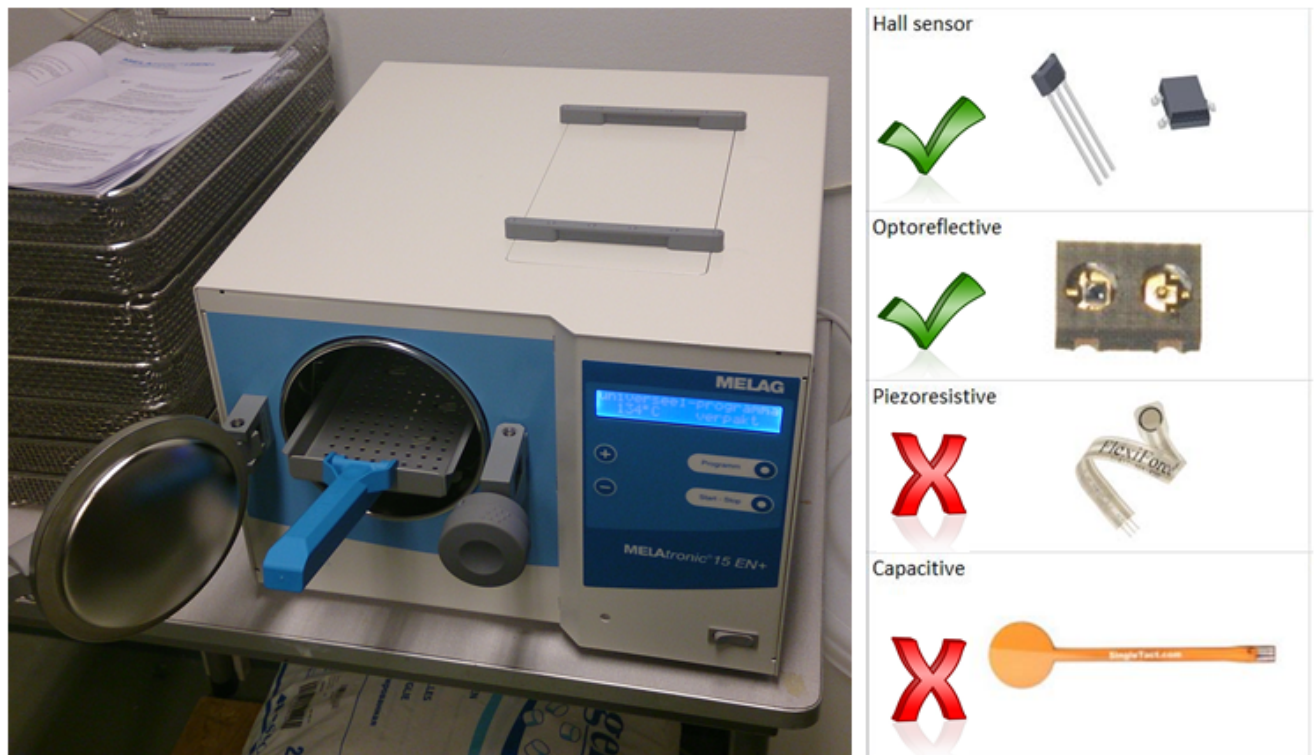
Figure 16: Autoclave at the Misit lab. The standard program was used, which uses hot steam at 134 degree Celsius, at a pressure of 2 bar for 20 minutes.

Multiple criteria selection

However, there are more arguments to consider than just the sterilization procedure. To make a well informed choice, an overview was created of all the pros and cons of each sensor (Fig. 17). Their respective working principles are also explained, because it is important to understand these fundamental principles as well, instead of just applying them blindly.

In conclusion, the Hall sensors were considered to have the best ratio of pros versus cons. They have three striking advantages. Firstly, they are can be sterilized by the standard autoclave procedure. Secondly, they are very easy to use because of their (ratiometric) linearity without the need for an amplifier. Finally, they are robust because of their completely sealed epoxy packaging. For instance, the optic sensor is much more vulnerable to being damaged or getting dirty, because the LED is exposed. Hall sensors are very cheap as well (€3 apiece) and they are said to have a good repeatability [63]. Their output-voltage levels are dependent on magnetic flux density at the most sensitive area of the device. Thus, the resolution in terms of distance measurement is determined by the change of magnetic flux density over a certain distance.

The biggest drawback is that these sensors cannot be directly applied to the titanium implant, because the titanium implant deforms not more than one or two micrometer under a load of 30 kilograms. Thus, it is very difficult to create the desired magnetic field over such a short distance. Therefore, it is required to build in a spring element that allows for bigger deformations. A spring element that could deform at least 0.5 mm was deemed to be sufficient to perform the measurement. After consultation with medical doctor Blaauw, we came to the conclusion that a deformation of less than 1 mm is still acceptable within the clinical perspective of maintaining the dimensions of the original implant.

Another drawback is that Hall sensors are sensitive to electromagnetic interference (EMI). However, thanks to increased EMI awareness and protection in modern hospitals, we can now use our mobile phones around medical equipment. Therefore, the Hall sensors are expected to remain undisturbed as well.
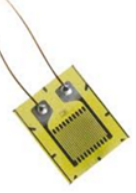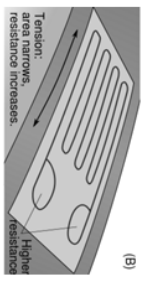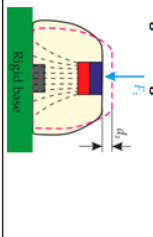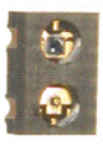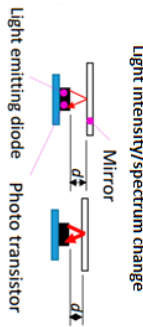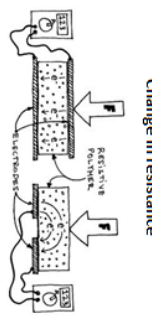
Sensor	Modulated parameter	Autoclave	Price	Resolution	Repeatability	Needs spring	Ease of use	Remarks
Strain gauge	Change in resistance	Once	€20,- a piece + €40,- glue	Good	Good	No	Difficult	Established product, Sensing range, Best resolution, Directly applied to Ti
Hall sensor	Change in magnetic field	Many times	€3,- a piece	Good (closeby)	Good	Yes	Easy	Influenced by EMI, Requires spring element, Robust, Linear output possible
Optoreflective	Light intensity/spectrum change	Many times	€3,- a piece	Good	Average	Yes	Difficult	Vision can be obscured, Ambient light interferes, Not very robust, Non linear, Requires spring element
Piezoresistive	Change in resistance	No	€16,- a piece	Bad	Bad	No	Easy	Not sterilizable by autoclave, Low repeatability, Bad resolution
Capacitive	Change in capacitance	No	€20,- a piece + €60,- electronics	Good	Good	No	Easy	Not sterilizable by autoclave, Linear calibration software, Minimal Detectable Force 20g

Figure 17: Overview of the working principle of each sensor and a comparison of their strengths and weaknesses. The Hall sensor was selected as the best option.

2.2. Linear guidance design

It is technically difficult to measure forces in all three orthogonal directions. Furthermore, measuring the force in the axial direction could already provide useful information and thus it was decided to measure the force only in this direction. In order to physically decouple the forces, three different possibilities for a linear guidance were identified: to use a sliding bearing, rolling bearing or parallel flexure. A rolling bearing small enough to fit in the implant is difficult to manufacture, so this option was disregarded. A benefit of the parallel flexure, is that it can function as a spring as well. Concept designs of a parallel flexure guidance and sliding bearing were made in SolidWorks (Fig. 18). This was done in order to get a feeling for the physical workspace of the design and explore the feasibility of our options. After experimenting with the geometry in Solidworks and Comsol, it appeared that the stresses in the parallel flexure exceeded the yield strength long before the desired deformation of 0.5 mm was reached. Therefore, it was decided to use the sliding bearing.
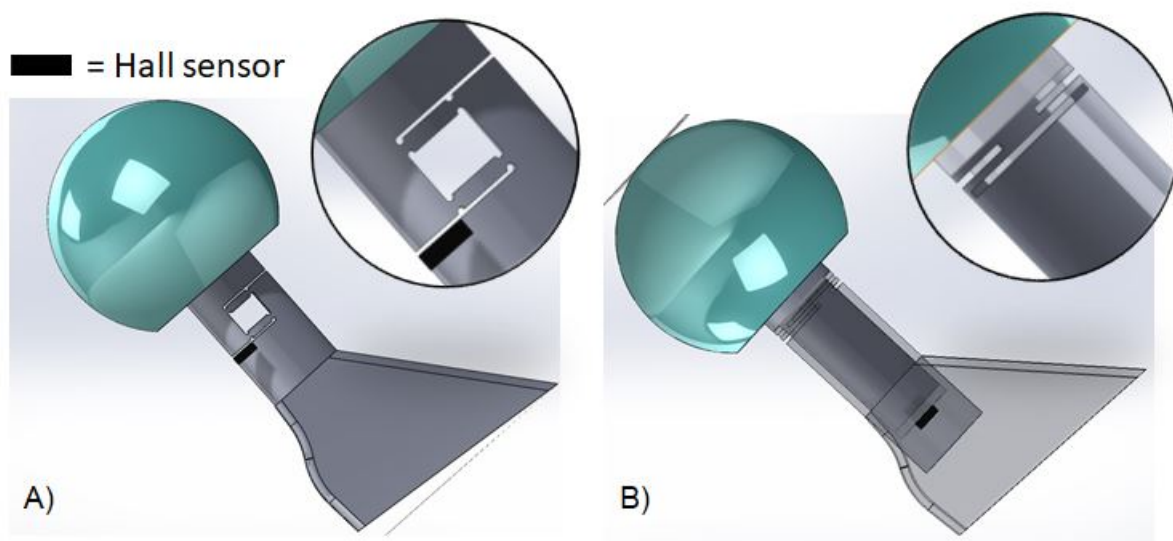
Figure 18: A) Design that uses a parallel flexure as a linear guidance and spring element at the same time B) Design that uses a sliding bearing in combination with a spring element. Designs were made in SolidWorks by the author.

2.3. Spring element design

Spring Requirements

The requirements read that the deformation should be sufficiently large, so the (Hall) sensor can detect it. On one hand, the minimal deformation of the neck should be at least 0.5mm. On the other hand, the maximum deformation of the neck should be less than 1mm under the maximum load of 40 kg, because the test implant should be representative for the final implant. This was decided in consultation with MD Bryan Blaauw. A spring element had to be added to obtain the desired deformation.

Furthermore, the available space for the spring element is limited. It has to fit inside a cylinder with a diameter of roughly 9mm. Therefore, the outer diameter of the spring must not be bigger than 8mm and its height should be as small as possible, because a larger height will leave less space for the linear guidance.

There are two parameters that a designer of a spring element can influence: the shape of the spring and the material it is made of. Both will be discussed next.

Spring shapes overview

Seven different spring shapes were investigated (Fig. 19). These basic spring elements can be put in series by stacking multiple elements on top of each other as shown in the second column. For the first four shapes the stresses and strains were calculated analytically. The analytical equation were taken from the 'Werktuigbouw formuleboekje' [64] (www.tribology-abc.com). For the other three shapes values from the Century Spring Corporation catalog on precision disc springs [65] were used. This way a quick comparison of the feasibility of these spring elements could be made. Given the dimensional constraints for the spring element, a maximum load of 400N and the desired deflection of at least 0.5mm, the minimal required height H force for each spring was estimated. The calculations will be explained in this chapter. Furthermore, some shapes, like the slotted disc and curved wave spring are more difficult to manufacture than the other shapes. This was also taken into consideration. Finally, the possible hysteresis of each spring has to be taken into account. The rubber spring will suffer from elastic hysteresis. The helical spring rotates under compression. This creates friction on the sliding rotating surface, which leads to hysteresis. The disc shaped springs expand on the outside circle and shrink on the inside circle under compression. This also creates sliding surfaces and thus hysteresis.

Next, the material choices and performed calculations for figure 19 will be explained into more detail, followed by a conclusion.
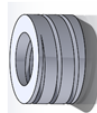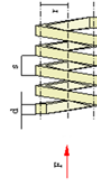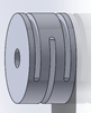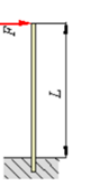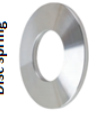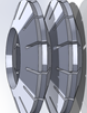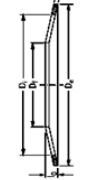
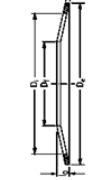| Basic element	Series	Material	Height needed	Max force	Manufacturing	Hysteresis	Analytical solution	Analytical equations
Compressed solid		NBR	1mm	Over 400 N	Easy	Yes (Elastic)	Yes	$A = \pi/4 \cdot (D_{out}^2 - D_{in}^2)$ $\sigma = \frac{F}{A}$
Helical		Ti-6Al-4V	5mm (2 coils)	± 400 N	Average	Yes (Sliding Rotation)	Yes	$\delta = \frac{44.9 \cdot n \cdot r^3 \cdot F}{d^4 \cdot G}$ $\tau = \frac{4.8 \cdot r \cdot F}{d^3}$ $\tau_{max} = \frac{\sigma_{yield}}{\sqrt{3}}$
Leaf spring		Ti-6Al-4V	4mm (2 flexures)	±130 N	Easy	No	Yes	$I = \frac{b \cdot h^3}{12}$ $\delta = \frac{F \cdot L^3}{3 \cdot E \cdot I} = \frac{4 \cdot F \cdot L^3}{E \cdot b \cdot h^3}$ $\sigma = \frac{F \cdot L \cdot h/2}{I} = \frac{6 \cdot F \cdot L}{b \cdot h^2}$
Disc spring		Ti-6Al-4V	2mm (stack of 2)	±400 N	Average	Yes (Sliding Surface)	Yes	$\delta = \frac{0.65 \cdot F \cdot r_{out}^2}{E \cdot t^3}$ $\sigma = \frac{F \cdot (1 - 2/3 \cdot r_{in}/r_{out})}{t^2}$
Disc slotted outside		SS*	1.5mm (stack of 2)	± 20 N	Difficult	Yes (Sliding Surface)	No	* Catalog
Disc slotted inside		SS*	1.5mm (stack of 2)	± 20 N	Difficult	Yes (Sliding Surface)	No	* Catalog
Curved wave Spring		SS*	4mm (stack of 2)	± 170 N	Difficult	No	No	* Catalog

Figure 19: Overview of seven different spring elements. Springs can be put in series to increase displacement. The diameter of all springs was limited to 8mm. The height needed to reach a displacement of 0.5mm and maximum loads were calculated analytically if possible. In the other cases values were obtained from the Century Spring Corp. precision disc spring catalog [65]. For the first prototype, the rubber ring was chosen as the best option. Abbreviations: NBR = Nitrile butadiene rubber, SS = Stainless steel

Materials

In this case we must use a biocompatible material, so we could use either a biocompatible elastomer, polymer, or metal as spring material. The material selection database CES Edupack [66] was used to find suitable materials.

Silicone rubber

The 'compressed solid' shape spring requires a very low E modulus. Therefore, silicone rubbers were investigated. Using a simple rubber element is advantageous, because it is small, can take high forces and is easy to obtain and use. However, there are three drawbacks of using rubber. The first one is that it cannot be sterilized with hot steam, due to the high temperature. Therefore, it is not reusable and the component must be replaced with a new one after each session. Thus, the manufacturing tolerances of the rings must be top notch to ensure repeatability when the spring is replaced, or else the device must be re-calibrated every time a new rubber spring element is inserted. The second drawback is that the stress-strain curve of rubber is non linear. However, this can be taken into account during calibration, by determining this relation. The third drawback is that rubber is a viscoelastic material. Therefore, some elastic hysteresis, force relaxation and creep can be expected. These depend on time, temperature and stress levels. These effects must not be ignored.

Polymers

There are also biocompatible polymers like: PMMA, PE, PEEK, PTFE (Teflon) or UHMWPE. However, these deform non-linear and do not have the right E modulus for our application.

Metals

A metal spring element is most suitable for the other six spring shapes. The benefits from metal is that it is not very sensitive to temperature changes and can therefore be sterilized with hot steam and it does not suffer from elastic hysteresis. Therefore, the material properties of biocompatible metals were investigated in the material selection database CES [66]. Biocompatible metals are: stainless steel, titanium (commercially pure or an alloy like Ti-6Al-4V), nickel-titanium alloys (like Nitinol), cobalt-chromium alloys or nickel-chromium alloys. Especially stainless steel and the titanium alloys Ti-6Al-4V and Nitinol are interesting for reasons that will be discussed next.

Stainless steel is used for most standardized spring elements that are sold on the internet. Therefore, these spring elements are easy to obtain. However, it is not the best material for a spring element, because its E modulus around 200 GPa, which is higher than for titanium, and its yield strength varies from 170-1000 MPa, which is lower than for titanium [66].

Titanium alloy Ti-6Al-4V, which the stem of the hip implant is made of, is commonly used for medical (and aerospace) engineering, because of its biocompatibility and high yield strength: $\sigma_y = 750 - 1200$ MPa [66]. It also has a relatively low E modulus: E = 110-120 GPa [66]. This high yield strength and low E modulus make Ti-6Al-4V especially suitable as a spring material. Since the implant is made of this material, it might even be possible to create a monolithic spring in the neck of the implant.

Nitinol is an alloy made from nickel and titanium. Nitinol is interesting because it has a very low E modulus and it is superelastic. This means the material can stretch about 8%, which is exceptionally large for a metal alloy. This superelasticity is caused by the phase transformation between the austenitic and martensitic phases of the crystal. There is a catch however, because the material shows large hysteresis after the 'transformation stress'. Therefore, the transformation stress should not be exceeded. The transformation stress and E modulus of Nitinol are $\sigma_t = 600$ MPa and $E = 50$ GPa [66]. In the end, it was decided not to use Nitinol, because the material is very expensive.

A metal should have a high yield strength and a low elastic modulus to be suitable as a spring. If these three materials are compared on their ratio of yield strength (MPa) to E modulus (GPa) we get: Stainless steel: $\sigma_y/E = 5$, Ti-6Al-4V: $\sigma_y/E = 10$ and Nitinol: $\sigma_t/E = 12$ [66]. Therefore, the titanium alloys are more suitable as spring materials. However, stainless steel springs are easier to obtain.

Calculations

Compressed solid

It would be very easy to use a simple compressible volume as a spring. Examples are: a rectangle, a disc shape or a ring shape. A simple ring or disc shape element is easy to make or buy and would fit nicely inside a cylindrical neck. Furthermore, a ring shape has the advantages that it has more space to expand than a disc shape when compressed and the magnetic field can pass through the middle uninterrupted. A simple calculation will now be made to estimate the viability of this option. If we compress a simple ring shaped element with an outer diameter of 8mm and an inner diameter of 6mm with a force of 400 Newton, this would induce a stress of 18 MPa (equation 1,2). This is below the yield strength of NBR rubber, which is approximately 20-30 MPa [66]. Rubber does not have a constant E modulus that can be used to make a simple calculation with equation 3, because rubber has a non-linear stress-strain curve. However, since we know the induced stress is 18 MPa, we can look up the strain in a stress-strain graph from literature. The stress-strain graph of silicone rubber in uniaxial compression is shown below (Fig. 20). According to this graph the rubber ring will be compressed to 20% of its length at this stress. This means a thickness of 1.25mm is required to reach a displacement of exactly 1mm.

$$A = \pi/4 \cdot (D_{out}^2 - D_{in}^2) = \pi/4 \cdot (8^2 - 6^2) = 22 \ mm^2 \tag{1}$$

$$\sigma = \frac{F}{A} = \frac{400}{22 \cdot 10^{-6}} = 18 \ MPa \tag{2}$$

$$\delta = \frac{F \cdot L}{A \cdot E} \ \ (not \ applicable \ to \ rubber) \tag{3}$$
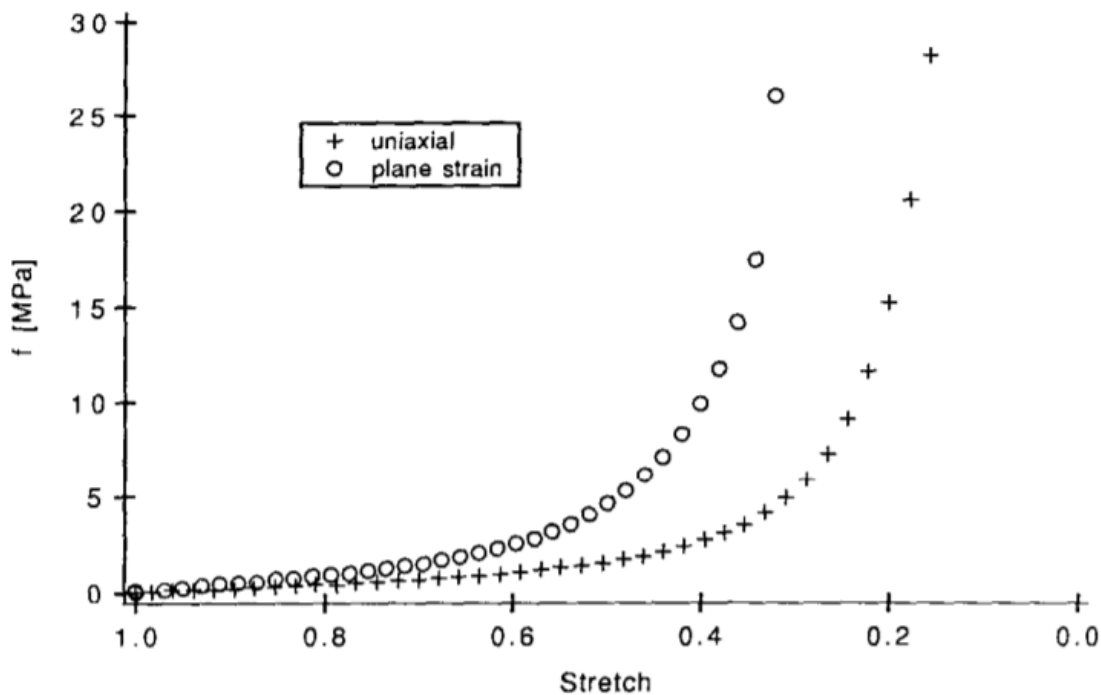

Figure 20: Stress-strain graph for uniaxial compression and plane strain compression of silicone rubber. For uniaxial compression a stress of 18 MPa corresponds to compressing the object to 20% of its original length. [67]

Therefore, a ring shaped rubber spring element would be suitable, as this will satisfy the requirements to have a displacement bigger than 0.5mm and smaller than 1mm at the maximum load of 400 Newton. The induced stresses are acceptable. The ring can be very small, which is advantageous. However, at this point in time the amount of elastic hysteresis in the rubber was still unknown. The results for the hysteresis test will be shown in chapter 3.
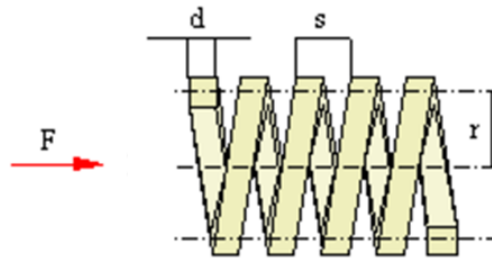
Helical spring

Figure 21: Dimensions of a helical compression spring. *Credit: http://www.tribology-abc.com*

Helical compression springs were also investigated. The deflection and shear stress in a helical spring are [64]:

$$\delta = \frac{44.9 \cdot n \cdot r^3 \cdot F}{d^4 \cdot G} \tag{4}$$

$$\tau = \frac{4.8 \cdot r \cdot F}{d^3} \tag{5}$$

The deflection must be at least 0.5mm and the stress must not exceed the yield strength. Notice from the equations that it is smart to increase radius r as much as possible, as this will increase the deflection to the power of 3 and increase the shear stress by the power of just 1. The number of windings n can also be increased, but this will also make the spring higher.

Assuming pure shear, we can use the von Mises equation to calculate the maximum allowable shear stress τ_{max} (Equation 3), given the yield strength of Ti-6Al-4V is 750-1200 MPa. (We take the lower boundary of 750 MPa.)

$$\tau_{max} = \frac{\sigma_{yield}}{\sqrt{3}} = \frac{750}{\sqrt{3}} = 433 \; MPa \tag{6}$$

The applied force and shear modulus of Ti-6Al-4V are:
$F = 400 \; N \; (Applied \; force)$
$G = 44 \; GPa \; (Shear \; modulus \; Ti - 6Al - 4V)$

Using the equations (4) and (5), a good estimation of the required spring dimensions can be obtained. The coil radius r was chosen as large as possible. Then, the thickness d was increased until the spring could support 400N. Eventually, the needed free length h that is needed to reach the desired deformation δ is calculated. The final dimensions are:
$r = 2.8 \; mm \; (Spring \; radius)$
$d = 2.4 \; mm \; (Thickness \; springwire)$
$D_{out} = 2 \cdot r + d = 8 \; mm \; (Spring \; outer \; diameter)$
$n = 2 \; (Number \; of \; coils)$
$s = 2.67 \; mm \; (Pitch \; of \; lead)$
$h = 5.34 \; mm \; (Free \; length \; spring)$

Results:
$\delta = 0.54 \; mm \; (Spring \; deflection)$
$\tau = 389 \; MPa \; (Shear \; stress)$
$k = 741 \; N/mm \; (Stiffness)$

Thus, if we would make a helical spring element from Ti-6Al-4V, we need a free length h of 5.34mm, thickness d of 2.4mm and radius r of 2.8mm in order to obtain the minimal deformation of 0.5mm under a load of 400N, while staying within the maximum allowable shear stress of 433 MPa.
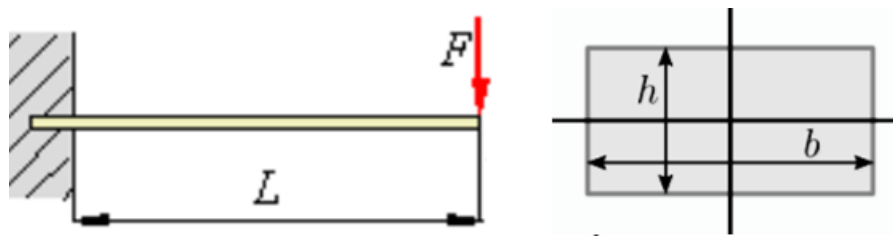
Leaf spring

Figure 22: Dimensions of a basic leaf spring element. *Credit: http://www.tribology-abc.com*

$$I = \frac{b \cdot h^3}{12} \tag{7}$$

$$\delta = \frac{F \cdot L^3}{3 \cdot E \cdot I} = \frac{4 \cdot F \cdot L^3}{E \cdot b \cdot h^3} \tag{8}$$

$$\sigma = \frac{F \cdot L \cdot h/2}{I} = \frac{6 \cdot F \cdot L}{b \cdot h^2} \tag{9}$$

Again, the deflection must be at least 0.5mm and the stress must not exceed the yield strength. Notice from the equations that it is smart to increase the length L as much as possible, because it increases the deflection to the power of three and increases the stress by the power of just one. Thus, it makes more sense to have a couple of long leaf flexures on top of each other, than a couple of short leaf flexures next to each other. If two leaf flexures are put in series, this will also remove the shortening effect.

The applied force was set to 130N, because the leaf flexure could not handle higher forces and still reach the desired displacement, without needing very thick flexures. Furthermore, the E modulus of Ti-6Al-4V was used:
$F = 130 \ N$
$E = 120 \ GPa$

The leaf flexures have to fit in the available space with a diameter of 8mm. Therefore, the length, width and height were chosen as:
$L = 6 \ mm$
$b = 5.29 \ mm$
$h = 0.89 \ mm$

Results:
$\delta = 0.25 \ mm$
$\sigma = 1116 \ MPa$
$k = 517 \ N/mm$

Thus, two leaf springs in series would be needed to reach the desired displacement of 0.5mm. The stress is quite high, but by making leaf springs with a varying cross section it could be possible to reach higher displacements at a lower stress level.
Milling leaf springs into the test neck would be a nice solution, because it creates a monolithic structure. Unfortunately, we would only have one shot at it, because DePuy only gave us one test neck to experiment with. It would be more sensible to use milling techniques to create the spring with the selected titanium alloy. However, it is unfortunate that the leaf springs can not handle loads of 400N.
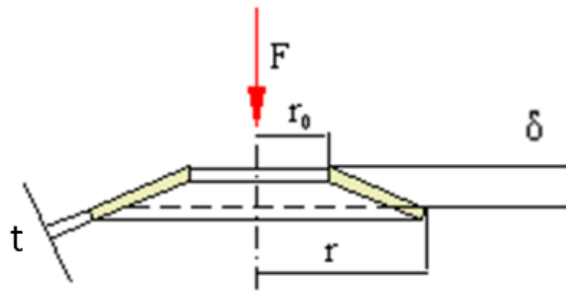
Disc spring

Figure 23: Dimensions of a disc spring. *Credit: http://www.tribology-abc.com*

$$\delta = \frac{0.65 \cdot F \cdot r_{out}^2}{E \cdot t^3} \qquad (10)$$

$$\sigma = \frac{F \cdot (1 - 2/3 \cdot r_{in}/r_{out})}{t^2} \qquad (11)$$

The formulas above are derived from the 'Werktuigbouw Formuleboekje' [64]. If we stack two disc springs, each one needs to displace at least 0.25mm under the load of 400N. The outer radius r was chosen as large as possible. The thickness was chosen as low as possible:
$F = 400 \ N$
$E = 120 \ GPa$
$D_{out} = 8 \ mm$
$r_{out} = 4 \ mm$
$r_{in} = 3 \ mm$
$t = 0.5 \ mm$

Results:
$\delta = 0.28 \ mm$
$\sigma = 800 \ MPa$
$k = 1442 \ N/mm$

Thus, according to these simple equations, two stacked disc springs with a thickness of 0.5 mm will be enough to obtain the required deflection at least 0.5 mm. This induces a stress of 800 MPa, which is just over the lower boundary of the yield strength of Ti-6Al-4V $\sigma_y = 750 - 1200$ MPa.

Slotted disc and curved wave springs
These springs are too complicated to have simple analytical equations. However, their dimensions, deflections and maximum loads were found in the Century Spring catalog [65].
The slotted disc springs have very low spring constants. This means they can easily reach the displacement of 0.5mm, but can not handle forces higher than 20N. Our requirement that their radius has to be smaller than 8mm still applies to all springs.
The curved wave springs can handle forces around 170N. If two of them are stacked on top of each other the displacement of 0.5mm can be reached. However, it would be difficult to attach them to each other, since the contact area is very small. Pre-stacked packages of these springs are also for sale, but not in many sizes. A nice benefit of this design is that the top and bottom rings make sure there are no sliding surfaces when the unit is compressed.

Conclusion
Concluding from figure 19, the rubber spring element was selected as the best option, because it is very small, can take high forces, produces the required displacement and is easy to obtain and use. However, at this point in time the amount of elastic hysteresis in the rubber was still unknown. The hysteresis test results will be shown in chapter 3.

2.4. Final design

The final design uses a cylinder that slides over the neck part (Fig. 24). The spherical head is clamped on top of the cylinder and does not slide. A linear Hall sensor is fixed inside the neck part. This sensor measures the magnetic flux density of the magnet that is fixed inside the cylinder. Between the neck and the cylinder is a rubber spring element that allows for small deformations (less than 1 mm when loaded with 40 kg).
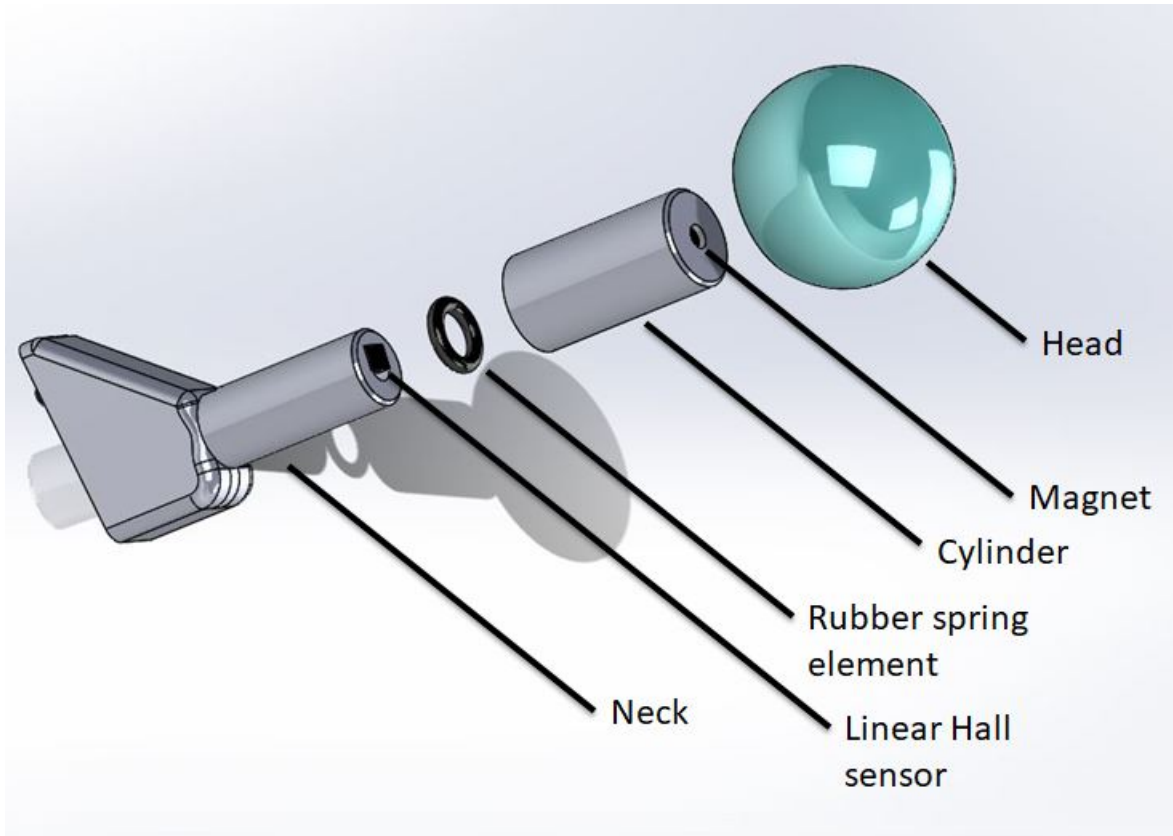

Figure 24: The final design as made in SolidWorks.

Sensor

The chosen sensor is the A1302 Hall sensor manufactured by Allegro. This is actually an integrated circuit. The integrated circuit contains a continuous-time, ratiometric, Hall circuit, a linear amplifier and a CMOS Class A output structure. It is optimized to accurately provide a voltage output that is linearly proportional to an applied magnetic field. The device has a quiescent output voltage that is 50% of the supply voltage. This is recommended to be 5 Volts, because this results in the highest linearity and symmetry. The sensor has a typical sensitivity of 1.3 mV/Gauss, at an ambient temperature of 25° C. Therefore, the sensor is saturated at a magnetic flux of:

$$B_{sat} = \frac{(V_{max} - V_{quiescent})}{sensitivity} = \frac{(5 - 2.5)}{0.0013} = 1923 \; Gauss. \tag{12}$$

Thus, if we want to use the Hall sensor to its full potential , the magnetic field should be such that it varies from zero to 1923 Gauss over the desired displacement of approximately 0.5 to 1 mm, The devices sensitivity changes slightly with temperature. It can serve at a temperature range from –40°C to 125°C and can be stored at a temperatures between –65°C and 170°C. This, combined with the waterproof epoxy packaging, explains why it can be sterilized with hot steam in the autoclave. Therefore, it is a robust sensor, which is suitable to use inside the human body.

Magnet

The disc shaped magnet is fixed inside the cylinder. The flux density of the magnet has the largest gradient when close to the magnet, especially if the magnet has a large H over D ratio. Therefore, it is possible for the Hall sensor to accurately measure small displacements when using such a magnet. A neodymium magnet with strength of M = 12200 Gauss (N38) and dimensions D = 5 mm and H = 1 mm was chosen, in order to obtain a large magnetic field gradient, while staying under the saturation value of the Hall sensor, which was calculated to be 1923 Gauss. The magnetic field as a function of the distance z can be calculated with the following equation [63]:

$$B(z) = \mu \cdot \frac{M}{2} \cdot \left(\frac{(z+H)}{\sqrt{(z+H)^2 + (D/2)^2}} - \frac{z}{\sqrt{z^2 + (D/2)^2}} \right) \tag{13}$$

- With μ the relative magnetic permeability

- M the magnetization of the magnet in Gauss

- H the height in of the magnet in m

- D the diameter of the magnet in m

This results in the following magnetic field-distance plot (Fig. 25), made in Matlab (Appendix C.2). The magnetic field gradient is largest between 0 to 2 mm distance from the magnet. Using the large gradient in this section will improve the resolution of our measurements.
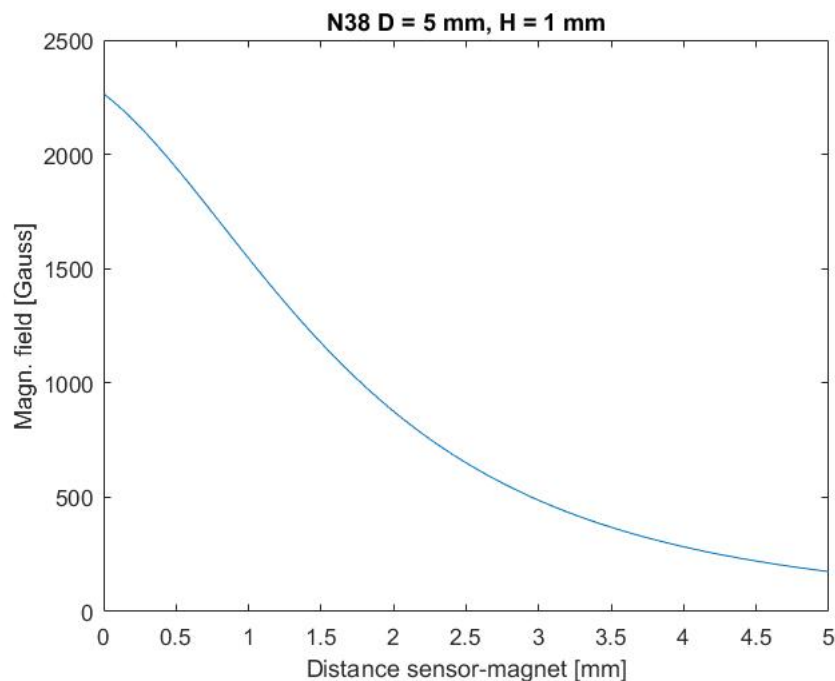

Figure 25: Magnetic field as a function of the distance z along the axis of the disc shaped magnet.

Spring element

The rubber ring shaped spring element was used, because it is small, can take high forces and is easy to obtain and use. At this point in time the amount of elastic hysteresis of the spring was still unknown.

Neck

A request was sent to DePuy company to obtain the CAD model of the real Corail trial necks. After a series of emails and phone calls, the request was unfortunately denied. Luckily, we had obtained a trail neck, and the dimensions of this neck were carefully measured with a caliper. Using these dimensions a SolidWorks model of redesigned neck suitable for instrumentation was made. A dimensional drawing of the designed neck can be found in appendix D.1. The neck connects to the original stem through a pin and hole. It features an axis on which a cylindrical component will be sliding. It has room for the linear Hall sensor and wiring, which runs through the axis. Production and material choices are discussed in chapter 4.

Cylinder

This part is a simple cylinder which can be made on a turning lathe. It has a cavity to fit the magnet and a hole to reach and remove the magnet if it needs to be replaced. We would like to minimize the friction as much as possible, by using a spacing between +0.005 mm and +0.010 mm between neck and cylinder. Using a tight spacing will prevent the mechanism from jamming. The friction will also be reduced by applying lubrication. The cylinder should also be able to fit inside the original trial head. There must not be any movement between the cylinder and the trial head. A dimensional drawing of the designed cylinder can be found in appendix D.2.

3

Prototype

A prototype was made in order to put the design to the test. This chapter consists of three parts. First, the assembly of the prototype will be shown in an exploded view and the material selection and manufacturing techniques will be explained. second, the calibration method will be presented and the results will be explained. Third, the subject of friction and lubrication will be discussed, together with the frictions tests that have been performed.

The rest of this page is intentionally left blank, so the description of the assembly and a photo of the assembly can be shown together on the next two pages.

3.1. Assembly and manufacturing

The assembly of the prototype consists of the following parts (Fig. 26):

1. Spherical head. A standard spherical test head was used. The diameter of the used test head was 32 mm. The depth of the hole was classified as +1, which means it adds 1 mm to the neck length. It was made by DePuy Synthes company.

2. Cylinder. The cylinder was made out of stainless steel on a turning lathe (turning machine). The final spacing between the cylinder and neck was: $\emptyset 9,410 - \emptyset 9,402 = 0.008$ mm. This tight spacing will prevent the mechanism from jamming.

3. Magnet. A Neodymium was used. The strength of the magnet was class N38. This corresponds to a strength of 1.22 Tesla. The dimensions of the magnet are: $\emptyset$ 5.00 x 1.00 mm.

4. Ring shaped spring element. The rings are all made of NBR. They were manufactured by Sanivesk. The dimensions of the chosen ring are: $\emptyset$in = 6.00, Thickness = 2.00 mm.

5. Linear Hall sensor. The linear Hall sensor with model number A1302 was chosen. The manufacturer was Allegro.

6. Neck part. The neck is 3D printed in metal, because a plastic neck would be too flexible. This way, the measurements would not be influenced by a bending neck. However, the first model was 3D printed in plastic, because it is a cheap and fast way to experiment with the shape of the design and to validate if it fits with the other components (stem, cylinder and sensor) as it should. In the final prototype, the neck is made out of stainless steel, which was 3D printed at the DEMO lab. Then, the surface was smoothened by milling. This resulted in a final diameter of 9,402 mm and a surface roughness of 0.2 µm, which is comparable to grinding. This roughness was Ra measured. Ra roughness is the arithmetic average of the absolute values of the height deviations in the profile, compared to the mean line of the profile.

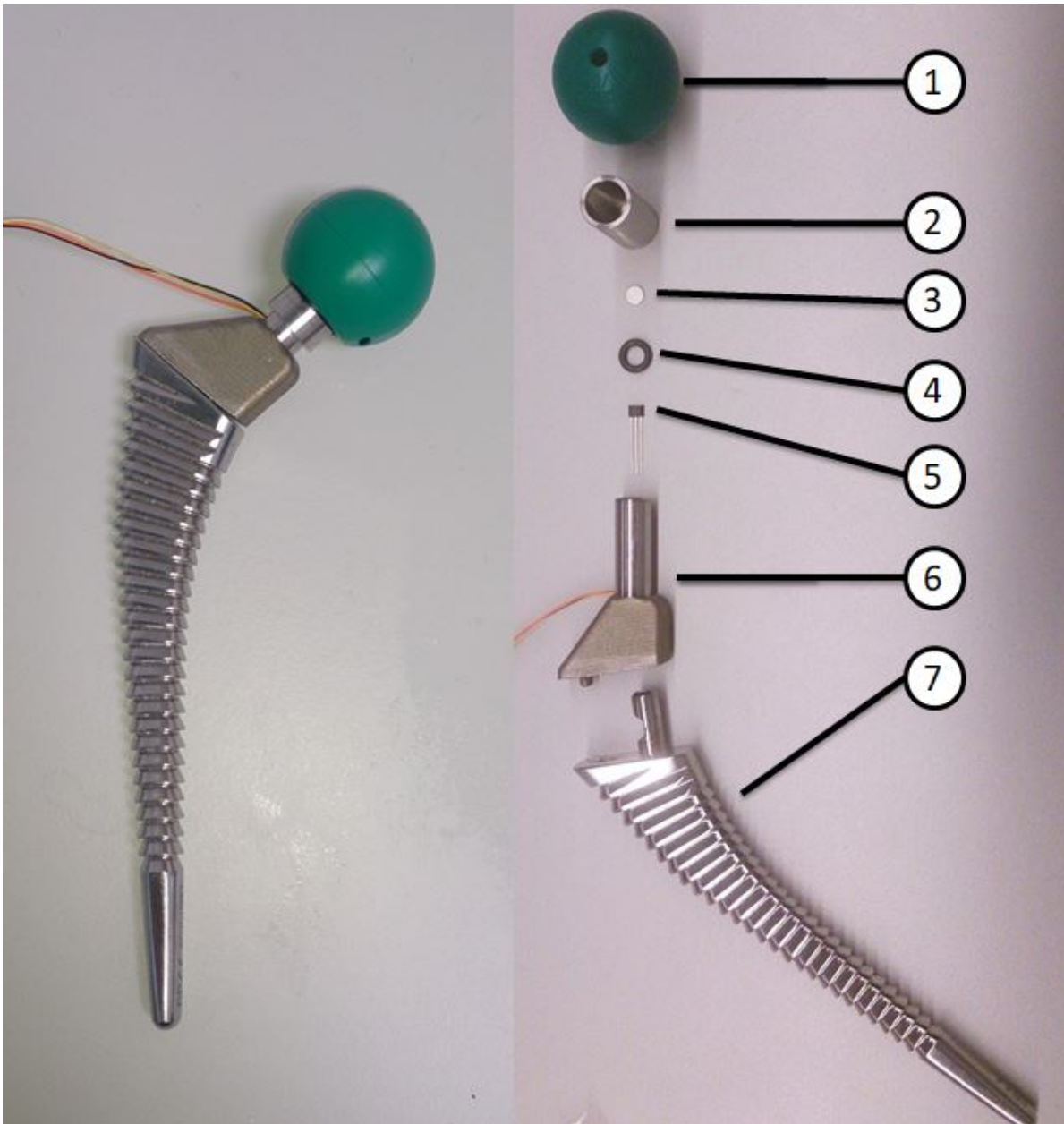7. Stem. A standard test stem was used.

Figure 26: Final prototype as used in the cadaver test. 1) Spherical head (Original), 2) Cylinder (Stainless steel, made by turning), 3) Magnet (Neodymium, Strength N38 = 1.22 Tesla, Ø 5.00 x 1.00 mm), 4) Ring shaped spring element (NBR, Øin = 6.00, Thickness = 2.00 mm, Sanivesk), 5) Linear Hall sensor (A1302 Allegro), 6) Neck part (Stainless steel, 3D printed and milled), 7) Stem (Original).

3.2. Calibration

Method

A universal materials testing machine was used to calibrate the prototype, by putting it under compression in a controlled fashion (Fig. 27). A aluminum cylinder was put on top of the prototype, to make sure the magnetic field was not disturbed by a steel object. The sensor output was calibrated with force readings from the testing machine. Steps of 0.05 mm were taken, in a range from 0 to 0.85 mm. At each step, the values for the sensor output voltage and compressive force from the materials testing machine were saved. The ring with Øin = 6,00 mm and a thickness of 2,00 mm had the best spring curve for our application (Fig. 28), because it deformed 0.82 mm at a load of 40 kg, which is within the requirements for minimal and maximal deformation. It is also noticeable that the deformation becomes non-linear at 90 Newton (0.55 mm). This can be caused by two things, namely that the rubber material behaves non-linear and that the rubber ring probably hits the side of the cylinder under the load of 90 Newton.

Relaxation

Five seconds rest were taken after each step of 0.05 mm. The dimples in the spring characteristic graph are caused by the force relaxation of the viscoelastic material during each 5 seconds of rest. All viscoelastic materials are stiffer when loaded fast than they are when loaded slow. This velocity dependent response is caused by the fluid-like behavior of the material. At high rates of loading the fluid is compressed as it attempts to flow from one region to another region of the material. This explains why force relaxation is dependent on time, temperature and stress.

Repeatability

Different rings of the same size and material were used to check if the fabrication tolerances of the rings are small enough (Fig. 29). It appeared that the rings are well fabricated and have little influence on the repeatability of the experiment. It has to be noted though, that subsequent stress stain curves are different from the first curve. This phenomenon is known as the Mullins effect, or strain softening [68]. During the first straining some entanglements are removed. This slightly decreases the stress required for subsequent cycles. The results shown in figure 29 are from the second compression of each ring.
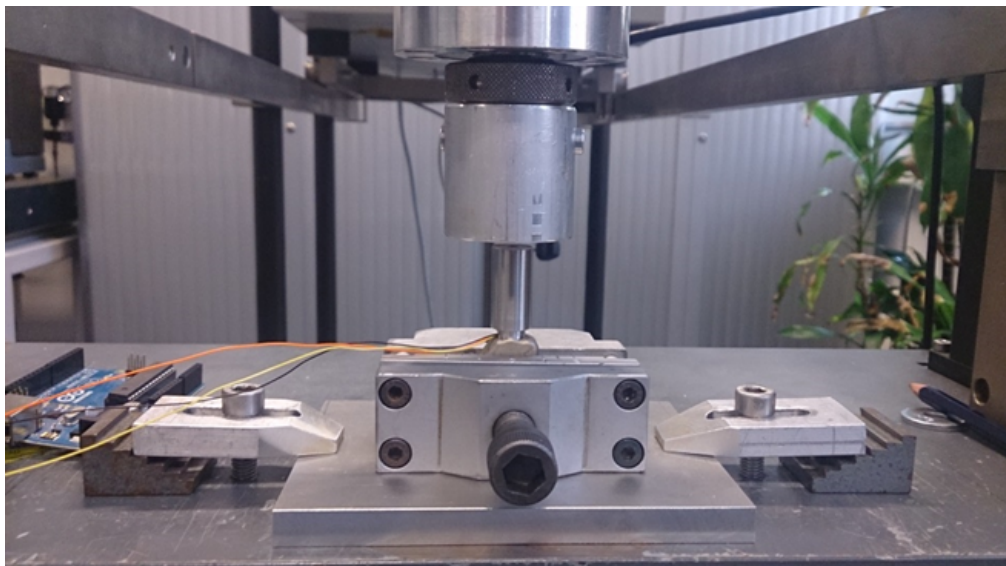

Figure 27: Measurement setup with the prototype clamped in vertical position underneath the universal testing machine.
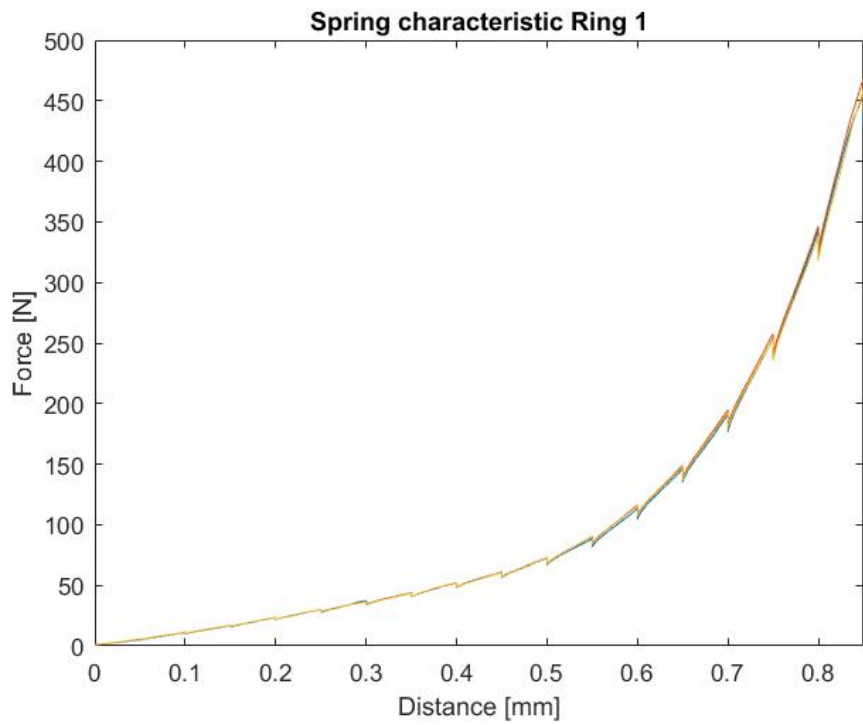
Figure 28: Spring characteristic of the ring with ⌀in = 6,00 mm and thickness 2,00 mm. Three measurements (of the same ring) are shown. Steps of 0.05 mm were taken, with 5 seconds rest in between. The dimples every 0.05mm are caused by the force relaxation of the viscoelastic material during each 5 seconds of rest.
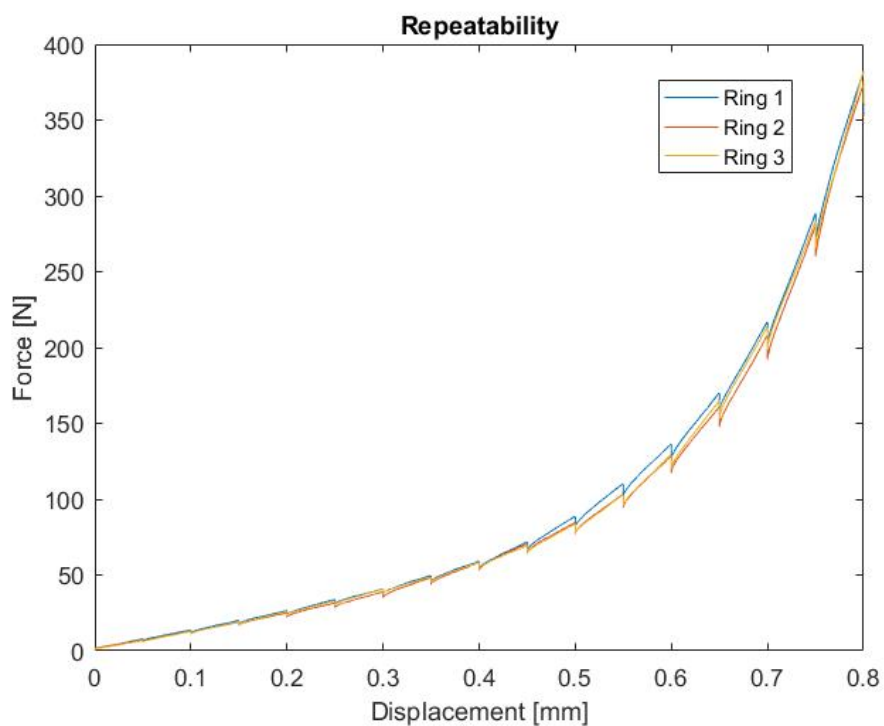

Figure 29: Three different rings of the same size and material were used to check if the fabrication tolerances of the rings are small enough to be negligible.

Analytical relation

Equation 14 describes the analytical relation between the force on the system and voltage of the sensor. This relation was determined by using the curve fitting tool in Matlab (Fig. 30). Later this formula was used to calculate the force F as a function of the output voltage V measured in real time during surgery. The relation was derived from the data of the vertical situation. Thus, friction is assumed to negligible.

$$F(V) = a_1 \cdot e^{-\left(\frac{V-b_1}{c_1}\right)^2} + a_2 \cdot e^{-\left(\frac{V-b_2}{c_2}\right)^2} \tag{14}$$

Corresponding coefficients are:
$a_1 = 3.449 \cdot 10^{18}$
$b_1 = 4.429$
$c_1 = 0.1322$
$a_2 = 2.955 \cdot 10^4$
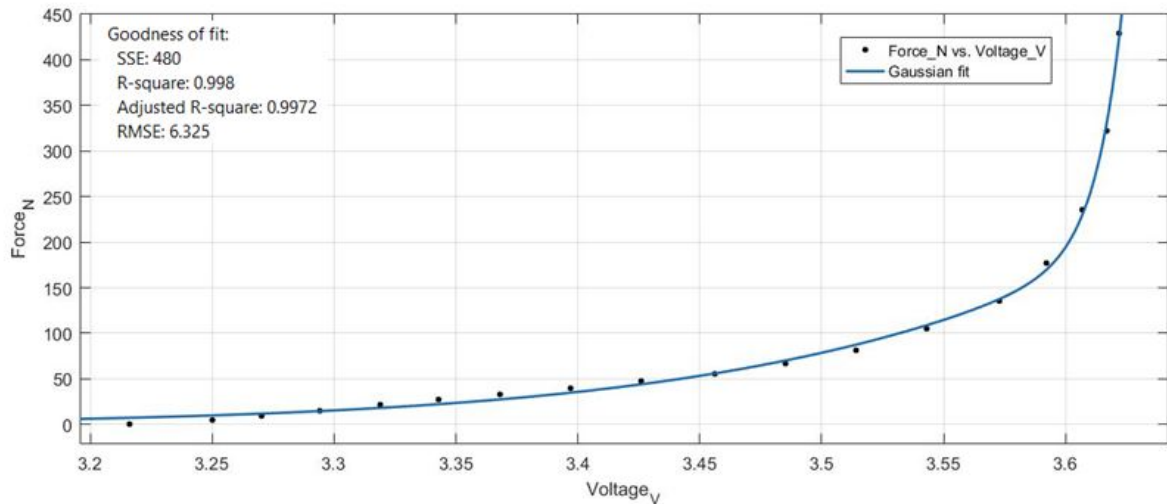$b_2 = 5.055$
$c_2 = 0.6385$

Figure 30: Equation: $F(V) = a_1 \cdot e^{-\left(\frac{V-b_1}{c_1}\right)^2} + a_2 \cdot e^{-\left(\frac{V-b_2}{c_2}\right)^2}$. Analytical relation determined with the curve fitting tool in Matlab that was used to calculate the force as a function of the output voltage. (Derived from the vertical situation and therefore assumed to have negligible friction.)

Resolution

The resolution of the Arduino UNO board can easily be calculated, since the board contains a 6 channel, 10-bit analog to digital converter. This means that it will map input voltages between 0 and 5 volts into integer values between 0 and 1023. This gives us a resolution between readings of: 5 Volts / 1024 units = 0.0049 Volts (4.9mV) per unit consistently. However, the resolution in terms of force measurement of the device is not constant, as the resolution increases non-linearly with the input force (Fig. 30), because of non-linear spring characteristic and non-linear increase in magnetic field density. From equation 1 we can calculate that a voltage of 3.2V corresponds to a input force of 6.38 Newton and the minimum step size of 4.9mV corresponds to a resolution of 0.28 Newton, which is 4.4% of the input force. At 3.6V the input force is 193 Newton and the minimum step size of 4.9mV corresponds to a resolution of 16.4 Newton, which is 8.5% of the input force. The requirements aimed at a resolution of 5 Newton. The achieved resolution is indeed lower than 5 Newton until the sensor output of 3.567 Volt, which corresponds to 130 Newton.
Furthermore, the noise level can not be excluded when determining the resolution. When

applying constant force (during calibration), the voltage output graphs sometimes alternated between two digital values. This means the noise level was not larger than one step or 4.9mV, which can correspond to a value between 0.28 and 16.4 Newton, depending on the input force.

Measurement frequency

The measurement frequency using the device with Arduino (UNO) and Matlab (R2016b) varied from 22 to 35 Hz. I found out later that the reason for this is that Matlab was slowed down because my laptop was not plugged in, which automatically triggers the windows power saver mode which lowers performance to save power. With the power saver mode setting turned off the frequency was 35 Hz consistently as it should have been during the measurements as well. This means the requirement of having a minimal measurement frequency of 32 Hz (as described in chapter 2.3) was sometimes met, but not in all of the results, because my laptop was not always plugged in during the measurements.

Alternatively, the prototype can also be used as a stand alone unit that functions without a laptop. This will increase the measurement frequency, because this does not require communication between Matlab and Arduino. The sampling rate when using Matlab with Adruino is relatively low (around 22-35 Hz), even when the baud rate (bits per second) is set to 115200. The Arduino code in appendix E uses the sensor output voltages on the analog pin of Arduino to calculate the forces in real time and shows them on a LCD display (Fig. 31). At the same time it saves the force, voltage and time data on a microSD card that is on a microSD shield attached to the Arduino. This way no laptop is required to show and save the data. However, this stand alone Arduino system cannot make a graph of the measured forces in real time. A graph is a very useful visualization to directly show the surgeon what is happening. Therefore, a laptop with Matlab (R2016b) was used in the cadaver session to make a graph of the measured force in real time (Matlab code appendix C.1). The setup with the laptop and the real time produced graphs of the cadaver session will be shown in Chapter 5.
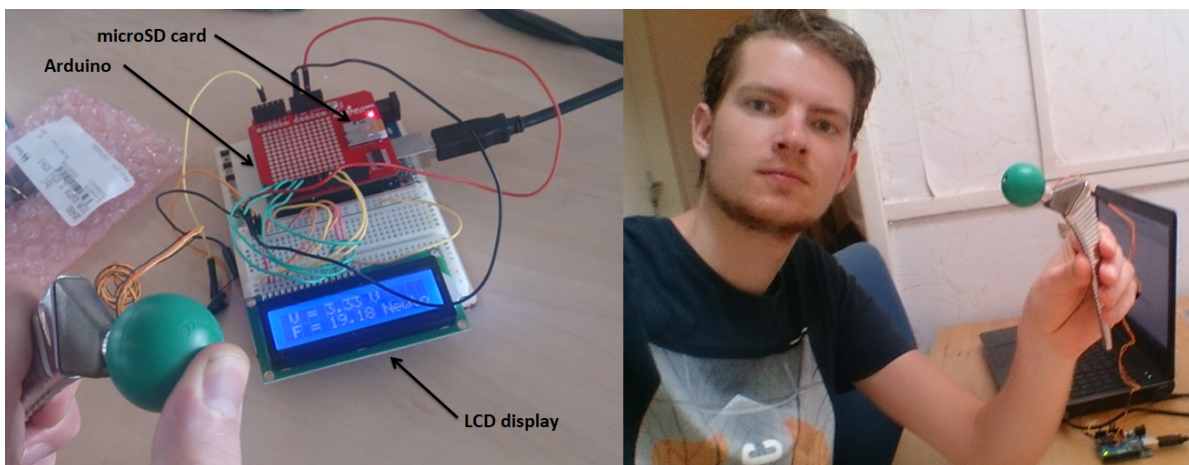

Figure 31: Left: The prototype as a stand alone unit using Arduino, a microSD card and a LCD display. This way no laptop is needed and the measurement frequency is higher. Right: Setup using Arduino and a laptop to make real time graphs of the measured forces.

3.3. Elastic hysteresis

The load cell still only moves in the vertical direction and measures the force F_{vert} in this direction. Steps of 0.05 mm were taken. We did not want to exceed 400 N, because it could damage the spring element. After reaching a force of approximately 400 N, steps of 0.05 mm were taken in the reversed direction until the starting point was reached again. This way a hysteresis loop was created (Fig. 34). The hysteresis loop is caused by the internal friction of the rubber spring element. Therefore, we should speak of elastic hysteresis in this case. The area in the center of the hysteresis loop is the energy that is dissipated as heat. Elastic hysteresis is larger when the loading and unloading is done quickly than when it is done slowly. This also explains the force relaxation mentioned before. It is not possible to remove this hysteresis completely, because it is inherent to the rubber material.

There is an inaccuracy when the load is decreasing due to the hysteresis (Fig. 32). When the load is decreased the displacement will not change according to the top line, but according to the bottom line. Therefore, the force indicated at decreasing loads will be higher than the actual force.
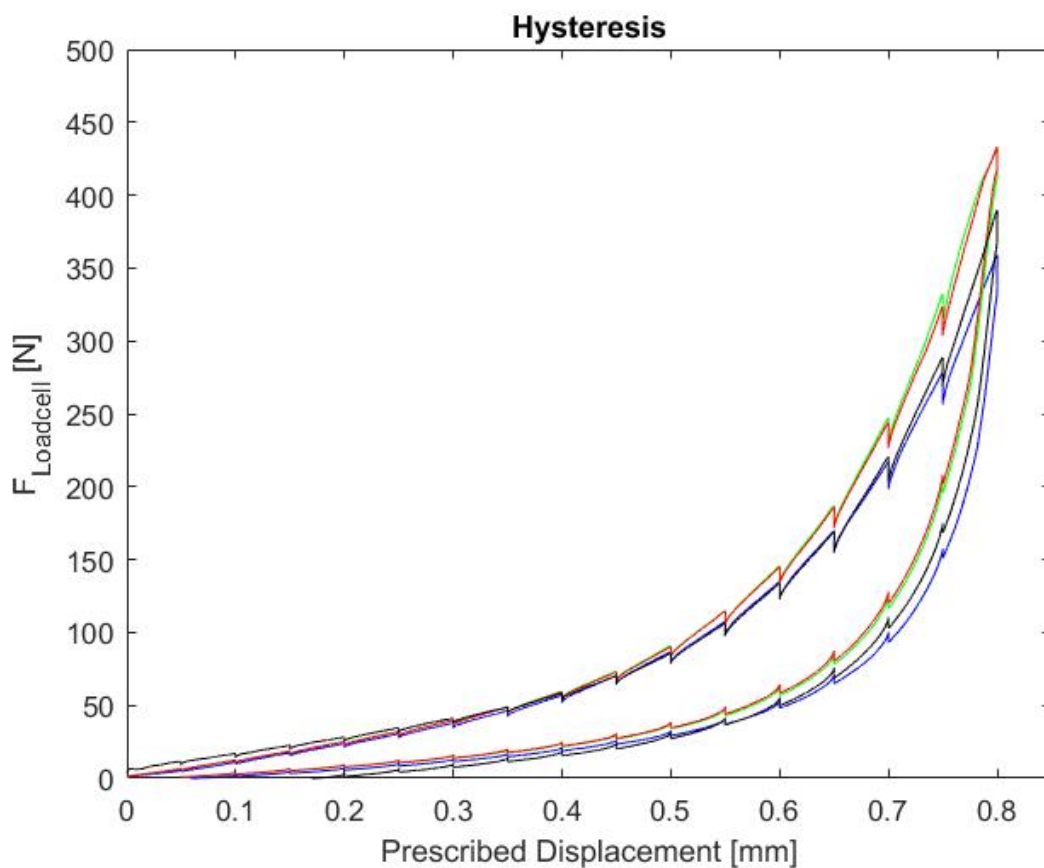

Figure 32: Results from the hysteresis test. The hysteresis loop is caused by the viscoelastic behavior of the rubber. Four measurements are shown.

3.4. Friction

The design contains a sliding element. Therefore, it is important to consider the effect of sliding friction. Factors that influence (dry) sliding friction are: surface roughness, adhesion between surfaces, surface deformation and surface contamination. A special case occurs when two surfaces of the same material are pressed together. In that case we speak of cohesive bonds instead of adhesive bonds. Cohesive bonds are generally stronger than adhesive bonds. The advantage of using a metal on a non-metal is that there is no metallurgic compatibility between the two surfaces. The advantage of using metal on metal is that we can machine it using milling and turning techniques, in order to obtain the extremely low surface roughness of 0.2 µm. Milling plastics is also possible, but it requires severe cooling and is therefore more difficult. In metal on metal contact, cohesive bonds between the atoms of both surfaces will be formed, which increases the friction. The contact area is bigger on smooth surfaces. This means there will be more cohesive bonds, thus more friction.

However, the decreased roughness of the surfaces lowers the friction caused by the ploughing effect. Another advantage of using metals, is that their strength and stiffness are are much higher than those of plastics. Therefore, the component is less likely to fail or deform.

Lubrication

Koch Uhrenöl Sorte 4 was used to lubricate the mechanism. This is a lubricating oil for watches. It is not biocompatible, but did not pose any problems in this case, because the first test was on a cadaver. When testing on living patients, a different lubricant must be chosen. For instance, Spectra lube instrument lubricant could be used, which is a biocompatible lubricant with rust inhibitor. It has a neutral pH of 6.5 and is water-based to allow for steam penetration during sterilization, which seems ideal for our application. Unfortunately, it is only shipped to the USA. Therefore, it was not used in our tests.

Friction tests

In the first friction test, the neck of the prototype was clamped under an angle of 45 degrees under the universal testing machine. We intended to measure the friction force caused by a force acting under an angle of 45 degrees. However, this measurement setup was not accurate, because the load cell can only push down vertically and the prototype also moved horizontally. An elaborate explanation of this faulty setup is given in appendix F. Luckily, the mistake in this test setup was discovered. With this knowledge, a second friction test with a better test setup was created.

In the second friction test, a new test setup was used (Fig. 33). This test setup consists of a mass that exerts a normal force F_n on the prototype through a wire and pulley. In order to observe the effect of friction, weights of 5 and 10 kilos were applied to create a normal force F_n of 50 and 100 N respectively. This way we could research the effect of friction on the system, when the force is not in the axial direction. Logically, more vertical force is required to obtain the same displacement due to the friction forces, as can be seen by the peaks moving to the left in (Fig. 34). The friction force is the difference between the vertical force without normal force applied and the vertical force with normal force applied. For example, we can read from the graph that at a normal force of 5 kilos causes a friction force of 30 N when 80 N of vertical force is applied. In the same way we can see that a normal force of 10 kilos causes a friction force of 60 N when 120 N of vertical force is applied.
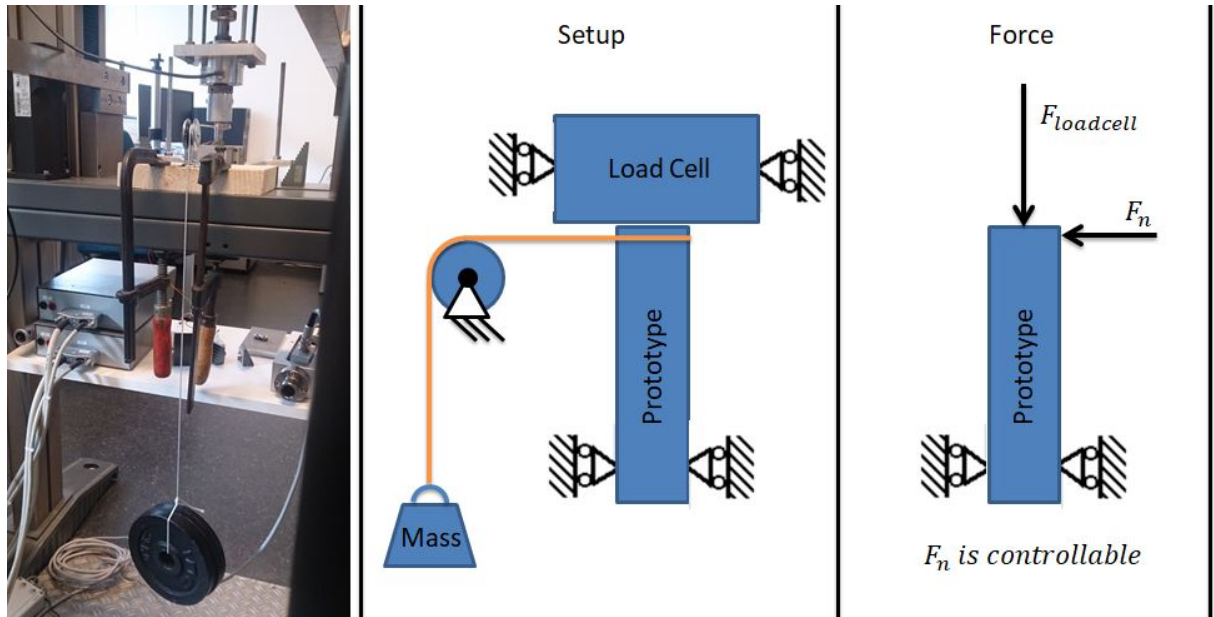
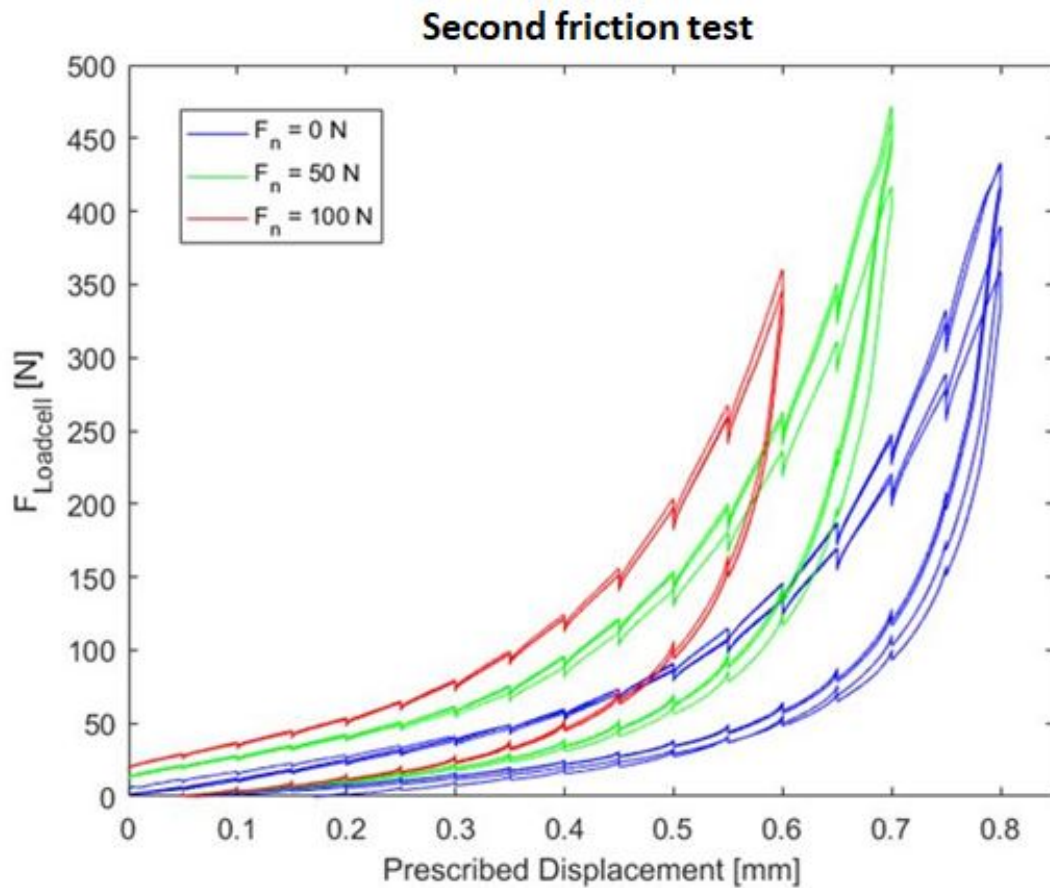Figure 33: Test setup as used in the second friction test.

Figure 34: Results from the second friction test. The hysteresis loop is caused by the viscoelastic behavior of the rubber. The force peaks moving to the left side are caused by friction. The friction results from the applied normal force F_n. Three measurements are shown for each load case.

Tapping test

This test had the same setup as the second friction test, meaning a normal force of 100 N was applied. However, in this test a constant displacement (Fig. 35) or a constant force (Fig. 36) was prescribed on the testing machine. Then, the prototype was tapped by hand three times in order to see if it was possible to 'shake out' the friction. Logically, the observed variable was the variable that was not prescribed. Three measurements are shown for each test. There is an observable effect when tapping the mechanism, but it does not seem possible to 'shake out' all the friction. In figure 35 the friction force is reduced by approximately 20 N due to the tapping, where the total friction force is around 100 N as estimated from figure 34 (Comparing the top red line to top blue line at a displacement of 0.5mm).
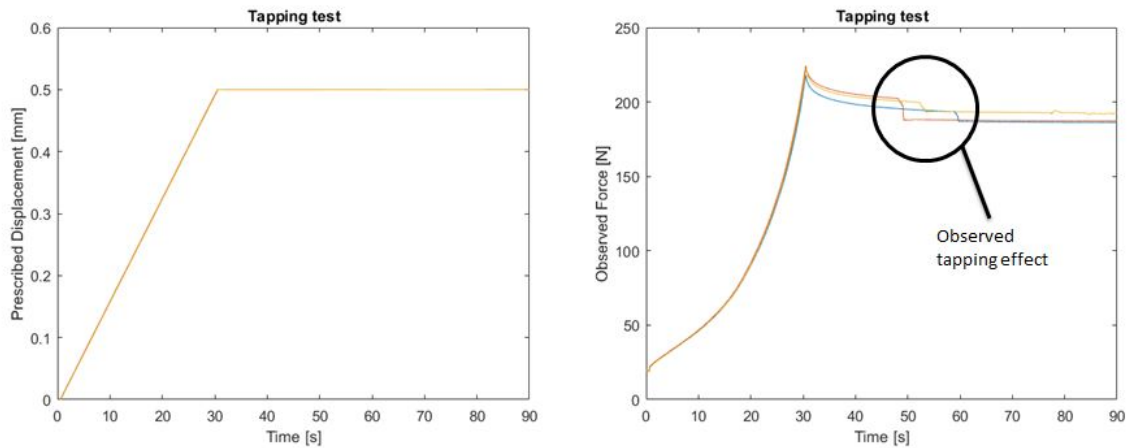

Figure 35: Observed effect when tapping against the mechanism three times to remove the static friction. In this case the displacement was controlled to be 0.5 mm and the force was observed.
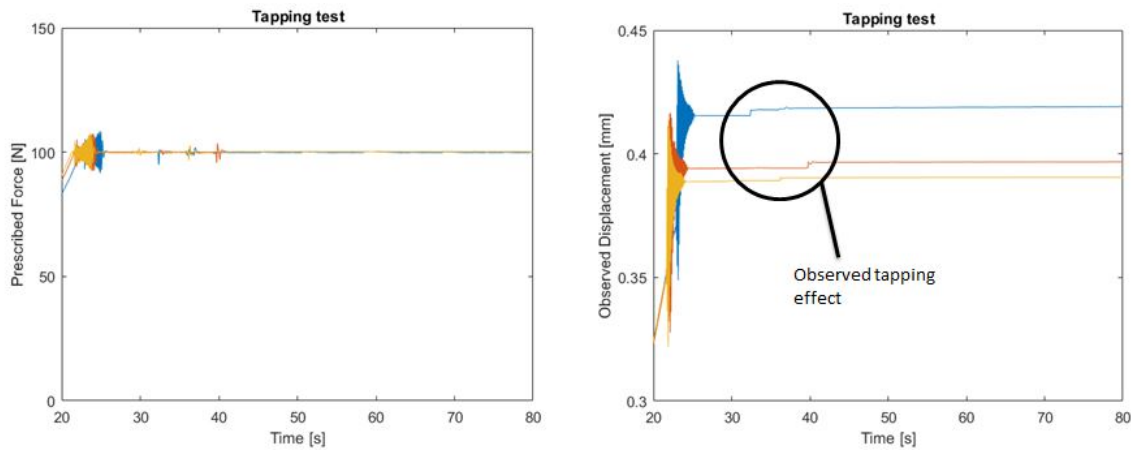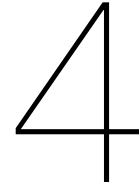

Figure 36: Observed effect when tapping against the mechanism three times to remove the static friction. In this case the force was controlled to be 100 N and the displacement was observed.

4

Cadaver test

On 22-6-2017 a cadaver test was performed in the Erasmus hospital in Rotterdam. In this chapter the test protocol and results will be shown.

4.1. Test protocol

1. Put the body in the supine position (lying on his back). The surgeon uses the anterior (frontal) approach.

2. Use the instrumented test neck with the ring and magnet that have been selected to have the best performance during calibration.

3. Use Arduino and Matlab to perform the measurements. This can reach a measurement frequency of 35 Hz, which is higher than the required 32 Hz. The Matlab code provided in appendix C.1 is used to make a graph of the force in real time.

4. Make recordings of 1 minute at a time. This should be around 2000 data points.

5. First test: The patient is lying straight in the supine position and is not moved. Measure the hip force in this position.

6. Second test: Attach a spring scale (Newton meter) to the leg. Now pull the leg in the inferior direction until there is no more force in the hip. Also, film the spring scale when pulling. The hip of the patient should be held during pulling, or else the patient might slide of the table.

7. Third test: Now the range of motion will be varied. Use a goniometer or set squire to determine the angle of the leg during this test. Hold the leg in one of the following angles for 5 seconds before moving on to the next position:

   - Internal rotation: 0, 45 and 90 degrees.
   - External rotation: 0, 45 and 90 degrees.
   - Adduction: 0 and 25 degrees.
   - Abduction: 0 and 25 degrees.
   - Flexion of both hip and knee: 0, 45 and 90 degrees.
   - Adduction and abduction till 25 degrees, combined with 45 degrees external rotation at the same time.

   (Hyperextension is not possible due to the patient lying in the supine position.)

8. Repeat this protocol for the other patients, depending on how many are available.

4.2. Results

First test

The first test shows the magnitude of the axial force while the patient is lying in the supine position. In appendix B it can be observed that the resulting force is almost completely in the axial direction in this position. Therefore, this could already give a quite precise indication of the soft tissue tension. In this case the force was 42 Newton (Fig 37), but it has to be taken into account that a cadaver was used. The leg had not yet been moved in any way when this measurement was made, so the muscles were still quite stiff. Still, the forces in a living patient are expected to be around 300-400 Newton according to literature [60], nearly ten times as high.

Second test

During the second test, the leg was pulled using a spring scale (Fig 38). A pulling force of 8.3 kg was needed in order to get a measurement of zero force in the prototype in the hip. This is higher than the force in the hip, because the soft tissues in the knee of the patient are also absorbing some force and the friction between the leg and the table is also influencing this result. The force in the hip did not return to 42 Newton after pulling, but instead it stayed at 25 Newtons. This can be explained by the fact that we are testing on a cadaver. Therefore, the muscles will not return to their original length after they have been stretched out.

The second test is in fact an objectified version of the shuck test. During the shuck test the assistant pulls the leg and the surgeon watches how far the head of the implant dislocates. In our objectified shuck test the pulling force exerted by the assistant with a spring scale is recorded, together with the compressive force inside the hip implant. This gives more objective insight into how much pulling force is required before the force in the hip becomes zero, which means that the prosthetic head will start moving or is moving away from the cup. The problem remains that there are still uncontrolled variables, like the friction between the leg and the table, the weight and compliance of the leg that is being pulled, the possible movement of the hip on the table and the effect of different levels of anesthesia. These variables influence the pulling force that is required to have zero compressive force in the hip. Still, adding this measurement will make the test more objective than it is now.
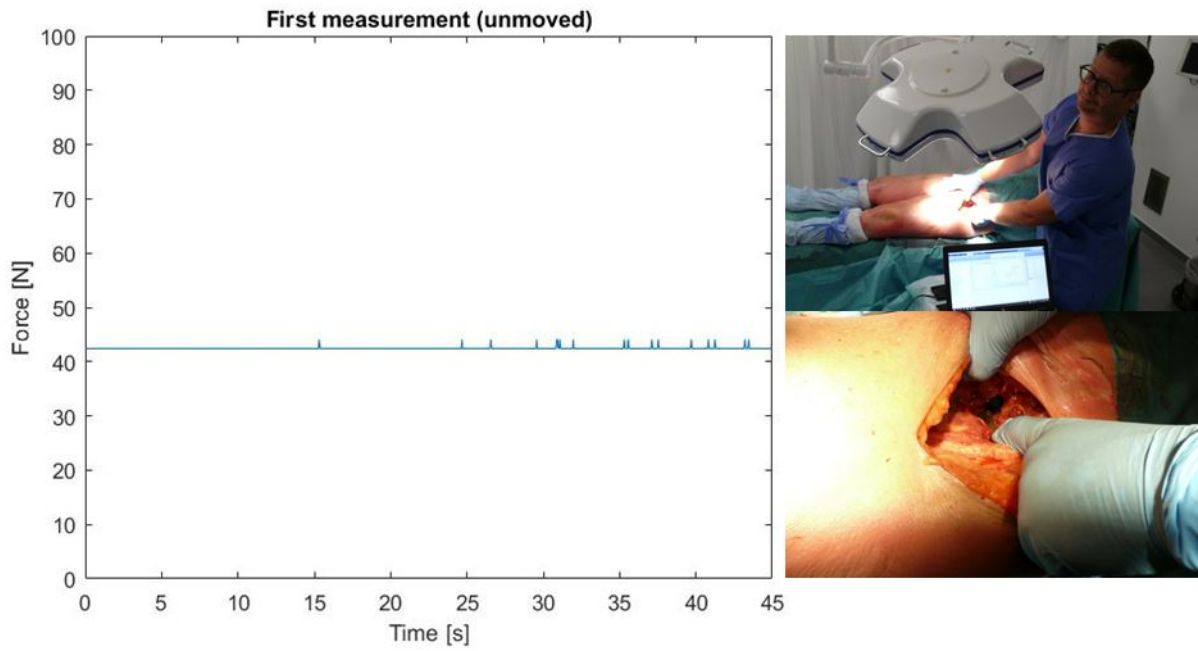
Figure 37: First test. Measurement directly after insertion of the device into the hip. The leg has not yet been moved in any way.
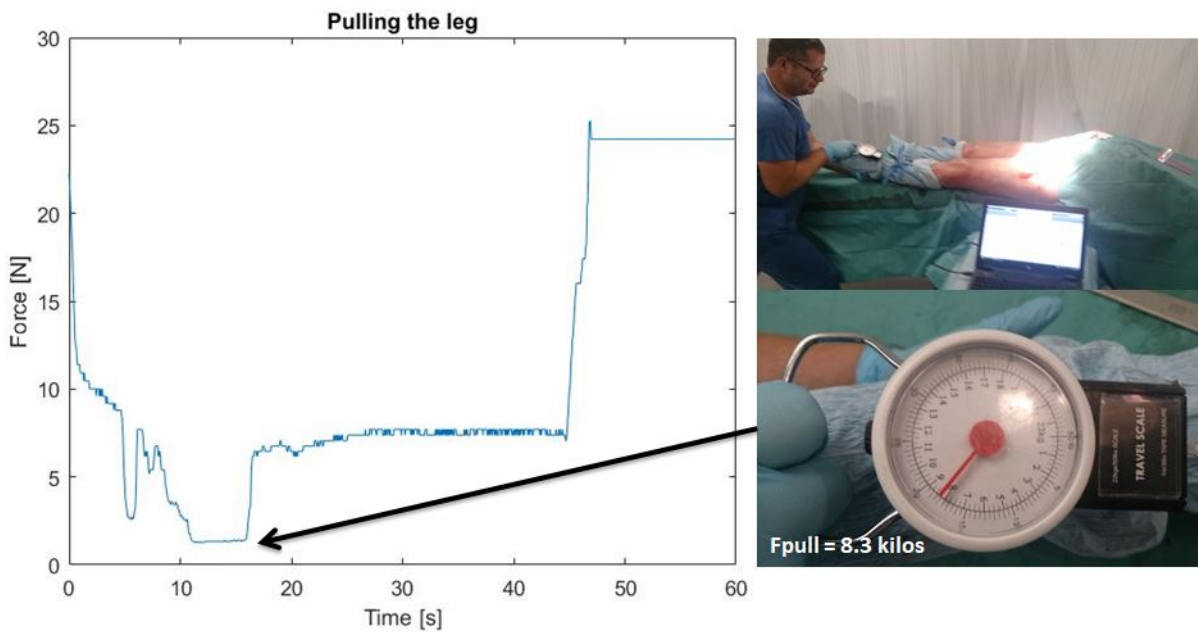

Figure 38: Second test. The leg was pulled using a spring scale. A pulling force of 8.3 kg was needed in order to get a measurement of zero force in the prototype in the hip. This is explained by the knee and ankle of the patient acting like spring elements and by the friction between the leg and the table.

Third test

In the third test the range of motion was varied by rotating the hip manually into different predetermined angles. The the axial force in the hip was recorded during these motions. These results are more difficult to interpret, because the resultant hip force is usually not in the axial direction during these movements. However, it might be possible to identify interesting patterns in the axial force recorded when repeating these movements. For example, during internal rotation there is a clear rise in axial force depending on the angle of rotation. The force peaks are getting lower during each repetition however, because the soft tissues of the cadaver got stretched out. In a living patient the results are expected to be more consistent. Furthermore, it should be noted that outcomes are influenced by the surgeons grip on the leg. It is noticeable in the results, because he lifts part of the weight of the leg.

The performed motions with predetermined angles are:

- Internal rotation: The leg was moved in internal rotation from 0 till 45 and then to 90 degrees (Fig. 39). This was measured at the foot with a set square. This was done three times in a row. The results were similar, although it was noticeable that the peak force slightly declined after each repetition. This could be explained by the soft tissues stretching further and further during each repetition, without returning to their original position, since we are working with a cadaver. The highest force measured was 101.2 Newton.

- External rotation: The leg was rotated externally. First to 90 degrees, then to 45 degrees and finally to 0 degrees (Fig. 40). This was measured with a set square. This movement was performed two times in a row. The highest force measured was 72.5 Newton.

- Adduction: The leg was adducted from 0 to 25 degrees (Fig. 41). This was measured with a goniometer on top of the leg. The highest force measured in this position was 97.6 Newton.

- Abduction: The leg was abducted from 0 to 25 degrees (Fig. 42). This was also measured with a goniometer on top of the leg. The highest force measured in this position was 121.8 Newton.

- Flexion: Both the hip and knee were flexed simultaneously (Fig. 43). At point 1 and 5 the leg and knee are flexed 90 degrees. At point 2, 3 and 6 the leg and knee were flexed 45 degrees. At point 4 the leg and knee were flexed 0 degree. Remarkably, there is a peak force when going from 45 to 0 degrees (after point 3 and 6). This could be explained by a pushing force that is unintentionally caused by the surgeon. Another explanation is that the soft tissues are causing this force peak. The highest force measured was 81.1 Newton.

- Adduction and abduction with external rotation: First the leg was rotated 45 degrees externally. Then it was held at this angle and subsequently adducted and abducted until 25 degrees in both directions (Fig. 44). This was done twice. This combination of rotations was suggested by the surgeon and provided clear force peaks. The highest force measured was 105.0 Newton.
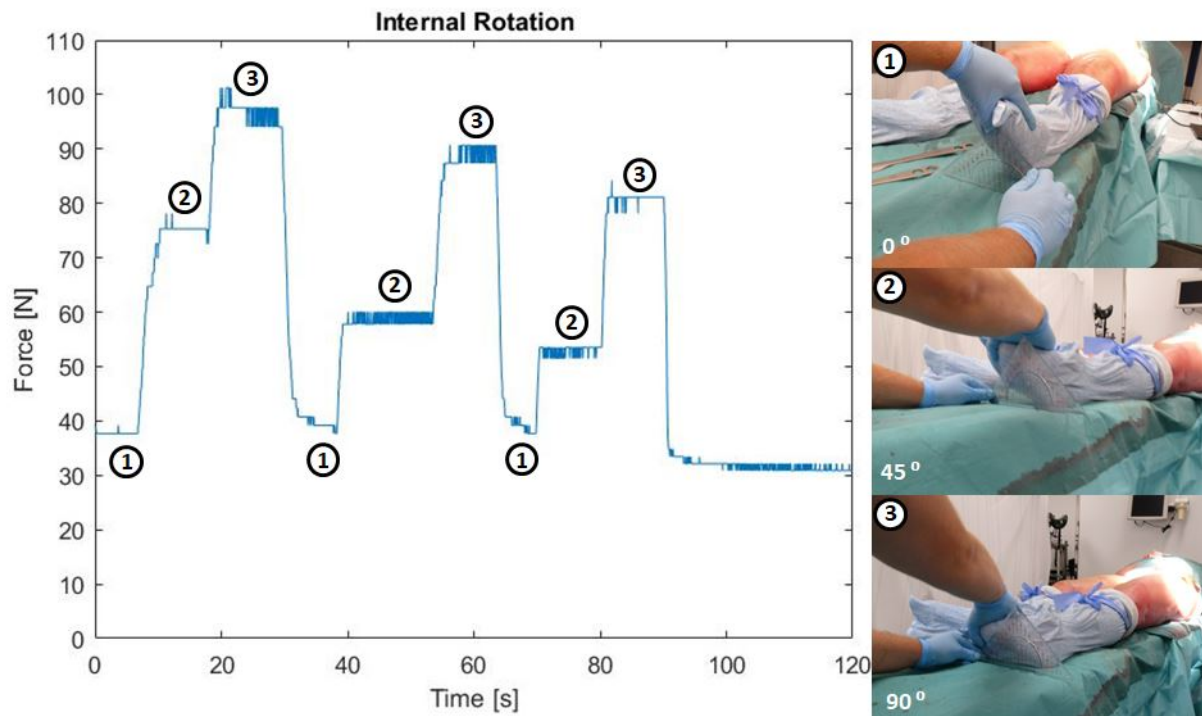
Figure 39: The leg is rotated internally to 45 and then to 90 degrees. This was measured with a large set squire at the feet, as can be seen in the picture. This test was performed three times in a row. The force declines with each repetition because of the soft tissues stretching.
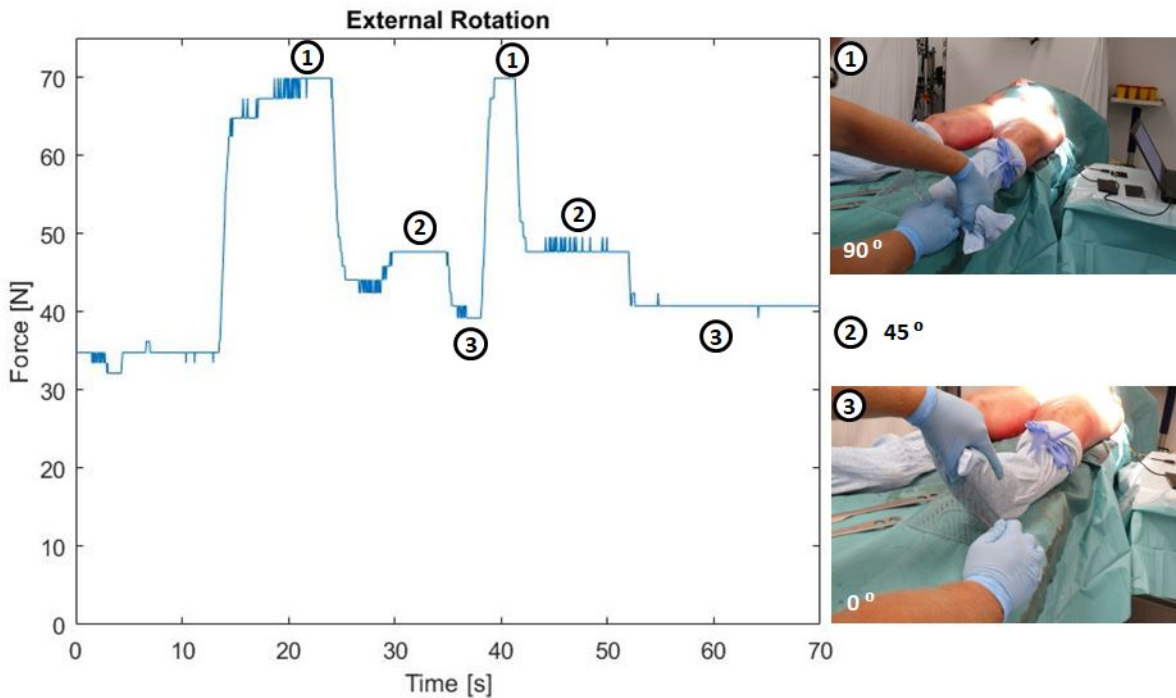

Figure 40: The leg is rotated externally to 45 and then to 90 degrees. This was measured with a large set squire at the feet, as can be seen in the picture. This test was performed two times in a row.
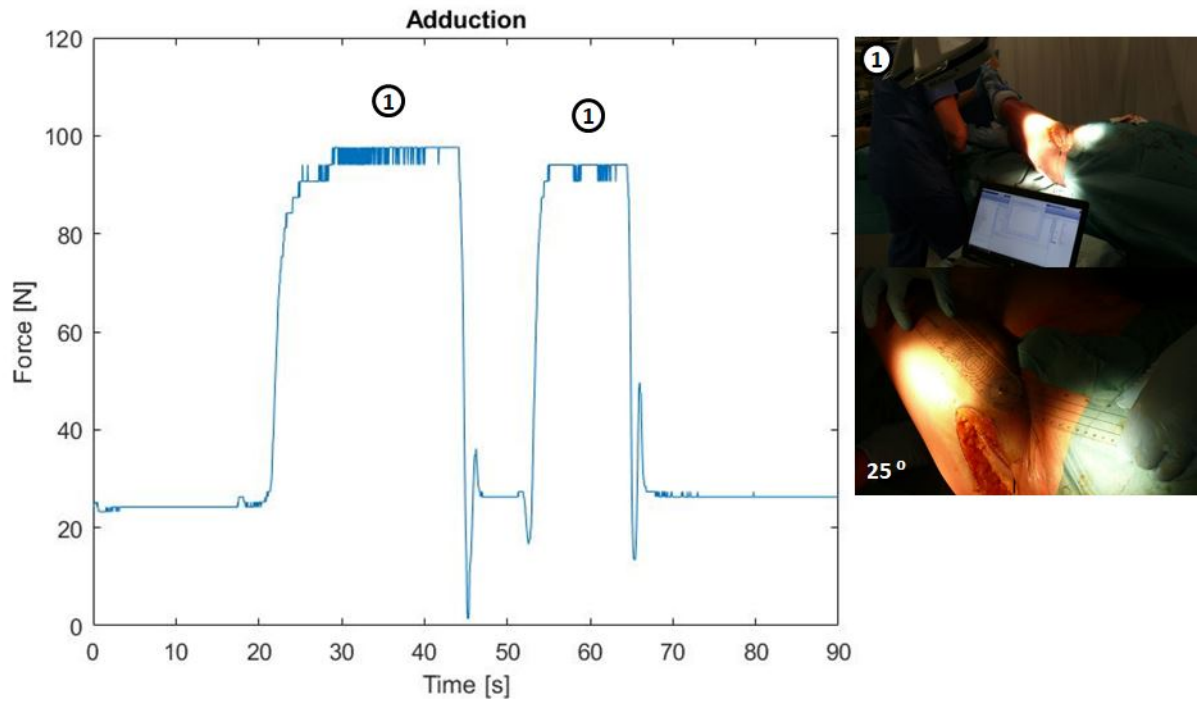
Figure 41: The leg is adducted to 25 degrees two times in a row. This was measured with a goniometer on top of the leg, as can be seen in the picture.
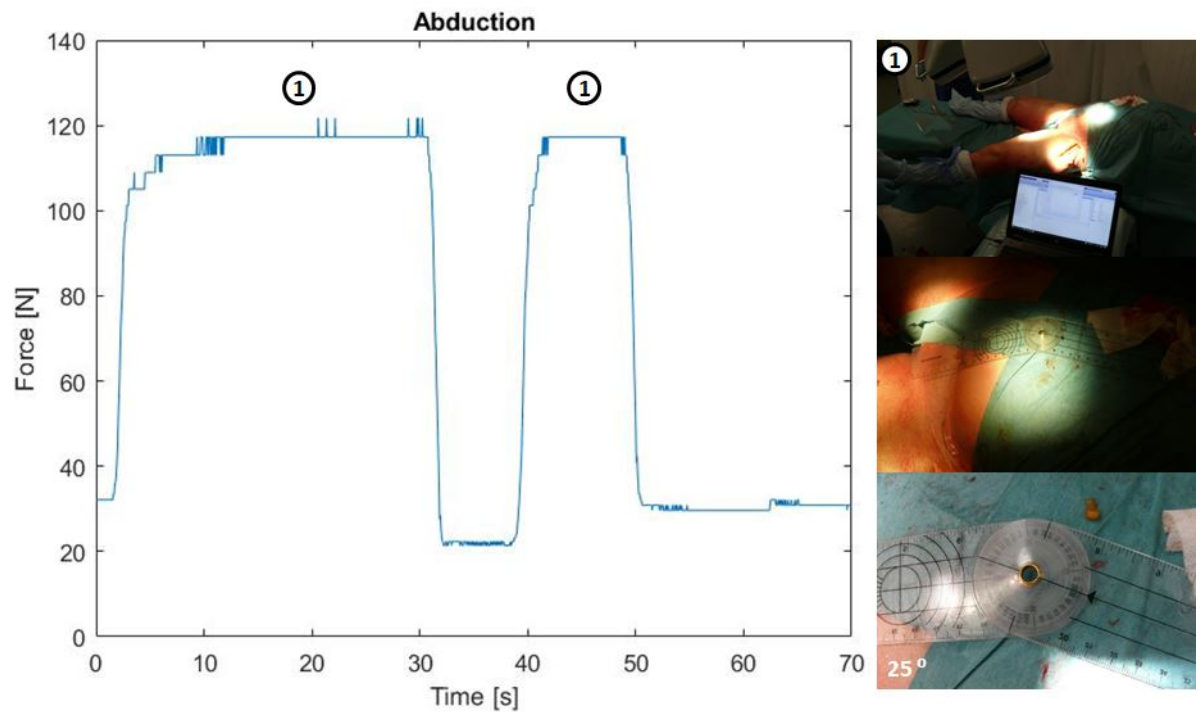
Figure 42: The leg is abducted to 25 degrees two times in a row. This was measured with a goniometer on top of the leg, as can be seen in the picture. The highest loads were recorded in this position.

Figure 43: The leg and knee are both flexed to 45 and then 90 degrees. This was done twice, as can be seen in the numbered pictures.

Figure 44: The leg is rotated externally to 45 degrees, while simultaneously being moved in adduction and abduction till 25 degrees. This was done twice, as can be seen in the numbered pictures.

5

Recommendations new design

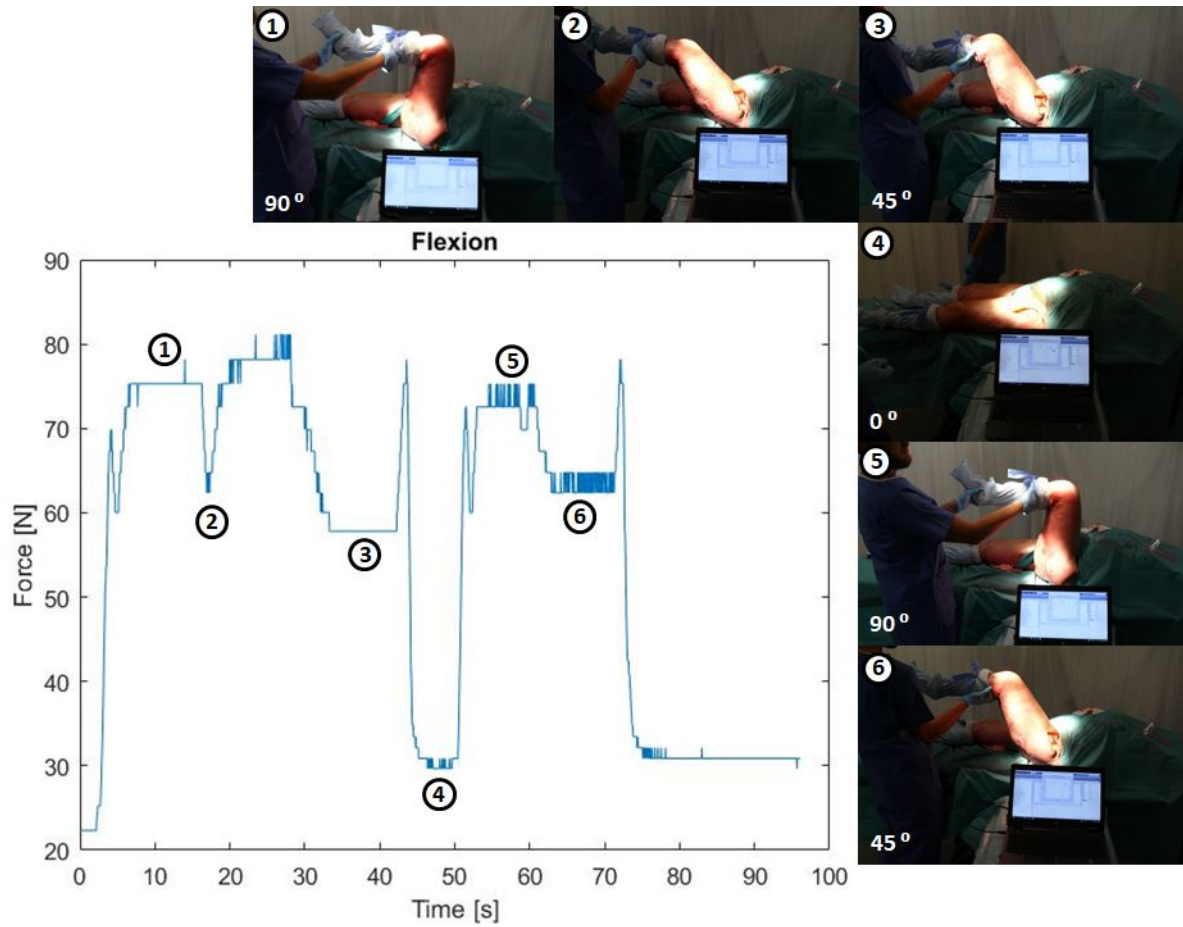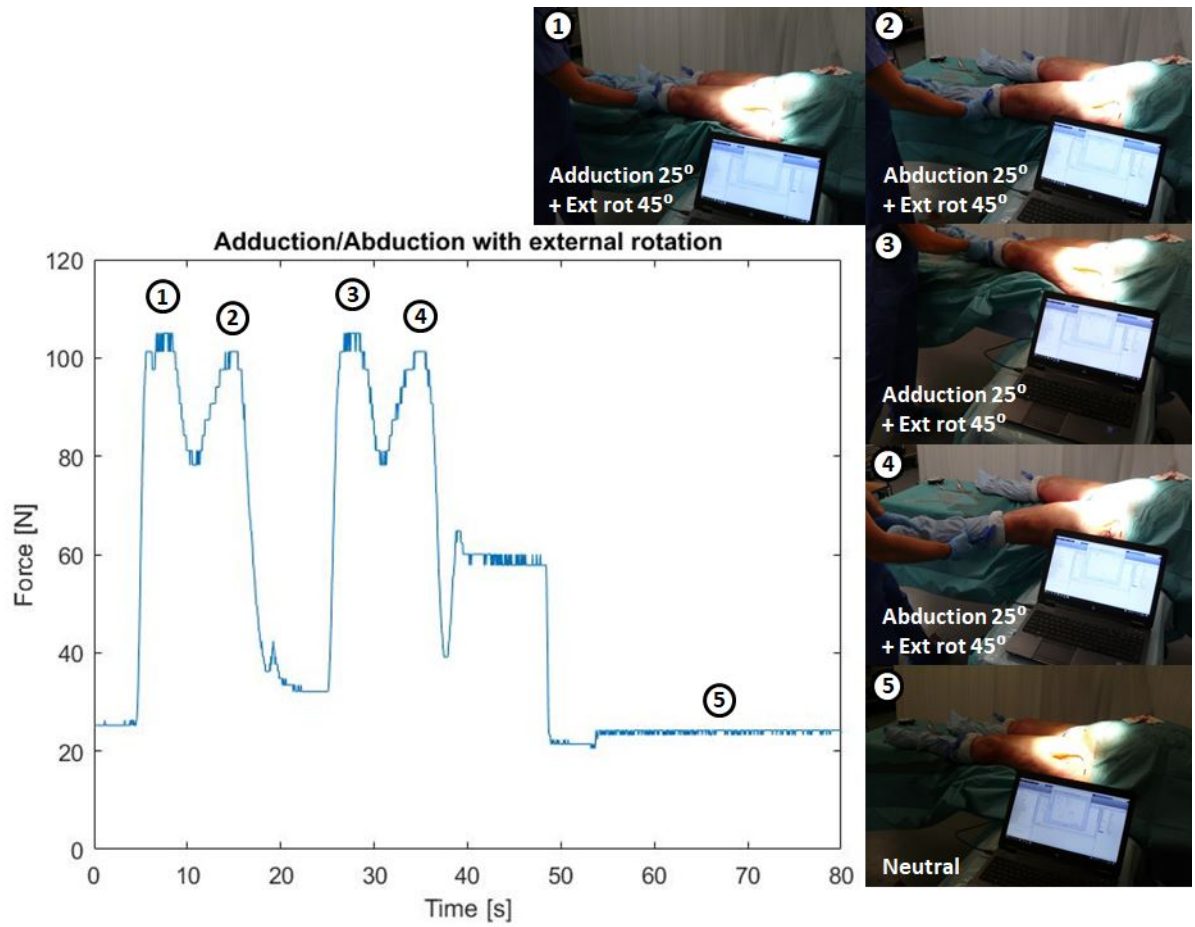Future research could invoke further improvements of the prototype. Two problems have occurred in the prototype: The elastic hysteresis caused by the rubber spring element and the friction of the sliding bearing. Solutions for these two problems will be discussed next. Furthermore, recommendations on how to improve the ROM tracking and interface are given.

Redesign spring element

The hysteresis of the rubber spring could be lowered by redesigning the spring from a different material. A metal spring would be preferable, because there is very little hysteresis in metal springs. Again, we look at figure 19 to choose a better candidate. The disc springs have only one disadvantage, which is that they might start sliding when compressed. This issue might be solved by clever design. The leaf spring element has the great advantage that we can make a monolithic unit of parallel flexures, thus there will be no sliding surfaces. Therefore, these two options were further investigated.

Double disc

Calculations in chapter 3 have shown that a double disc shaped spring made from the titanium alloy Ti-6Al-4V is possible option, but it is problematic that the two surfaces of the disc springs can slide over each other in unpredictable ways. Two solutions were found for this problem (Fig. 45). A possible solution to this problem is to put a cylinder in the middle that keeps them in place. Another solution is to make grooves on the connecting surfaces of the disc springs, so no sliding will occur.

Double leaf

It is not possible to get both the desired stiffness and deflection with metal leaf springs that have to fit inside the space of the previous rubber spring. It was decided to lower the force range to the one in the cadaver test, being maximally 130N, because neuromuscular blocking agents will be used during the surgery, so the forces might be more in the range of the ones measured in the cadaver session than the ones in living patients. This way a spring element from Ti-6Al-4V was designed that has the desired deflection of 0.5mm. It fits in the cylinder and is 5mm high. It hits the stop limit before the yield strength is reached, which is at a load of 130N. Therefore, it will not be plastically deformed under higher loads (Fig. 46).

Friction

On top of that, the friction could be lowered by choosing two materials for the neck and cylinder that are not metallurgically compatible. For instance, plastic on metal or ceramic on metal combinations generally have less friction than metal on metal. Since plastics are not stiff enough for our application, it is recommended to use a biocompatible ceramic material, such as zirconia, combined with a metal like stainless steel or a titanium alloy. The roughness (Ra measured) of both surfaces can be reduced to 0.1 µm or less by turning, grinding, honing or superfinishing. This in combination with an adequate spacing between +5 and +10 µm will keep friction forces to a minimum.

ROM tracking

The measurement of the hip angles can be much improved. Many studies use a simple goniometer, like the one in the lower right picture of figure 42, to measure the angles. A more accurate method would be to use a simple camera tracking system with or without markers on the body. An example is given in Pfister et al. [69], 2014, which compares Microsofts Kinect system with a 10-camera Vicon Nexus 3D motion capture system. The Kinect system consists of an infrared light projector, an infrared camera and a color video camera. The infrared light that is reflected is converted into depth data. This is combined with the data from the color camera to distinguish shapes. This enables the Kinect to track and record 3D human motion without using controllers or markers. Unfortunately, they found that the current Kinect system was not yet accurate enough to perform clinical measurements. However, with future improvements it may become an ideal and affordable solution to measure the ROM in clinical settings.

Interface

Such a motion tracking system could be connected to a touchscreen, which shows the current angular position of the leg and a target position. When the target position is reached the surgeon or assistant can press an OK button on the screen to proceed to the next target position. Every time the force data is recorded and eventually the system could make a post analysis based on all the obtained force data.

Another improvement would be to express the results in percentage bodyweight of the patient, because the hip force is naturally higher in heavier patients.
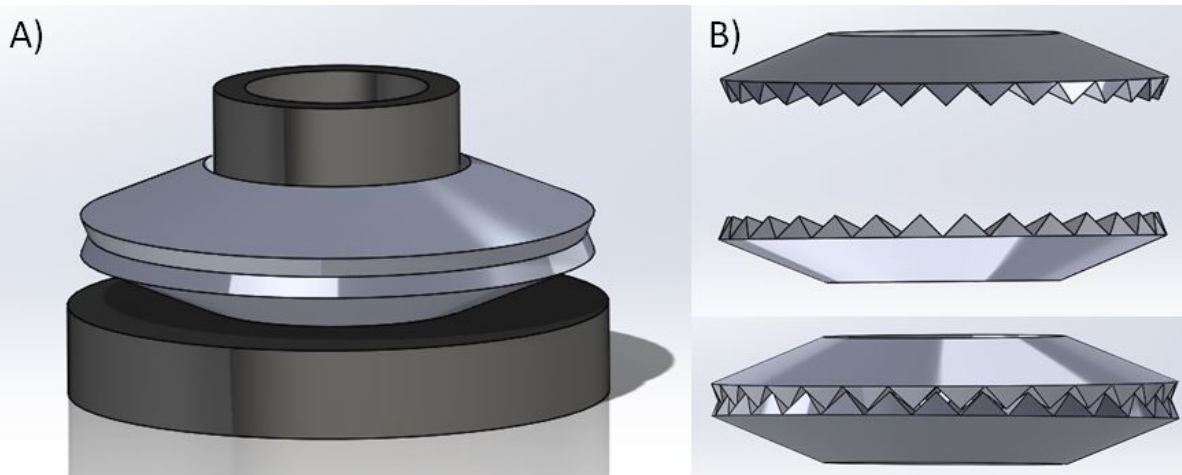
Figure 45: Two solutions to prevent the disc springs from sliding. Left: Using a cylinder. Right: Using a zig-zag edge.
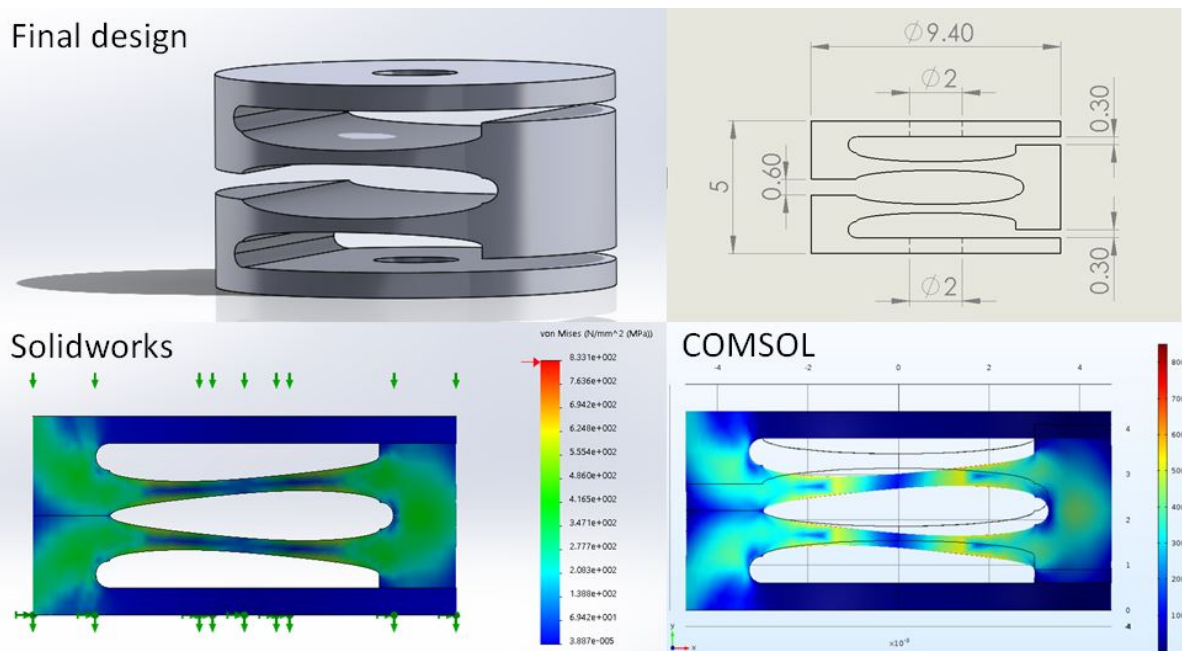

Figure 46: Top: SolidWorks model of the double leaf spring element with parabolic cuts for an improved stress distribution and higher deflection. Dimensions are indicated. Bottom: FEM calculation of the stress during maximal deformation in SolidWorks (left) and COMSOL (right). The maximum stress was approximately 830 MPa in both simulations.

Discussion

The aim of this thesis was: *"To create a sterilizable instrument that measures the compressive force in the axial direction of the neck of the hip implant during surgery."* This measured axial force in combination with a standardized ROM test could be used to objectively assess the soft tissue tension during surgery. Based on literature it is expected that this instrument will be a helpful tool for inexperienced surgeons in particular, because errors made by the surgeon are the biggest cause of early failures [4], [5], and inexperienced surgeons registered twice as much dislocations as experienced surgeons [6]. Thus, the instrument could improve the success rate and quality of total hip arthroplasty by reducing the number of early failures caused by dislocation resulting from the inexperience of the surgeon.

The created prototype succeeded in this goal. The prototype can be completely sterilized by the standard autoclave sterilization procedure. Therefore, it is a reusable device. Furthermore, the instrument can be quickly inserted. It takes a matter of seconds to insert the instrument into the body once the stem is in place and then connect it to a monitor. Thus, the surgery will not take much longer than usual. Moreover, the monitor shows a graph of the hip force in real time that is intuitive to understand. This is easy to understand for doctors and nurses with little technical knowledge.

There is also room for improvement. It is important note that the system is accurate when the load is increased from zero to a value, but is inaccurate when the load is decreased, because of the elastic hysteresis (Fig. 32). Therefore, the force indicated at decreasing loads will be higher than the actual force. To tackle this problem of elastic hysteresis, two possible redesigns for a spring element were presented in chapter 5 (Fig. 45-46). These new spring elements will not show elastic hysteresis, because they are made from metal. In the toothed disc spring design there might still be some stick slip effects due to sliding surfaces. In the parallel leaf spring design there will definitely not be any sliding surfaces, because the spring is monolithic and the shortening effect is compensated by the double leaf flexure. Since there are no sliding surfaces, no stick-slip effects will occur that can cause hysteresis effects. Both designs can deform the desired distance of 0.5mm. However, the disc spring design can take higher forces than the leaf spring design. Intraoperative force measurements should be performed to investigate how high the hip forces really are when the patient is under anesthesia with neuromuscular blocking agents applied.

Furthermore, there is friction in the device if a force is exerted in the lateral direction. Part of the friction force can be removed by tapping against the mechanism (Fig. 35). Still, there is too much friction in the mechanism. The friction could be lowered by choosing two materials for the neck and cylinder that are not metallurgically compatible. Plastic is not stiff enough. Therefore, it is recommended to use a ceramic, for instance zirconia, on a metal. The roughness of both surfaces can be reduced by for instance turning, grinding, honing or even superfinishing.

A cadaver test was performed with the developed device. This gave insight into the force in the hip during rest, when pulling the leg and during the range of motion. Although there were inaccuracies due to the elastic hysteresis of the rubber spring and friction between axis and cylinder, it was already possible to distinguish consistent patterns during repeated measurements.

It is necessary to create a standardized test, because the axial force in a static situation does not contain enough information to be a complete soft tissue tension test. However, when moving the hip in a certain path, interesting patterns can occur. For example, the

double force peak from figure 44 that occurs when moving the hip in adduction and abduction in while applying constant external rotation. A hypothesis can be made that these force peaks must be symmetrical when the soft tissue tension of the hip is correct. A proposal for a standardized test is shown in Appendix G. Notice that the hypothesis is based on pattern recognition and not on absolute values. This test can be used in future research, to find out if the axial force measured during these ROM tests provides enough information to assess the soft tissue tension.

This thesis put the basis for a project proposal for IMDI3, which is a collaboration between TU Delft, ACMIT, DePuy (a Johnson&Johnson company), the Elkerliek hospital and the Erasmus medical center.

Conclusion

The goal of this thesis was: *"To create a sterilizable instrument that measures the compressive force in the axial direction of the neck of the hip implant during surgery."* This measured axial force in combination with a standardized ROM test could be used to objectively assess the soft tissue tension during surgery. It is expected that this instrument will be a helpful tool for inexperienced surgeons, because literature shows that errors made by the surgeon are the biggest cause of early failures and inexperienced surgeons registered twice as much dislocations as experienced surgeons. Therefore, the instrument could improve the success rate and quality of total hip arthroplasty by reducing the number of early failures caused by dislocation resulting from the inadequate soft tissue tension created by inexperienced surgeons.

The goal of the thesis was successfully achieved by creating a force measurement system that measures the hip force in the axial direction. The complete system with sensor can be sterilized by the standard sterilization procedure, which is cleaning by hot steam in an autoclave. Thus, it is reusable. The device can be inserted in a matter of seconds once the stem is in place. When connected to a monitor, a graph of the axial force that is intuitive to understand is shown in real time.

A cadaver test was performed with the developed device. It was possible to distinguish consistent force patterns during repeated measurements.

The rubber spring element showed too much elastic hysteresis. The discussion concluded that the monolithic leaf spring design is better alternative, as long as the forces that have to be measured during surgery are lower than 130 Newton.

Based on what was learned from the cadaver test and from literature, a standardized test proposal with hypothesis was made. This test should serve as a guideline to get consistent and useful results in future research. This future research should investigate if the axial force measured during these ROM tests provides enough information to objectively assess the soft tissue tension, or if more information is required.
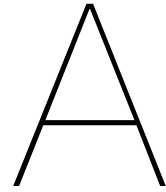
Anatomy & motions of the hip

This appendix contains an overview of the relevant bone sections, ligaments, muscles, motions and anatomical planes of the hip. If the reader encounters an unknown word in the report considering one of these topics, it can be found here.

Bone sections

The most relevant bone sections are shown below (Fig. A.1). The reader should be familiar with these terms, because they are used throughout this report.
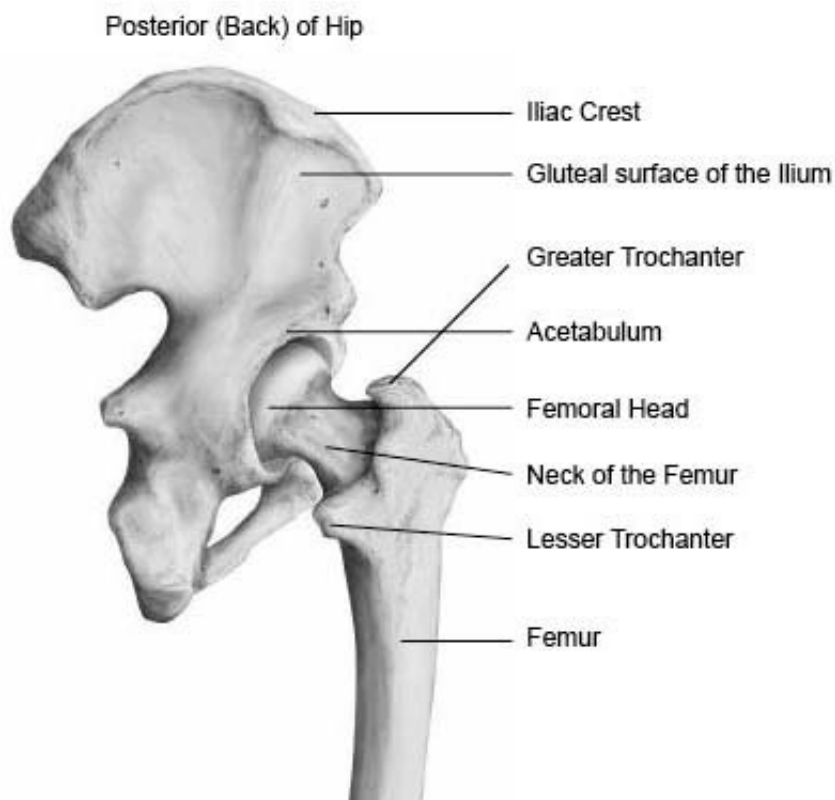

Figure A.1: Posterior view of the bones of the hip. *Image credit: www.healthpages.org*

Ligaments of the hip

The ligaments of the hip joint increase stability. They can be divided into two groups: intracapsular and extracapsular.

Intracapsular

The only intracapsular ligament is the ligament of the head of the femur. It is a relatively small ligament (not shown). It is removed during total hip surgery.

Extracapsular

There are three extracapsular ligaments (Fig. A.2):

Iliofemoral: Located anteriorly. It originates from the ilium and attaches to the intertrochanteric line in two places, giving it a Y shaped appearance. It prevents hyperextension of the hip joint.

Pubofemoral: Located anteriorly and inferiorly. It prevents excessive abduction and extension.

Ischiofemoral: Located posteriorly. It originates from the ischium of the pelvis and attaches to the greater trochanter of the femur. It prevents excessive extension of the hip joint.
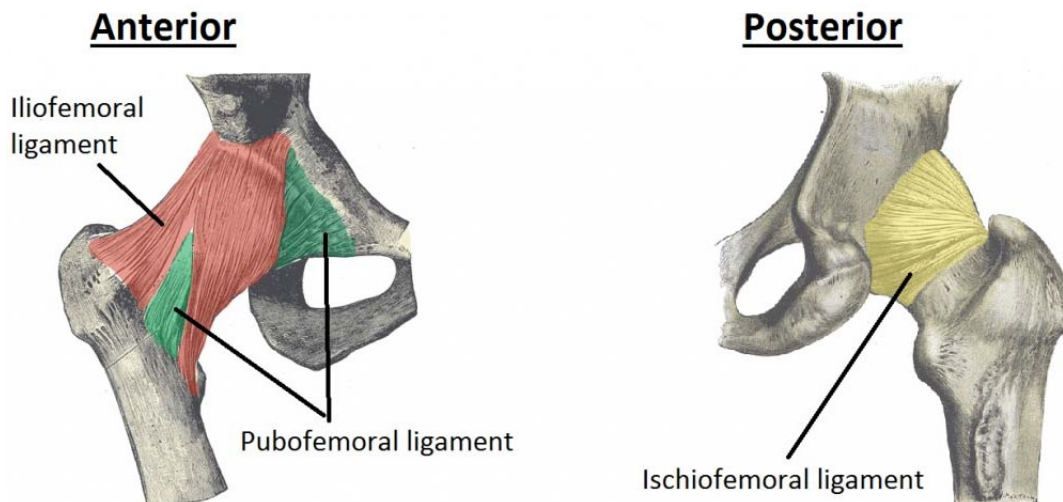

Figure A.2: Anterior view and posterior view of the ligaments of the hip. *Image credit: www.teachmeanatomy.info*

Relevant muscles

Johnston et al. [18], 1979, and Heller et al. [19], 2005, studied which muscles in the lower limb influence hip motion and modeled them. According to Johnston et al. (Fig. A.3) the relevant muscles for hip movement are:

1 Sartorius muscle
2 Rectus femoris
3 Gracilis muscle
4 Pectineus
5 Adductor longus
6 Adductor brevis
7-9 Adductor magnus
10 Gluteus maximus
11-13 Gluteus medius
14-16 Gluteus minimus
17 Tensor faciae latae
18 Piriformis
19 Obturatorius internus
20 Gemellus superior
21 Gemellus inferior
22 Quadratus femoris
23 Obturatorius externus
24 Biceps femoris
25 Semitendinosus muscle
26 Semimembranosus muscle
27 Iliopsoas
28 Vastus
29 Gastrocnemius
30 Soleus

Figure A.3: Overview of the relevant muscles regarding hip motion [18].
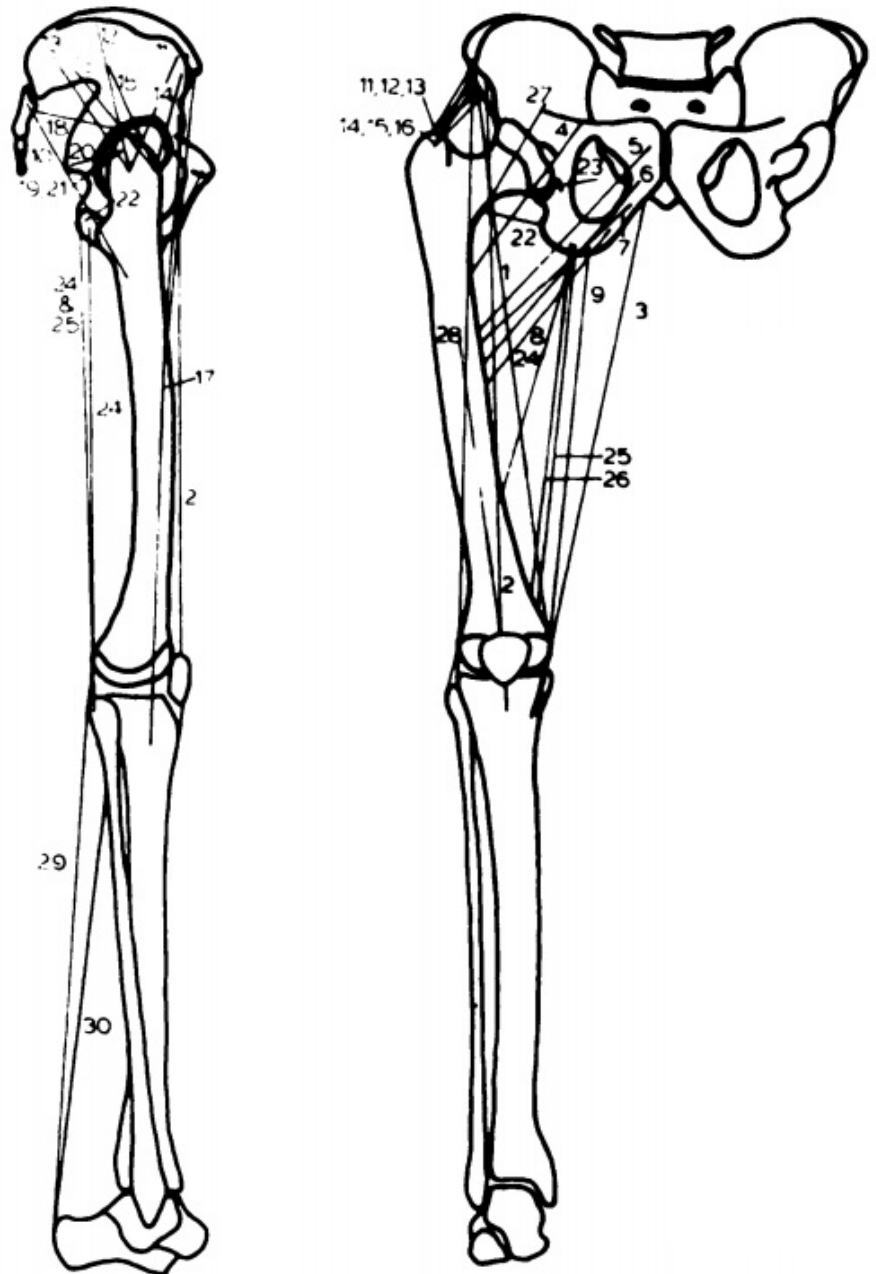
Motions and muscles

The muscles mentioned before can affect different hip motions (Fig. A.4). Listed below are all the possible movements of the hip. Next to them are the principle muscles responsible for these movements [70]:

Flexion: Iliopsoas, rectus femoris, sartorius
Extension: Gluteus maximus, semimembranous, semitendinosus and biceps femoris
Abduction: Gluteus medius, gluteus minimus and the deep gluteals (piriformis, gemelli etc)
Adduction: Adductors longus, brevis and magnus, pectineus and gracillis
Lateral rotation: Biceps femoris, gluteus maximus, and the deep gluteals (piriformis, gemelli etc.)
Medial rotation: Gluteus medius and minimus, semitendinosus and semimembranosus
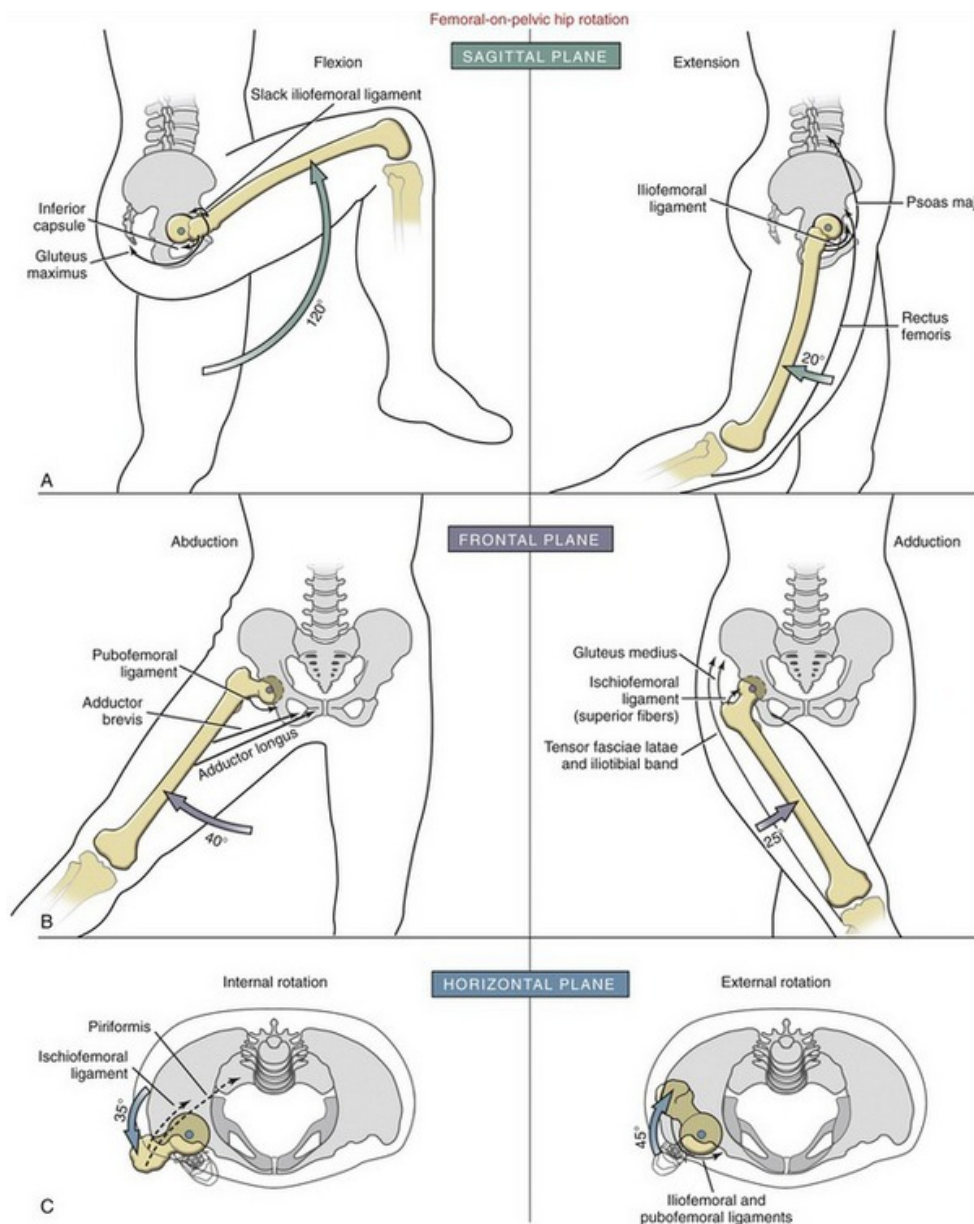

Figure A.4: Overview of possible hip motions and related muscles and ligaments. The approximated maximum range of each motion is given in degrees. *Image credit: www.clinicalgate.com*

B
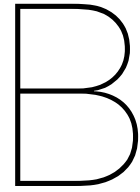
Data Hip III implant

The six figures on the next three pages were obtained from www.orthoload.com [35]. They show data of the hip joint forces in the Hip III implant during 'isometric contraction' with the patient in the supine position. Isometric contraction means the joint angle and muscle length do not change during contraction. The resultant force points almost in the axial direction, but tends to point slightly in the superior direction. This can be seen most clearly in the frontal plane.

Figure B.1: Hip III implant; Supine Position; Isometric contraction; Patient 2 [35].

Figure B.2: Hip III implant; Supine Position; Isometric contraction; Patient 3 [35].

Figure B.3: Hip III implant; Supine Position; Isometric contraction; Patient 4 [35].

Figure B.4: Hip III implant; Supine Position; Isometric contraction; Patient 5 [35].
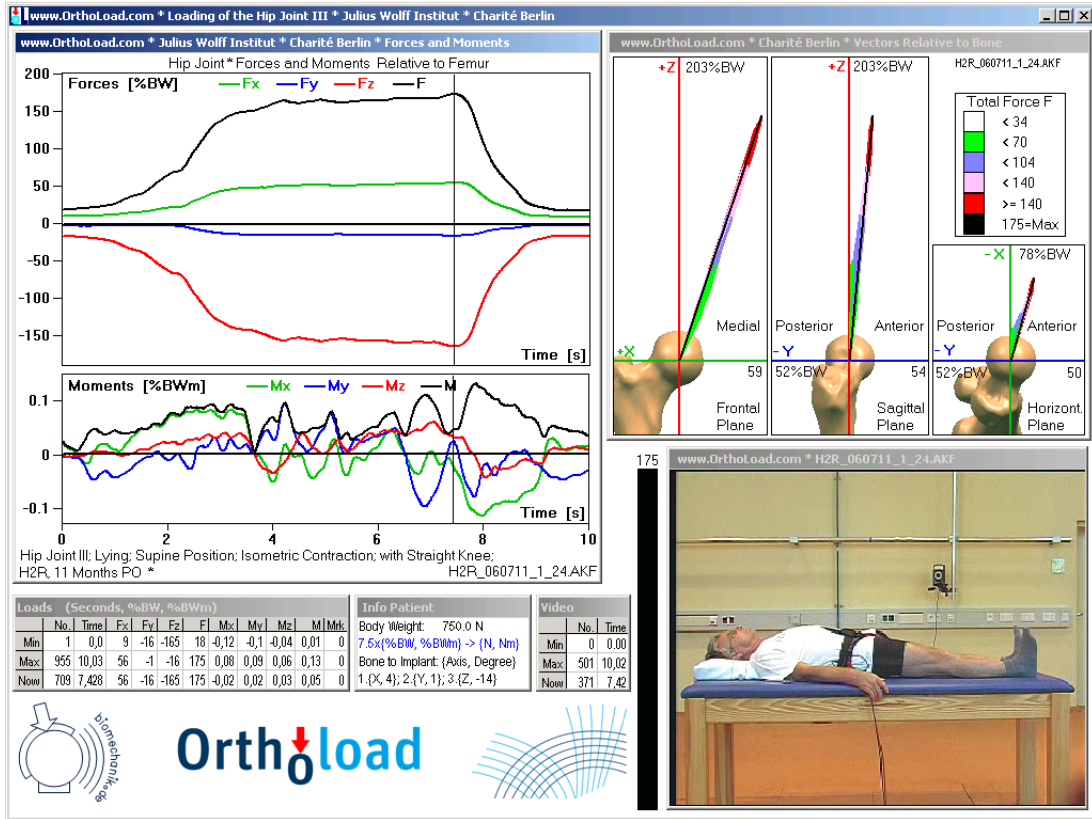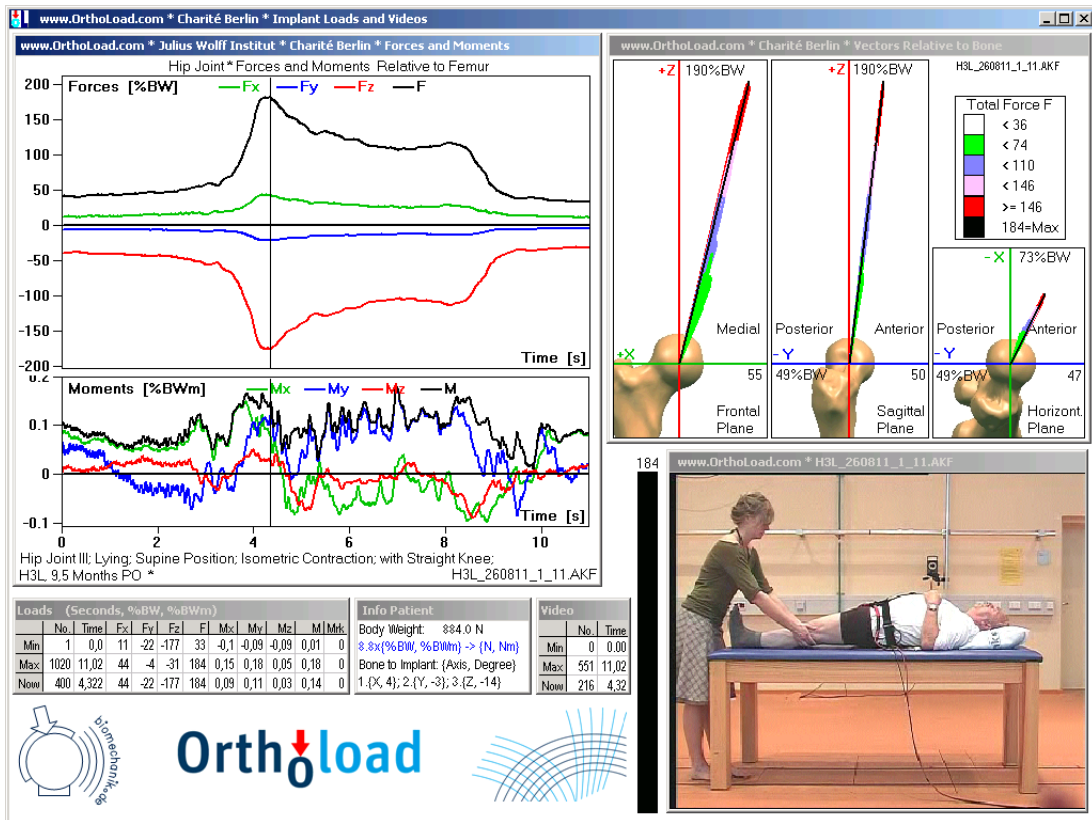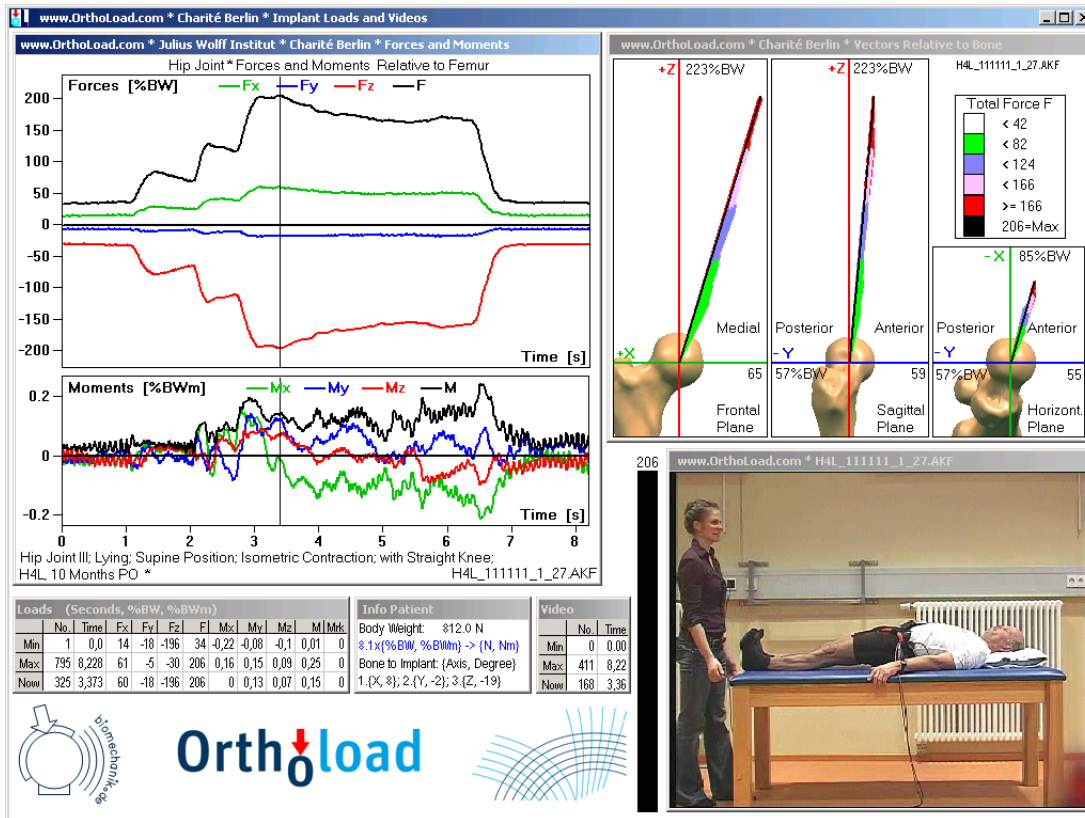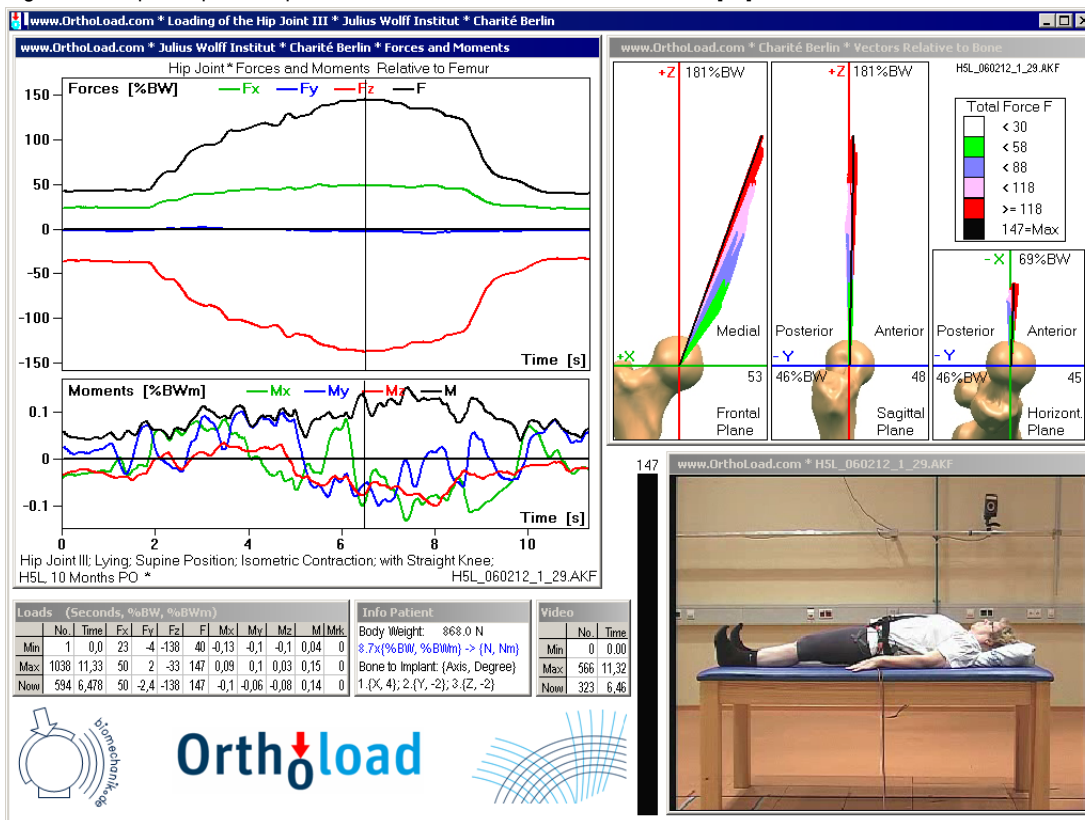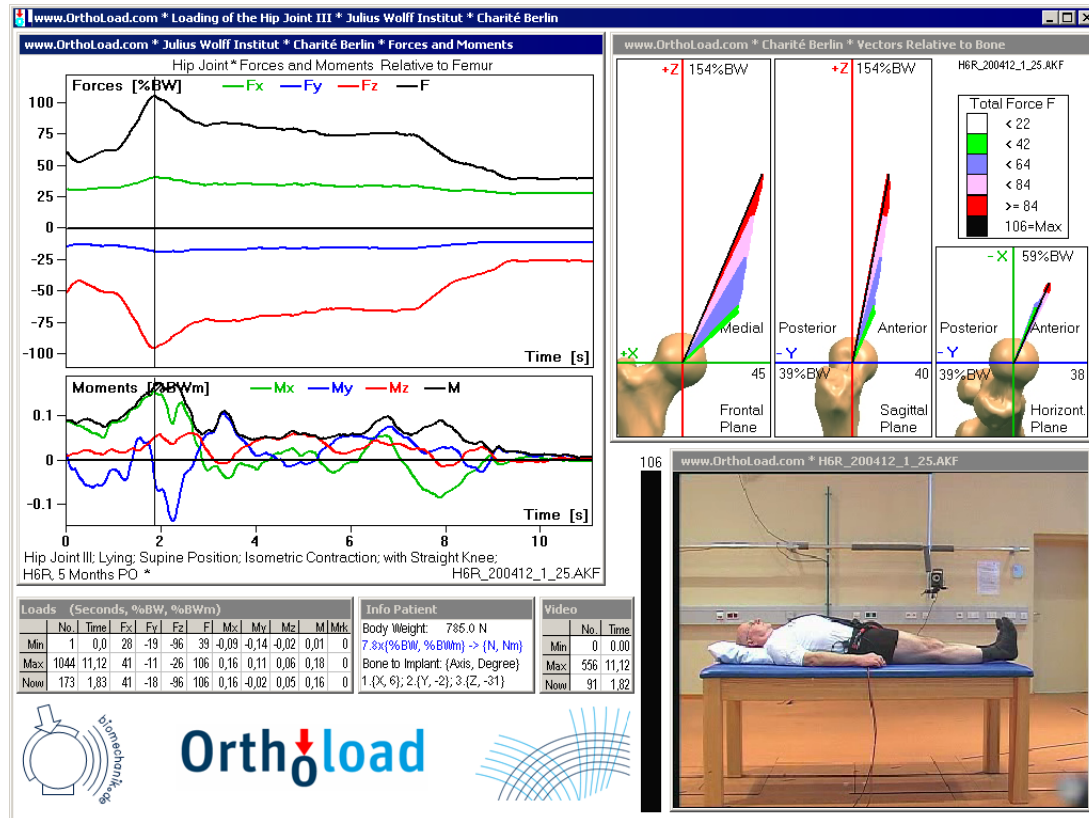
Figure B.5: Hip III implant; Supine Position; Isometric contraction; Patient 6 [35].
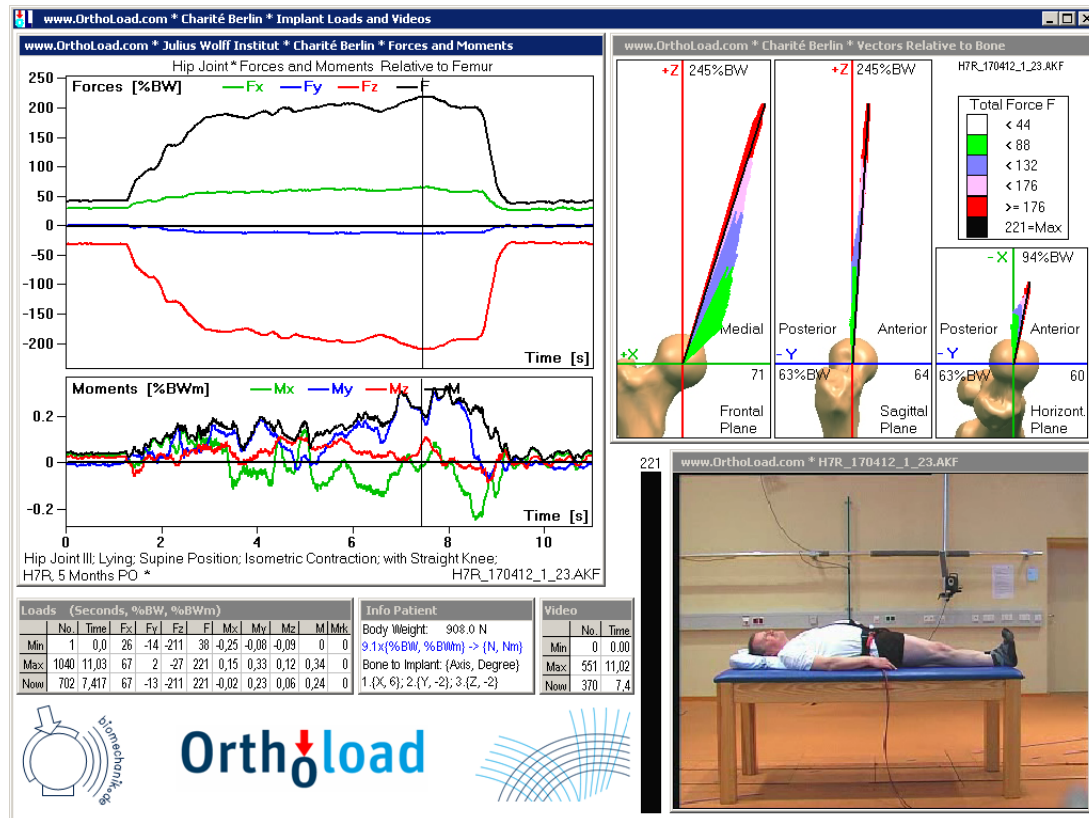
Figure B.6: Hip III implant; Supine Position; Isometric contraction; Patient 7 [35].

C
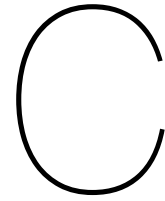
Matlab code

Arduino-Hall-sensor.m

```matlab
1  This code reads the Lin Hall sensor output on Arduinos analogue pin
2  and plots the calculated forces or magnetic field in real time.
3  Dieter van der Pol  31-5-17
4
5  Clean
6  clc
7  clear all
8  close all
9
10 Connect
11 a = arduino('COM3','Uno'); % Connect to Arduino Uno
12
13 Define constants
14       T =            0;    % Create time variable for while loop
15     t(1) =           0;    % Create time vector
16   t_end =           10;    % Choose end time in seconds
17    Sens =     1.3/1000;    % Sensitivity in Volt. A1302: 1.3mV = 1 Gauss
18 nofield =          2.5;    % No magnetic field = 2.5V output
19       n =        90000;    % Number of datapoints
20      a1 =    3.449e+18;    % Constants from calibration
21      b1 =        4.429;
22      c1 =       0.1322;
23      a2 =    2.955e+04;
24      b2 =        5.055;
25      c2 =       0.6385;
26
27 Measurement loop
28 while T < t_end
29     for i = 1:n
30     tic
31     V(i) = abs(readVoltage(a,'A3')-2.5)+2.5;    % Read analogue pin
32     % Comp(i) = V(i) - nofield;                 % Optional calc. Gauss
33     % gauss(i) = abs(Comp(i)/(Sens));           % Optional calc. Gauss
34     F(i) = a1*exp(-((V(i)-b1)/c1)^2) + a2*exp(-((V(i)-b2)/c2)^2); %
35         Caclulate Force from Voltage
36     pause(0.001)                                % Pause briefly so we can
           plot
37     % plot(t,V)                                 % Optional plot
```

```matlab
37      % plot(t,gauss)                          % Optional plot
38      plot(t,F)                                % Plot forces in real time
39      xlabel('Time [s]')
40      % ylabel('Volt [V]')
41      ylabel('Force [N]')
42      elapsedTime = toc;
43      T = T + elapsedTime;                     % Keep track of time
44      t(i+1) = T;                              % Expand time vector
45      if T >= t_end                            % Quit if end time reached
46          break
47      end
48      end
49 end
50
51 Save output voltage and time vector
52 Volt_time = [V; t(1:length(t)-1)];           % Save voltage and time
53 % save Volt_time.mat
54
55 Calculate measurement frequency
56 Freq = length(t)/t(end);                      % Depends on CPU speed
```

Magnet.m

```matlab
% This code calculates the magnetic field density as function of
% distance. It also calculates the saturation value of the Hall sensor.
% Dieter van der Pol    31-5-17

% Clean
clc
clear all
close all

% Define constants
Sens = 1.3*10^-3;    % Sensitivity A1302 Hall sensor = 1.3 mV/Gauss
z_0 = 0*10^-3;       % Initial distance sensor-magnet
z_max = 5*10^-3;     % Max distance sensor-magnet
Hm = 1*10^-3;        % Height magnet 1mm
Dm = 5*10^-3;        % Diameter magnet 5mm
mu = 1;              % Relative magn. perm. materiaal/lucht
M  = 12200;          % Br = 12200 Gauss = 1.22 Tesla for N38
n = 100;             % Number of steps

% Calculate saturation value Hall sensor
B_max_detectable = 2.5/(Sens); % Saturation value of sensor in Gauss

% Calculate field strength at surface of magnet
B_z0 = mu*M/2 * ((z_0 + Hm)/sqrt((z_0 + Hm)^2 + (Dm/2)^2) - z_0/sqrt(z_0^2
     + (Dm/2)^2)); % Fieldstrength at initial distance

% Calculate magnetic field density as a function of axial distance z
for i = 1:n
z(i)    = z_0 + i*(z_max-z_0)/n; % Distance sensor-magnet
B_z(i) = mu*M/2 * ((z(i) + Hm)/sqrt((z(i) + Hm)^2 + (Dm/2)^2) - z(i)/sqrt(
     z(i)^2 + (Dm/2)^2)); % Magnetic field density as a function of axial
     distance z
end

% Change in magnetic field density over entire distance z
Delta_B = B_z0-B_z(n);

% Create figure with graph
plot([z_0*1000, z*1000],[B_z0, B_z])
xlabel('Distance sensor-magnet [mm]')
ylabel('Magn. field [Gauss]')
title('N38 D = 5 mm, H = 1 mm')
```
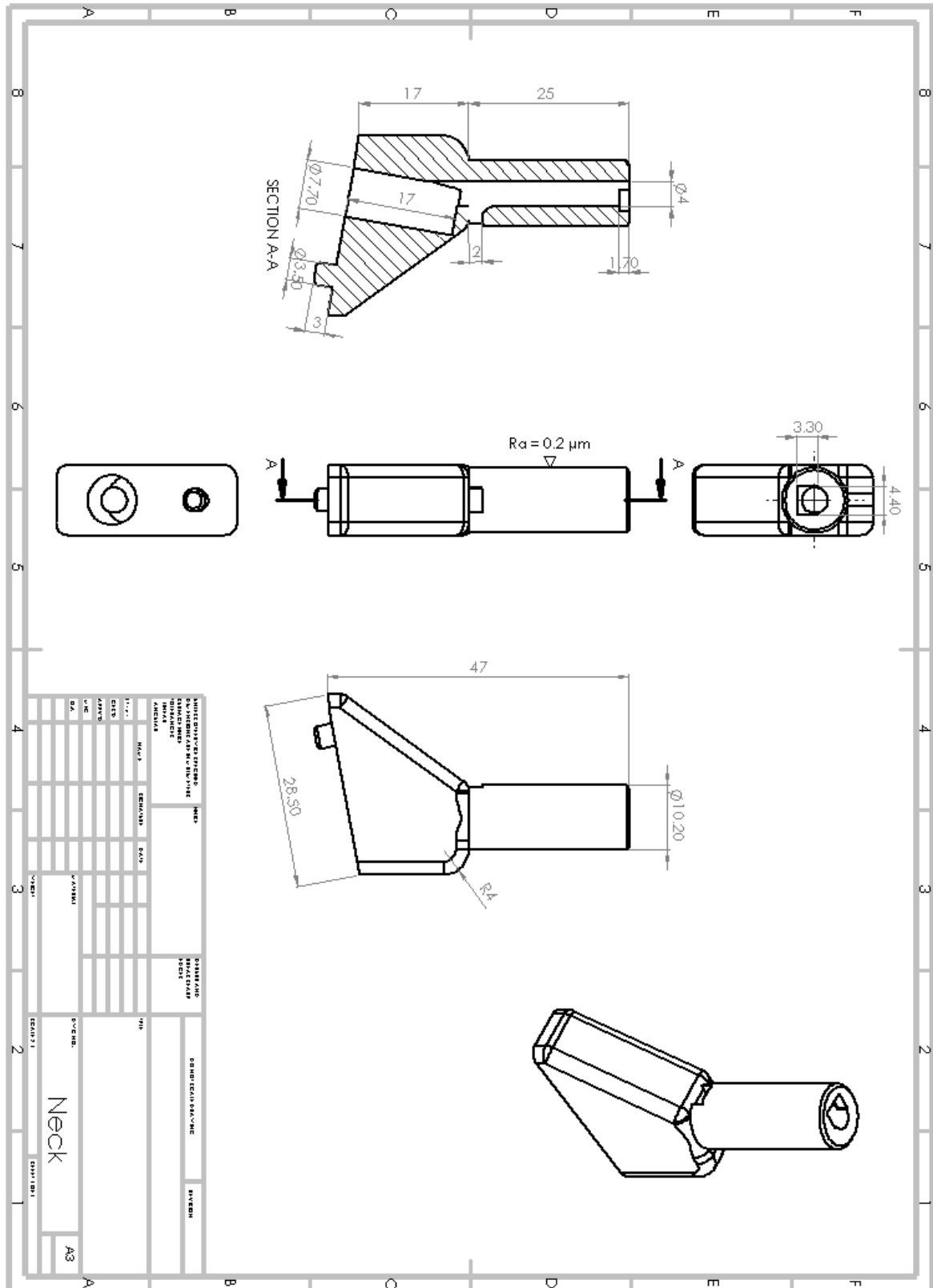
D
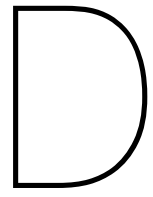
Dimensional drawings

Figure D.1: Dimensional drawing of the neck component. The final neck was 3D printed in stainless steel and smoothened by milling to a diameter of 9,402 mm and a surface roughness of Ra = 0.2 μm.
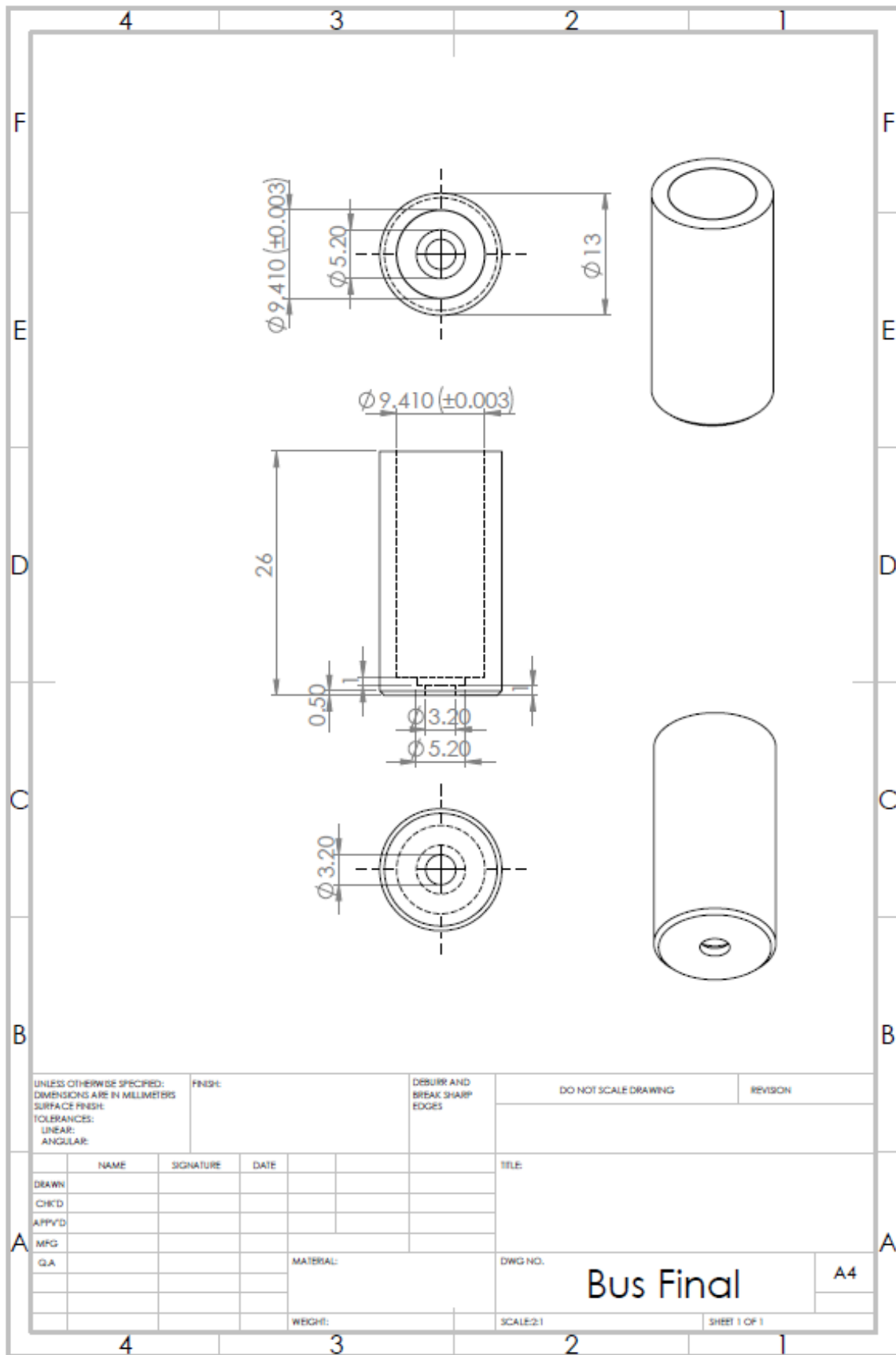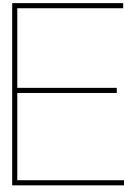
Figure D.2: Dimensional drawing for turning machining the cylindrical component. The material used was stainless steel.

E

Arduino code

The instrumented prototype can function without a laptop using this Arduino code. The code is named: Arduino-LCD-SD.ino. It uses the sensor output voltages on Arduino's analog pin to calculate the forces in real time and displays them on a LCD display. It also saves the data on a SD card.

```
1  // Made by: Dieter van der Pol, 15-7-17

3  // Include the library codes:
   #include <SD.h>
5  #include <LiquidCrystal.h>

7  // Initialize the library with the numbers of the interface pins, NOTE: pin 8, 11 and 13 go
        to the hex converter. Don't use them for the screen.
   LiquidCrystal lcd(10, 9, 5, 4, 3, 2);

9
   // On the Ethernet Shield, CS is pin 4. Note that even if it's not
11 // used as the CS pin, the hardware CS pin (10 on most Arduino boards,
   // 53 on the Mega) must be left as an output or the SD library
13 // functions will not work.

15 // Chip Select pin is tied to pin 8 on the SparkFun SD Card Shield
   const int chipSelect = 8;

17
   void setup()
19 {
     // Set up the LCD's number of columns and rows:
21   lcd.begin(16, 2);
     // Open serial communications and wait for port to open:
23   Serial.begin(9600);
     while (!Serial) {;} // wait for serial port to connect. Needed for Leonardo only

25
     Serial.print("Initializing SD card...");
27   // Make sure that the default chip select pin is set to
     // output, even if you don't use it:
29   pinMode(chipSelect, OUTPUT);

31   // See if the card is present and can be initialized:
     if (!SD.begin(chipSelect)) {
33     Serial.println("Card failed, or not present");
       // don't do anything more:
35     return;}

37   Serial.println("card initialized.");
   }

39
   void loop()
41 {
     unsigned long timeStamp = millis();
43   // Read sensor voltage on pin A0
     int raw = analogRead(3);    // Range : 0..1024
```

```
45    // Define constants
      float a1 =   3.449e+18;
47    float b1 =      4.429;
      float c1 =     0.1322;
49    float a2 =  2.955e+04;
      float b2 =      5.055;
51    float c2 =     0.6385;

53    // Uncomment this to get a raw reading for calibration of no-field point
      // long compensated = raw - NOFIELD;          // adjust relative to no applied field
55
      // Perform calculation
57    float V = 5.000000-(raw * 0.004883);      // Reverse field to positive and adjust scale
        from 8 bits to V = raw*5/1024
      float F = a1*exp(-pow((V-b1)/c1, 2)) + a2*exp(-pow((V-b2)/c2, 2));   // Relation as
        determined in Matlab fitting toolbox
59
      //Output on Serial monitor for debugging
61    Serial.print(" t = ");
      Serial.print(timeStamp);
63    Serial.print(" ms,");
      Serial.print(" Raw =   ");
65    Serial.print(raw);
      Serial.print(", V = ");
67    Serial.print(V);
      Serial.print(" V,");
69    Serial.print(" F = ");
      Serial.print(F);
71    Serial.println(" Newton");

73    lcd.setCursor(0, 0);
      lcd.print(" V = ");
75    lcd.print(V);
      lcd.print(" V ");
77    lcd.setCursor(0, 1);                         // Set the cursor to column 0, line 1 (
        note: line 1 is the second row, since counting begins with 0):
      lcd.print(" F = ");
79    lcd.print(F);
      lcd.print(" Newton ");
81
      // Make a string for assembling the data to log:
83    String dataString = "";

85    // Open the file. note that only one file can be open at a time,
      // so you have to close this one before opening another.
87    // This opens the file and appends to the end of file
      // if the file does not exist, this will create a new file.
89    File dataFile = SD.open("datalog.txt", FILE_WRITE);

91    // If the file is available, write to it:
      if (dataFile)    {
93
        //write to uSD card
95        dataFile.print(" t = ");
          dataFile.print(timeStamp);
97        dataFile.print(" ms,");
          dataFile.print(" Raw =   ");
99        dataFile.print(raw);
          dataFile.print(", V = ");
101       dataFile.print(V);
          dataFile.print(" V,");
103       dataFile.print(" F = ");
          dataFile.print(F);
105       dataFile.println(" Newton");

107       dataFile.close();}  //close file

109       delay(50);           // Delay of 50 ms equals 1000/50 = 20 Hz
      }
```

F
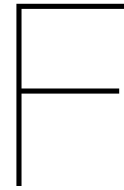
Faulty friction test

In the first friction test, the neck of the prototype was clamped under an angle of 45 degrees under the universal testing machine (Fig. F.1). We intended to measure the friction force caused by the normal component of the force acting under an angle of 45 degrees. However, this measurement setup was not accurate, because the movement of the cylinder in the vertical directions also requires an equal movement in the horizontal direction (Fig. F.2). The problem was that the cylinder could not move freely in this direction, because it was pressed against the load cell. Notice that the load cell can only push down vertically. If the load cell could move horizontally with the prototype there would not be a problem. Since the load cell could not move horizontally, the horizontal force F_{hor} resulted and this led to incorrect results. Luckily, the mistake in this test setup was discovered. With this knowledge, a second friction test with a better test setup was created.

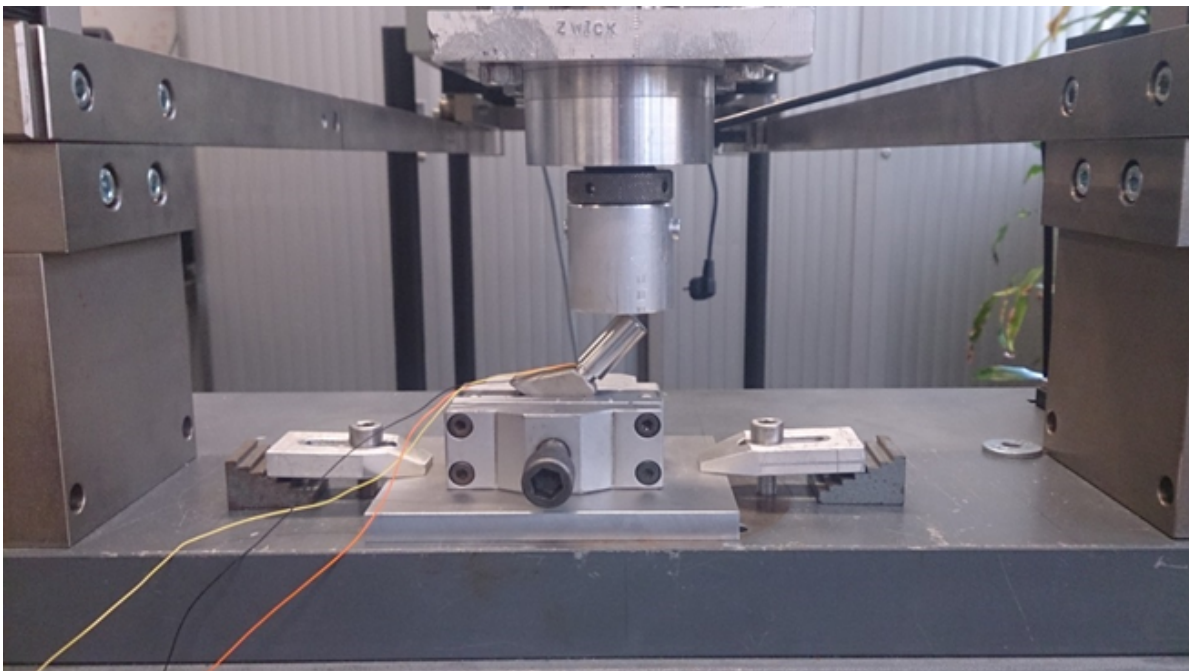Figure F.1: This incorrect test setup was used for the first friction test. It has the prototype clamped under an angle of 45 degrees underneath the testing machine.
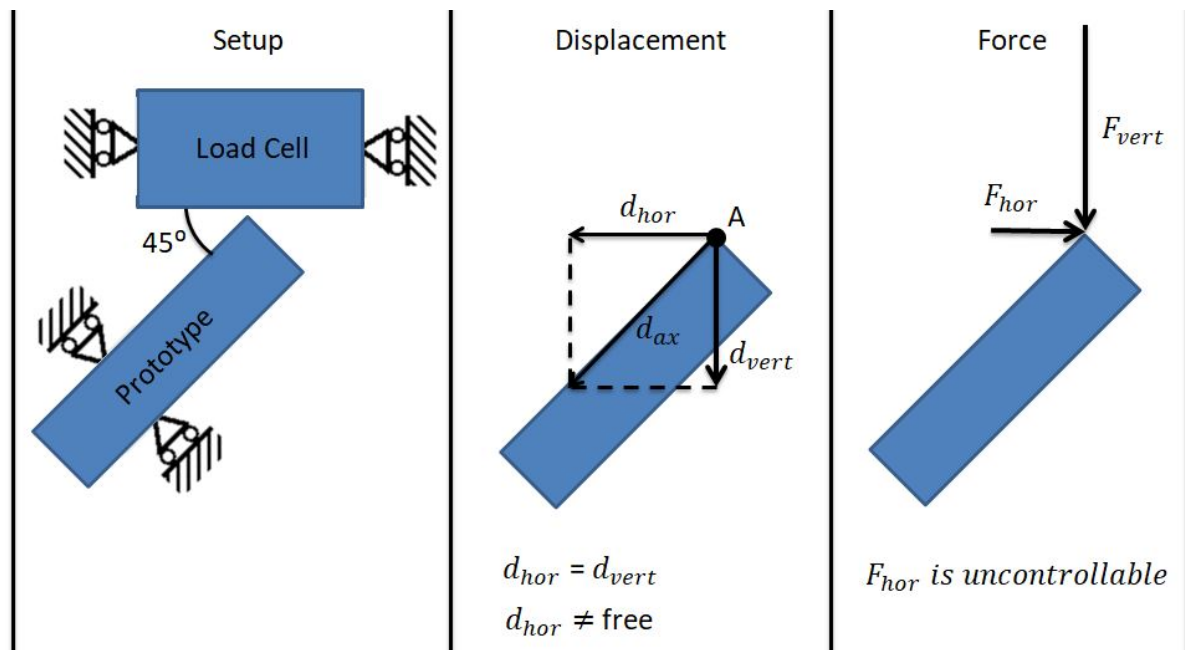
Figure F.2: This drawing shows the prototype tries to move in the direction d_{hor} when the load cell pushes down. However, the prototype could not slide freely in this direction. Therefore, there was an uncontrollable horizontal force that led to incorrect results.

G

Standardized test proposal

A standardized test protocol would help the surgeon to get consistent and useful results in future research. Therefore, two standardized test proposals were made. The assumption was made that the placement of the implant components is correct, no regional anesthesia is used and the patient has no muscular diseases, because this would create misleading measurement results.

Standardized test protocol

1. Put the patient in the supine position.

2. Insert the instrumented implant.

3. Hold the leg under the ankle.

4. Lift the leg just above the table while keeping the knee and ankle in the neutral position.

5. Hold the leg in 0 degrees external rotation.

6. Move the leg in 25 degrees abduction and adduction consecutively.

7. Repeat this movement three times.

8. The force vector of the resultant hip force is expected to rotate around the y axis during this motion (Appendix B, Fig. B.1, Frontal Plane). During this motion the hip force will reach a maximum, then a minimum and then another maximum similar to Figure 44. **Hypothesis**: The force peaks are symmetrical during this motion, if the hip has the correct soft tissue tension.

9. Check the range of motion. If the hip force is too high this will be evident, because the range of motion will be limited.

10. Check if the hip dislocates by applying a combination of flexion and external rotation. If the hip force is too low, the hip will now dislocate.

11. If the hip force is too high or too low, the surgeon should act accordingly by choosing a different trial head. Then repeat the protocol.

12. All the axial force patterns must be saved during these iterations, so the right force patterns can be distinguished from the wrong ones.

13. When the hip force is appropriate, the surgeon can place the final implant with the chosen dimensions.

A similar hypothesis can be made for internal-external rotation or internal-external rotation combined with abduction and adduction.

Bibliography

[1] Robert B Bourne and Cecil H Rorabeck. Soft tissue balancing: the hip. *The Journal of arthroplasty*, 17(4):17–22, 2002.

[2] Pencho Kosev, Bojan Valentinov, Yordan Andonov, and Cvetan Sokolov. Soft tissue balancing in total hip arthroplasty. *Journal of IMAB–Annual Proceeding Scientific Papers*, 21(1):752–756, 2015.

[3] Donald Longjohn and Lawrence D Dorr. Soft tissue balance of the hip. *The Journal of arthroplasty*, 13(1):97–100, 1998.

[4] J Stuart Melvin, Tharun Karthikeyan, Robert Cope, and Thomas K Fehring. Early failures in total hip arthroplasty—a changing paradigm. *The Journal of arthroplasty*, 29(6): 1285–1288, 2014.

[5] Slif D Ulrich, Thorsten M Seyler, Derek Bennett, Ronald E Delanois, Khaled J Saleh, Issada Thongtrangan, Michael Kuskowski, Edward Y Cheng, Peter F Sharkey, Javad Parvizi, et al. Total hip arthroplasties: what are the reasons for revision? *International orthopaedics*, 32(5):597–604, 2008.

[6] Urban Hedlundh, LENNART Ahnfelt, C-H Hybbinette, J Weckström, and HANS Fredin. Surgical experience related to dislocations after total hip arthroplasty. *Bone & Joint Journal*, 78(2):206–209, 1996.

[7] JAMES G Wright, SALLY Rudicel, and AR Feinstein. Ask patients what they want. evaluation of individual complaints before total hip replacement. *Bone & Joint Journal*, 76(2):229–234, 1994.

[8] Rosamond J Tansey, Gemma L Green, and Fares S Haddad. Large diameter heads: Is bigger always better? In *Seminars in Arthroplasty*, volume 26, pages 16–19. Elsevier, 2015.

[9] G Lecerf, MH Fessy, R Philippot, P Massin, F Giraud, X Flecher, J Girard, P Mertl, E Marchetti, and E Stindel. Femoral offset: anatomical concept, definition, assessment, implications for preoperative templating and hip arthroplasty. *Orthopaedics & Traumatology: Surgery & Research*, 95(3):210–219, 2009.

[10] Alexander Huppertz, Sebastian Radmer, Patrick Asbach, Ralf Juran, Carsten Schwenke, Gerd Diederichs, Bernd Hamm, and Martin Sparmann. Computed tomography for preoperative planning in minimal-invasive total hip arthroplasty: radiation exposure and cost analysis. *European journal of radiology*, 78(3):406–413, 2011.

[11] Thierry Scheerlinck. Primary hip arthroplasty templating on standard radiographs: a stepwise approach. *Acta Orthop Belg*, 76(4):432, 2010.

[12] Manish Dastane, Lawrence D Dorr, Rupesh Tarwala, and Zhinian Wan. Hip offset in total hip arthroplasty: quantitative measurement with navigation. *Clinical Orthopaedics and Related Research®*, 469(2):429–436, 2011.

[13] Henry D Atkinson, Karanjeev S Johal, Charles Willis-Owen, Steven Zadow, and Roger D Oakeshott. Differences in hip morphology between the sexes in patients undergoing hip resurfacing. *Journal of orthopaedic surgery and research*, 5(1):76, 2010.

[14] Ian S Rice, R Lee Stowell, Purab C Viswanath, and Gary J Cortina. Three intraoperative methods to determine limb-length discrepancy in tha. *Orthopedics*, 37(5):e488–e495, 2014.

[15] Palaniappan Lakshmanan, Shabhaz MY Ahmed, Richard GN Hansford, and David J Woodnutt. Achieving the required medial offset and limb length in total hip arthroplasty. *Acta Orthopædica Belgica*, 74(1):49, 2008.

[16] Monika Michalíková, Lucia Bednarcikova, Martin Petrík, Jozef Zivcak, and Richard Rasi. The digital pre-operative planning of total hip arthroplasty. *Acta Polytechnica Hungarica*, 7(3):137–52, 2010.

[17] Markus O Heller, Georg Bergmann, Georg Deuretzbacher, Lutz Claes, Norbert P Haas, and Georg N Duda. Influence of femoral anteversion on proximal femoral loading: measurement and simulation in four patients. *Clinical biomechanics*, 16(8):644–649, 2001.

[18] RICHARD C Johnston, RA Brand, and RD Crowninshield. Reconstruction of the hip. a mathematical approach to determine optimum geometric relationships. *The Journal of Bone & Joint Surgery*, 61(5):639–652, 1979.

[19] MO Heller, Georg Bergmann, J-P Kassi, Lutz Claes, NP Haas, and GN Duda. Determination of muscle loading at the hip joint for use in pre-clinical testing. *Journal of biomechanics*, 38(5):1155–1163, 2005.

[20] BW Stansfield, AC Nicol, JP Paul, IG Kelly, F Graichen, and G Bergmann. Direct comparison of calculated hip joint contact forces with those measured using instrumented implants. an evaluation of a three-dimensional mathematical model of the lower limb. *Journal of biomechanics*, 36(7):929–936, 2003.

[21] Seamus O'Brien. Femoral offset in total hip replacement: A study of anatomical offset in the northern ireland population. *International Journal of Orthopaedic and Trauma Nursing*, 18(3):162–169, 2014.

[22] Stephen Petis, James L Howard, Brent L Lanting, and Edward M Vasarhelyi. Surgical approach in primary total hip arthroplasty: anatomy, technique and clinical outcomes. *Canadian Journal of Surgery*, 58(2):128, 2015.

[23] Ofir Chechik, Morsi Khashan, Ran Lador, Moshe Salai, and Eyal Amar. Surgical approach and prosthesis fixation in hip arthroplasty world wide. *Archives of orthopaedic and trauma surgery*, 133(11):1595–1600, 2013.

[24] Kazunari Kuroda, Tamon Kabata, Toru Maeda, Yoshitomo Kajino, and Hiroyuki Tsuchiya. Do we need intraoperative radiographs for positioning the femoral component in total hip arthroplasty? *Archives of orthopaedic and trauma surgery*, 134(5): 727–733, 2014.

[25] Jens Dargel, Johannes Oppermann, Gert-Peter Brüggemann, and Peer Eysel. Dislocation following total hip replacement. *Deutsches Ärzteblatt International*, 111(51-52):884, 2014.

[26] Matthew S Austin, William J Hozack, Peter F Sharkey, and Richard H Rothman. Stability and leg length equality in total hip arthroplasty. *The Journal of arthroplasty*, 18(3):88–90, 2003.

[27] Chitranjan S Ranawat and JoséA Rodriguez. Functional leg-length inequality following total hip arthroplasty. *The Journal of arthroplasty*, 12(4):359–364, 1997.

[28] Mark N Charles, Robert B Bourne, J Roderick Davey, A Seth Greenwald, Bernard F Morrey, and Cecil H Rorabeck. Soft-tissue balancing of the hip. *J Bone Joint Surg Am*, 86(5):1078–1088, 2004.

[29] M Naito, K Ogata, and I Asayama. Intraoperative limb length measurement in total hip arthroplasty. *International orthopaedics*, 23(1):31–33, 1999.

[30] Sathappan S Sathappan, Daniel Ginat, Vipul Patel, Michael Walsh, William L Jaffe, and Paul E Di Cesare. Effect of anesthesia type on limb length discrepancy after total hip arthroplasty. *The Journal of arthroplasty*, 23(2):203–209, 2008.

[31] Rajesh Malhotra. *Mastering Orthopedic Techniques: Total Hip Arthroplasty*. JP Medical Ltd, 2011.

[32] Sam W Wiesel. *Operative techniques in orthopaedic surgery*. Lippincott Williams & Wilkins, 2012.

[33] Total hip replacement surgery video. Retrieved from: www.youtube.com. Accessed: 2016-11-16.

[34] Verena Schwachmeyer, Philipp Damm, Alwina Bender, Jörn Dymke, Friedmar Graichen, and Georg Bergmann. In vivo hip joint loading during post-operative physiotherapeutic exercises. *PloS one*, 8(10):e77807, 2013.

[35] Data hip iii implant. Retrieved from: https://orthoload.com, Accessed: 25-11-2016.

[36] Mohsin I Tiwana, Stephen J Redmond, and Nigel H Lovell. A review of tactile sensing technologies with applications in biomedical engineering. *Sensors and Actuators A: physical*, 179:17–31, 2012.

[37] Nils W Rydell. Forces acting on the femoral head-prosthesis: a study on strain gauge supplied prostheses in living persons. *Acta Orthopaedica Scandinavica*, 37(sup88):1–132, 1966.

[38] G Bergmann, F Graichen, J Siraky, H Jendrzynski, and A Rohlmann. Multichannel strain gauge telemetry for orthopaedic implants. *Journal of biomechanics*, 21(2):169–176, 1988.

[39] F Graichen and G Bergmann. Four-channel telemetry system for in vivo measurement of hip joint forces. *Journal of Biomedical Engineering*, 13(5):370–374, 1991.

[40] G Bergmann, G Deuretzbacher, M Heller, F Graichen, A Rohlmann, J Strauss, and GN Duda. Hip contact forces and gait patterns from routine activities. *Journal of biomechanics*, 34(7):859–871, 2001.

[41] Graichen Bergmann, F Graichen, and A Rohlmann. Hip joint contact forces during stumbling. *Langenbeck's Archives of Surgery*, 389(1):53–59, 2004.

[42] G Bergmann, F Graichen, A Rohlmann, P Westerhoff, B Heinlein, A Bender, and R Ehrig. Design and calibration of load sensing orthopaedic implants. *Journal of biomechanical engineering*, 130(2):021009, 2008.

[43] G Bergmann, F Graichen, A Rohlmann, A Bender, B Heinlein, GN Duda, MO Heller, and MM Morlock. Realistic loads for testing hip implants. *Bio-medical materials and engineering*, 20(2):65–75, 2010.

[44] Georg Bergmann, Alwina Bender, Jörn Dymke, Georg Duda, and Philipp Damm. Standardized loads acting in hip implants. *PloS one*, 11(5):e0155612, 2016.

[45] Graichen Bergmann, F Graichen, and A Rohlmann. Hip joint loading during walking and running, measured in two patients. *Journal of biomechanics*, 26(8):969–990, 1993.

[46] Georg Bergmann, Friedmar Graichen, Antonius Rohlmann, and Holger Linke. Hip joint forces during load carrying. *Clinical orthopaedics and related research*, 335:190–201, 1997.

[47] G Bergmann, H Kniggendorf, F Graichen, and A Rohlmann. Influence of shoes and heel strike on the loading of the hip joint. *Journal of Biomechanics*, 28(7):817–827, 1995.

[48] Graichen Bergmann, F Graichen, and A al Rohlmann. Is staircase walking a risk for the fixation of hip implants? *Journal of biomechanics*, 28(5):535–553, 1995.

[49] G Bergmann, M Correa da Silva, G Neff, A Rohlmann, and F Graichen. Evaluation of ischial weight-bearing orthoses, based on in-vivo hip joint force measurements. *Clinical Biomechanics*, 9(4):225–234, 1994.

[50] G Bergmann, A Rohlmann, and F Graichen. [in vivo measurement of hip joint stress. 1. physical therapy]. *Zeitschrift fur Orthopadie und ihre Grenzgebiete*, 127(6):672–679, 1988.

[51] Philipp Damm, Joern Dymke, Robert Ackermann, Alwina Bender, Friedmar Graichen, Andreas Halder, Alexander Beier, and Georg Bergmann. Friction in total hip joint prosthesis measured in vivo during walking. *PloS one*, 8(11):e78373, 2013.

[52] Philipp Damm, Verena Schwachmeyer, Joern Dymke, Alwina Bender, and Georg Bergmann. In vivo hip joint loads during three methods of walking with forearm crutches. *Clinical Biomechanics*, 28(5):530–535, 2013.

[53] Philipp Damm, Alwina Bender, and Georg Bergmann. Postoperative changes in in vivo measured friction in total hip joint prosthesis during walking. *PloS one*, 10(3):e0120438, 2015.

[54] Friedmar Graichen, Georg Bergmann, and Antonius Rohlmann. Hip endoprosthesis for in vivo measurement of joint force and temperature. *Journal of Biomechanics*, 32(10): 1113–1117, 1999.

[55] G Bergmann, F Graichen, and A Rohlmann. Hip joint forces in sheep. *Journal of biomechanics*, 32(8):769–777, 1999.

[56] G Bergmann, J Siraky, A Rohlmann, and R Koelbel. A comparison of hip joint forces in sheep, dog and man. *Journal of Biomechanics*, 17(12):907–921, 1984.

[57] Yoshito Otake, Naoki Suzuki, Asaki Hattori, Hidenobu Miki, Mitsuyoshi Yamamura, Nobuhiko Sugano, Kazuo Yonenobu, and Takahiro Ochi. Evaluation of hip dislocation in a patient after total hip arthroplasty by intraoperative measurements of soft-tissue-generated forces and with a 4d muscle model. *INTERNATIONAL JOURNAL OF COMPUTER ASSISTED RADIOLOGY AND SURGERY*, 1:239–241, 2006.

[58] Yoshito Otake, Naoki Suzuki, Asaki Hattori, Hidenobu Miki, Mitsuyoshi Yamamura, Kazuo Yonenobu, Takahiro Ochi, and Nobuhiko Sugano. System for intraoperative evaluation of soft-tissue-generated forces during total hip arthroplasty by measurement of the pressure distribution in artificial joints. *Computer Aided Surgery*, 12(1):53–59, 2007.

[59] Otto Müller, Wolfgang J Parak, Markus G Wiedemann, and Franz Martini. Three-dimensional measurements of the pressure distribution in artificial joints with a capacitive sensor array. *Journal of biomechanics*, 37(10):1623–1625, 2004.

[60] M Higa, H Tanino, H Ito, T Matsuno, T Sato, and SA Banks. Intraoperative soft-tissue tension measurements during total hip arthroplasty. *Proceedings of the 55th Transactions of Orthopaedic Research Society*, page 2029, 2009.

[61] Lucia Beccai, Stefano Roccella, Alberto Arena, Francesco Valvo, Pietro Valdastri, Arianna Menciassi, Maria Chiara Carrozza, and Paolo Dario. Design and fabrication of a hybrid silicon three-axial force sensor for biomechanical applications. *Sensors and Actuators A: Physical*, 120(2):370–382, 2005.

[62] Ana Luisa Trejos, Abelardo Escoto, Dustin Hughes, Michael D Naish, and Rajni V Patel. A sterilizable force-sensing instrument for laparoscopic surgery. In *5th IEEE RAS/EMBS International Conference on Biomedical Robotics and Biomechatronics*, pages 157–162. IEEE, 2014.

[63] Hongbo Wang, Greg de Boer, Junwai Kow, Ali Alazmani, Mazdak Ghajari, Robert Hewson, and Peter Culmer. Design methodology for magnetic field-based soft tri-axis tactile sensors. *Sensors*, 16(9):1356, 2016.

[64] Anton van Beek. *Werktuigbouw.nl Formuleboekje*. Microcentrum, 2015.

[65] Precision disc springs catalog. Retrieved from: `http://www.centuryspring.com`, Accessed: 15-06-2017.

[66] Ces edupack. 2017.

[67] Ellen M Arruda and Mary C Boyce. A three-dimensional constitutive model for the large stretch behavior of rubber elastic materials. *Journal of the Mechanics and Physics of Solids*, 41(2):389–412, 1993.

[68] Robert A Shanks et al. General purpose elastomers: structure, chemistry, physics and performance. In *Advances in Elastomers I*, pages 11–45. Springer, 2013.

[69] Alexandra Pfister, Alexandre M West, Shaw Bronner, and Jack Adam Noah. Comparative abilities of microsoft kinect and vicon 3d motion capture for gait analysis. *Journal of medical engineering & technology*, 38(5):274–280, 2014.

[70] Muscles and motions of the hip. Retrieved from: `http://teachmeanatomy.info`. Accessed: 20-10-2016.